Graz University of Technology
Institute for Railway Engineering and Transport Economy

Evaluation of attrition tests for railway ballast

Dissertation

June 2013

Dipl.-Ing. Holger Bach
Matrikelnummer: 0031068

Supervisor:
Peter Veit
Univ.-Prof. Dipl.-Ing. Dr.techn.

www.ebw.TUGraz.at

Tradition

„Dieses haben unsere Vorfahren aus gutem Grunde so geordnet, und wir stellen es aus gutem Grunde nun wieder ab.“ (“Just as our ancestors made such arrangements for a good reason, we now abandon them for a good reason”)

Georg Christoph Lichtenberg (1742–1799), Sudelbücher Heft C (234)

Acknowledgements

This doctoral thesis is an interdisciplinary study. Carried out at the Institute for Railway Engineering, it covers aspects of rock and soil mechanics, engineering geology, mineralogy, mechanics of granular media, statistics, machine vision and transport economics.

Making extensive use of the testing facilities at the Faculty of Civil Engineering and Geosciences, a multitude of laboratory tests were carried out over the course of the present study. I would thus like to thank the following people for their help: Matthias Lenz and Gregor Brunnsteiner at the Institute of Technology and Testing of Building Materials, Josef Linder and Uwe Fülöp at the Laboratory for Construction Engineering, Manfred Blümel at the Laboratory for Rock Mechanics, and in particular, Mario Wiesberger at the Institute for Railway Engineering.

Many thanks go to my dear colleagues (past and present) at the Department of Civil Engineering. Their friendship has been a continuous source of support. In particular I would like to thank Armin Berghold, Markus Enzi, Georg Neuper, Stefan Walter, Krzysztof Wilczek, Christian Lackner and Nedim Radoncic.

The financial support provided by Christoph Kuttelwascher at ÖBB Infra AG and Wolfgang Zottl at the ÖBB Research & Development Division is greatly appreciated. I also wish to thank Thorgeir Helgason of Petromodel Ltd., Iceland, for his support concerning the functionality of the Petroscope measuring device, and Helfried Breymann of HTL Saalfelden, for providing me with his point load test results.

Numerous laboratory tests were carried out and considerable theoretical work was contributed by master's students at the Faculty of Civil Engineering and Geosciences. Many thanks to Maria Cepeda Fernandez, Rita Fuchs, Katrin Hollersbacher, Anna Christina Neubauer, Peter Pixner, Martin Schöck and Elisabeth Uhlig, for all their diligent work.

I would like to express my deepest gratitude to Vera Hofer of the Institute of Statistics and Operations Research at Graz University and Christine Latal of the Institute for Applied Geosciences. They always offered prompt help when asked for assistance and contributed many valuable suggestions. Prof. Kurosch Thuro of TU Munich very kindly agreed to act as my co-supervisor and provided valuable support in the form of extensive experience in rock abrasion and tool wear. Many thanks! Finally, my supervisor, Prof. Peter Veit must be thanked for his constant support and guidance and for believing in the scientific and economic relevance of the TU Graz railway ballast test project, its feasibility, and in me.

Eidesstattliche Erklärung

Ich erkläre an Eides statt, dass ich die vorliegende Arbeit selbstständig verfasst, andere als die angegebenen Quellen/Hilfsmittel nicht benutzt, und die den benutzten Quellen wörtlich und inhaltlich entnommene Stellen als solche kenntlich gemacht habe.

Graz, am 25.06.2013 _____

Abstract

The use of poor quality ballast leads to shorter tamping intervals, a shorter ballast lifespan, and thus to increased life cycle costs. Railway companies employ specific quality control testing methods in order to ensure the desired mechanical behavior (i.e. resistance to fragmentation and to abrasion). In part, such tests have been used without change for several decades. The tests are meant to simulate the loads acting upon the ballast in track. Some tests results are highly variable and often show poor repeatability. The reasons for this remain unclear. Several possibilities for improvement have been suggested, for example, use of alternative test evaluation methods, adjustment of test procedures, and even the use of completely new test methods.

It is common belief that a given test result allows one to estimate the performance of ballast lifespan in track for the respective rock type. But this is only the case if the load regimen of the testing method resembles the loads acting upon the ballast particles in track. Thus, both the load level in track and the respective attrition test load level have to be estimated.

Using numerical models, load transfer from the vehicle axle via rail and sleeper into and through the ballast layer was simulated. The concept of 'coordination number' was then used to quantify the particle-to-particle loads within the ballast layer.

The evaluation comprised five attrition tests (Los-Angeles test, Swiss Impact test, Deval Attrition test, LCPC Abroy test und Cerchar test) and eleven rock types. The specific load level for each of the test methods was estimated. The measuring device „Petroscope®4D" was used to characterize the geometry of all particles in the respective sample. This allowed for classification of the test methods into the attrition categories "fragmentation", "rounding" and "abrasion" and for finding factors of influence with respect to deviations in the results obtained. In order to quantify the impact of variability in petrographic composition on test result deviation, tests were performed using samples of previously sorted subclasses.

Based on these findings, recommendations for efficient application and optimized test evaluation are given. The use of a wide range of samples from Austria's leading suppliers of ballast means that quality assessment is based on an extensive range of data.

Kurzfassung

Der Einsatz von Bahnschotter minderer Qualität führt zu verkürzten Stopfintervallen, einer Verringerung der Lebensdauer und damit erhöhten Lebenszykluskosten. Um die gewünschten mechanischen Eigenschaften (namentlich Schlagzähigkeit, Kantenstabilität und geringe Abradierbarkeit) sicherzustellen, werden von den Eisenbahnunternehmen Prüfverfahren festgeschrieben, die z.T. schon seit Jahrzehnten unverändert angewandt werden. Diese Verfahren sollen die im Gleis auf den Schotter wirkenden Belastungen simulieren. Die Versuchsergebnisse unterliegen teilweise erheblichen Schwankungen, deren Ursache z.T. noch ungeklärt ist. Zur Verbesserung dieser Situation sind sowohl alternative Auswertemethoden an etablierten Tests, Weiterentwicklungen in der Versuchsdurchführung und der Einsatz gänzlich neuer Verfahren denkbar.

Nur wenn das Lastregime der Testverfahren die mechanische Belastung des Schotters im Gleis zutreffend widerspiegelt, kann davon ausgegangen werden, dass aus einem Testergebnis auf die Lebensdauer der betreffenden Schottersorte im Gleis geschlossen werden kann. Daher ist sowohl das Lastregime im Schotterbett abzuschätzen als auch die im Zuge der Labortests auf die Probe einwirkenden Lasten.

Zunächst wurde mittels numerischer Methoden der Lastabtrag von der Fahrzeugachse über den Gleisrost und die Schwelle in und durch das Schotterbett modelliert. Zur Abschätzung der auftretenden Korn-zu-Korn-Kontaktkräfte im Schotterbett wurde das Konzept der Kontaktpunktanzahl herangezogen.

An fünf etablierten und alternativen Prüfverfahren (Los-Angeles Test, Druckfestigkeit am Haufwerk nach SN 670 830b, Deval Test, LCPC Abroy Test und Cerchar Test) wurden Reihentests mit elf Schottersorten vorgenommen und deren Lastregime analysiert. Hierbei wurde die Korngeometrie aller Körner der Probencharge mittels des Prüfgeräts „Petroscope®4D" präzise aufgemessen. Daraus konnten Anhaltspunkte über die Ursachen auftretender Streuungen gefunden und eine genaue Einordnung der Verfahren in die drei Verschleißkategorien „Kornbruch", „Kantenbruch" und „Abrasion" vorgenommen werden. Der Einfluss der Variabilität in der petrographischen Zusammensetzung der Probencharge auf die Ergebnisstreuungen konnte durch Tests mit zuvor händisch in Subgruppen getrennten Proben quantifiziert werden.

Aus diesen Erkenntnissen wurden Empfehlungen für einen zielführenden Einsatz und eine optimierte Auswertung der Verfahren zusammengestellt. Die umfangreichen Versuchsreihen mit Proben der wichtigsten österreichischen Schotterlieferanten erlaubte weiterhin auch eine Einschätzung der jeweiligen Schottergüte auf einer breiten Datenbasis.

Table of contents

1 Introduction

1.1 Background and problem statement

Railway ballast is a mass product. To build one kilometre of railway line some 7,000 tonnes of ballast are required (Österreichische Bundesbahnen (ÖBB) 2002). Austrian Railways alone have an annual demand of some 1 million tonnes p.a. (Kuttelwascher 2011).

The life cycle costs of ballast are not governed by purchase or transport cost, but by the cost of maintenance work such as tamping and ballast cleaning. These operations are necessary due to the fact that railway ballast is subject to attrition, caused by the large forces acting within the ballast layer.

Tamping becomes necessary whenever track position reaches a critical value. The main cause of track settlement is rearrangement of the ballast particles within the ballast layer (i.e. rotation and displacement) and particle fragmentation. Settlement remains small as long as the angular ballast particles prevent substantial realignment between neighbouring particles. However, as soon as edges and corners break ("chipping") and particle angularity decreases (i.e. particles become more rounded), particle readjustments become easier. Thus, stability of the particle edges is a quality criterion for railway ballast.

Ballast cleaning is carried out when the percentage of fines (i.e. particles with a diameter smaller than 22.4 mm) reaches a critical value (typically 30 % to 40 %; also called fouling of ballast). The fines fill the voids in-between the larger particles and thus increase ballast bed stiffness. This in turn leads to larger wear of other track components such as sleepers and rails. Furthermore, fines decrease permeability of the ballast bed and thus impede rainwater drainage.

Fines are generated by mechanical loads acting within the ballast layer and derive from infiltration from the ballast surface, e.g. due to wagon spillage or airborne dirt. One category of fines results from particle fragmentation, chipping and abrasion (polishing). Thus, resistance to wear (abrasion) and fragmentation constitute quality criteria for railway ballast.

Both tamping and ballast cleaning operations entail temporary track closure and incur downtime costs (establishment of bus replacement services, train diversions, and delays etc.). Such downtime costs can often be equal to or even exceed track maintenance costs.

Introduction

As there are only limited possibilities for a substantial decrease of load level acting upon the ballast layer, the frequency of maintenance such as tamping and ballast cleaning is governed by the ballast quality. It is thus obvious that high quality ballast can reduce life cycle costs.

The TU Graz „Standard Track Kilometer" model (described in Selig (2009)) is used to quantify increased maintenance costs caused by inferior ballast. A „Standard Track Kilometer" is a track section which is characterized by parameters such as axle load per day, radius, rail type, sleeper type etc. It is assumed that, for a given load, all track section with the same „Standard Track Kilometer" will react in a similar manner (Bach, Enzi 2013).

Tab. 1 shows the chosen Standard Track Kilometer classes. The two classes cover some 35% of the ÖBB network.

Standard Track Kilometer	load class [GMT]	radius class [m]	rail type	sleeper type
1	45,000 – 70,000	> 600	60E1	concrete
2	30,000 - 45,000	> 600	60E1	concrete

Tab. 1: chosen Standard Track Kilometer classes

It is assumed that inferior ballast reduces service life of the track. In Tab. 2, a service life decrease of just 1 to 2 years is assumed and the respective difference in annuity is calculated.

Standard Track Kilometer	service life [a]	annuity [€/a]	difference in annuity [€/a]
1	30	30,415	-
	29	31,407	992
	28	32,470	2,055
2	36	22,248	-
	35	22,845	597
	34	24,208	1,960

Tab. 2: annuities for different service life assumptions

Tab. 2 depicts the relevance of ballast quality for the entire life cycle costs of the track. This illustrates an economical demand for appropriate test procedures and sufficiently dense test intervals.

Ballast quality standards are usually subdivided into those covering geometrical and those covering mechanical requirements. Most railway companies' quality assurance systems specify that these tests be performed biannually for every supplier.

Such quality control systems exhibit specific shortcomings with considerable economic impact: Test intervals for mechanical properties are fairly wide. Thus, an unsatisfactory test result may lead to a ban on the respective supplier for the time remaining to the next test date. For logistic reasons the material tested on-site and shown to be of inferior quality may still be used, although in such cases the supplier is not paid. Thus, the customer saves on the purchase price but faces increased expenses for maintenance. Clearly, the accuracy and reliability of the mechanical tests is of great importance to assess the mechanical behaviour.

Time series of test results have existed for many decades. While such values exhibit large variability, the reasons for the strong fluctuations remain unclear. Possible explanations revolve around factors such as: deviation of petrographic composition and particle geometry within one sample; blasting and crushing technique; processing techniques; storage and transport logistics; production tolerance; wear limits of measuring equipment; insufficient sample size; and suitability of result parameters.

1.2 Objectives and scope of research

This study aims at estimating the load regime of attrition tests and its connection to the load regime in track. The impact of the magnitude of a given axle load and train speed on the sleeper load and the correponding particle-to-particle point load within the ballast layer is estimated, using both experimental results from the respective literature as well as numerical analysis.

With respect to the specific load regime, reasons for variabilities in test results are sought, and their magnitudes are estimated.

Test evaluation incorporates three established test methods: the Los-Angeles test, the Swiss compression test, and the Deval Attrition test. In addition, two test methods for estimating tool wear in drilling and tunnelling equipment are examined: the LCPC Abroy test and the Cerchar test.

The impact of deviation in petrographic composition is investigated by defining subclasses of rock types, based on macroscopic characteristics (colour, texture, particle shape and angularity) and carrying out separate tests with pre-sorted samples for the Abroy test, the Cerchar test and the Los-Angeles test. Attrition test results are compared with the corresponding values for mineral hardness.

Machine vision is used to determine particle shape and angularity in order to estimate the impact of these parameters on test result variability for two test methods, i.e. for the Deval Attrition test and for the Los-Angeles test.

Samples for the tests originate from the Autria's eleven most important suppliers of railway ballast, and thus incorporate a wide range of rock types.

1.3 Thesis structure

In section 2, experimental findings together with the results of numerical analysis are used to quantify the magnitude of a sleeper load for a given axle load, bogie geometry and train speed. The sleeper load is transmitted to the subsoil via a small number of load chains, causing large point loads at particle–to-particle contact points. Based on experimental data, theoretical considerations, and on results from numerical particle models, the magnitude of these point loads is estimated, using the concept of 'coordination number'.

Section 3 defines attrition types and shape characteristics. Techniques for measuring these characteristics are introduced, with an emphasis on concepts based on machine-vision. To enable comparison of different test types, a quasi-objective characteristic number for the degree of fragmentation is needed. Two such concepts are introduced.

Section 4 describes the testing procedure of the five test types evaluated and aims at an estimation of the load regime of the Los-Angeles test and the Deval Attrition test, based on geometric and kinematic considerations.

Section 5 contains a petrographic and geometric characterization of the eleven rock types used in the course of this study. Results of the test series are presented. The analysis lays special emphasis on the magnitude of the result deviation and on those factors behind such deviations. For the Los-Angeles test, an alternative evaluation method is derived on the basis of a comparison with the degree of fragmentation.

Section 6 gives an overview of the load regime of the test methods evaluated, using the classification of three attrition types described in section 3 and the test results from section 4. Based on the magnitude of the test result deviation and the sample size, strategies for obtaining a satisfactory confidence level for the results are then discussed.

The extensive data generated with samples from all eleven rock types allows for a comparison of the overall quality of the evaluated ballast types. A method for result normalization is introduced and performance ranking is shown for different choices of a representative test mix. Test results are compared to the load magnitude in track at the particle level, based on the relationship developed in section 2.

2 Loads and contact forces in the ballast layer

Quality control testing procedures for railway ballast are intended to simulate the load level in track. Based on the test result for a given test and a given sample, inferences may thus be drawn with respect to the expected performance of the respective ballast type in track. Thus, for a comparison of laboratory test load level and load level in track, an estimation of both load levels is necessary.

In this chapter, an estimation of the particle-to-particle forces in the ballast layer as a function of the macroscopic load (i.e axle load) is undertaken. In section 2.1, a finite-element model is used to derive sleeper loads from axle loads. In section 2.2, the stress level within the ballast layer is estimated. Here, the ballast layer is still regarded as being a continuum. In section 2.3, based on experimental findings and on data from the relevant literature, the obtained stress magnitudes are converted into particle-to-particle forces.

2.1 Axle loads and sleeper loads

Load transfer from the axle to the subsoil is via the rail, the rail pad, the sleeper and the ballast layer. Load transfer in the longitudinal direction is governed by the rail profile and the elasticity of the rail pad, of the sleeper, of any under sleeper pad (USP) and of the ballast layer.

Several traditional methods exist for estimating such load transfers, most of them are based upon WINKLER's half-space concept (Winkler 1867) and on ZIMMERMANN's simplification of the system whereby rail pad, sleeper, ballast layer and subsoil are taken to be a continuous and elastic support, such that the result is then mainly governed by the bedding factor (Zimmermann 1941).

As a more up-to-date alternative, numerical methods also exist. They allow for a more realistic modelling of the elasto-plastic material behaviour of ballast and subsoil and the geometry of the sleeper and the ballast layer.

The author carried out a numerical parameter study (Bach 2012), using a rather simple two-dimensional finite-element model (Fig. 1) of a track section 16 metres in length, using software code ABAQUS. The model includes rail, rail pads, sleepers, ballast layer and subsoil.

Loads and contact forces in the ballast layer

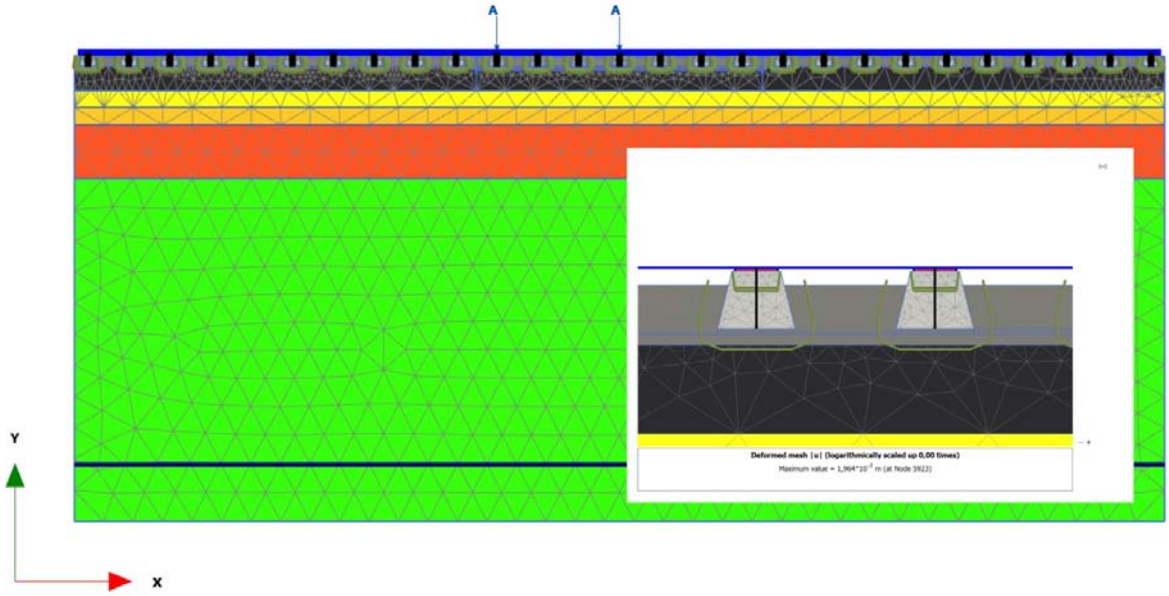

Fig. 1: numerical simulation – plot of model and detail with sleeper

All objects, except for the rail, are modelled using continuum elements. The rail is modelled as a beam element. The origin of co-ordinates is situated 8 metres from the left corner and at the level of the rail. Ballast and subsoil layers are retrained horizontally along the model perimeter, the rail is not. Relative displacements ("slip") between rail and rail pad, and between sleepers and the ballast layer, are modelled. Tab. 3 gives the material parameters applied, including the interface friction angle R_{inter}. All values are with reference to 1 m unit width.

object	constitutive law	spec. weight	Elasticity	ν	c	φ	R_{inter}
		γ [kN/m³]	E [MPa]	[-]	[kPa]	[°]	[-]
Rail60E1	Elastic	78.5	2.10E+08	0.150			
rail pad	Mohr-Coulomb	10	4.45E+04	0.010	1	78.69	0.67
Sleeper	Elastic	25	4.20E+07	0.200			
Ballast	Mohr-Coulomb	24	3.00E+05	0.200	50	45	0.67
Subsoil layer 1	Elastic	21	2.00E+05	0.275			
Subsoil layer 2	Elastic	21	1.75E+05	0.275			
Subsoil layer 3	Elastic	21	1.50E+05	0.275			
Subsoil layer 4	Elastic	21	1.00E+05	0.275			

Tab. 3: numerical simulation – material parameters

Typical axle loads and speed levels were simulated (Tab. 4; F: single axle; FR: freight train; CO: commuter train; IC: intercity train) and the impact of these parameters upon the load and displacement magnitude in the ballast layer and subsoil was investigated.

Loads and contact forces in the ballast layer

Model	Axle load	axle-center dist.	velocity	velocity factor
	F [kN]	a* [m]	v [km/h]	k_V [-]
F100	250	(single axle)	<<	1.000
FR00	250	1.8	<<	1.000
FR80	250	1.8	80	1.213
CO00	120	2.4	<<	1.000
CO80	120	2.4	80	1.213
IC00	180	2.4	<<	1.000
IC80	180	2.4	80	1.213
IC140	180	2.4	140	1.532

Tab. 4: numerical simulation – list of calculations (velocity factor (Führer 1978))

All simulations are static. The passing of an axle or a bogie was being simulated as a series of successive load steps. Axle loads were modelled as point loads (see the arrows marked "A" in Fig. 1), which were successively relocated by one sleeper spacing (i.e. by 60 cm), starting at the left edge of the model. In order to take account of the load increase due to dynamic phenomena, FÜHRER's velocity factor k_v (Führer 1978) was included. Other factors of influence, such as wheel and rail imperfections (see Gerstberger, Knothe & Wu (2003) for example), were neglected.

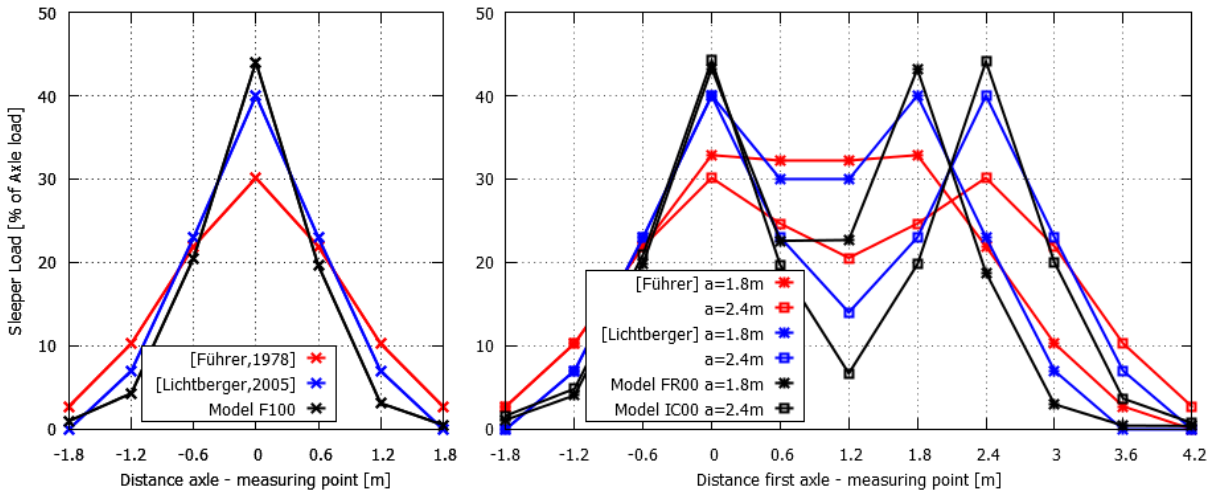

Fig. 2: axle load distribution for single axle (left) and bogie (right) - (Lichtberger 2010) and (Führer 1978) models vs. numerical calculations

Fig. 2 compares the results of two traditional models (Führer (1978) and Lichtberger (2010)) with the numerical study. To simulate a two axle bogie, the impacts of two single axles were superimposed. The numerical study is agrees well with LICHTBERGER's results, but less well with those of FÜHRER, which are based on a wider longitudinal load distribution. The respective sleeper load level is given in Fig. 3. Due to the superposition of the two axle loads of one bogie and the non-linear response of the ballast layer, the ratio of axle load and sleeper load is not constant (see Fig. 7; p. 17).

Loads and contact forces in the ballast layer

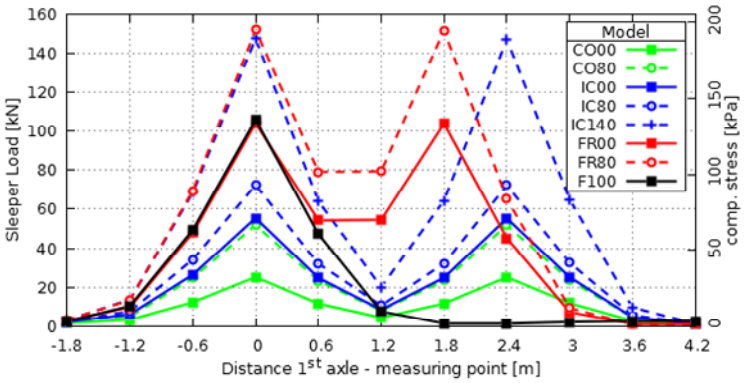

Fig. 3: numerical simulation – sleeper load – impact of axle load, axle-center distance and velocity

The values accord well with (Aikawa 2009)'s experimental findings. AIKAWA attached 75 force sensors to the sleeper's undersurface (see Fig. 4 left) and recorded the distribution of the sleeper load in the cource of an axle passage.

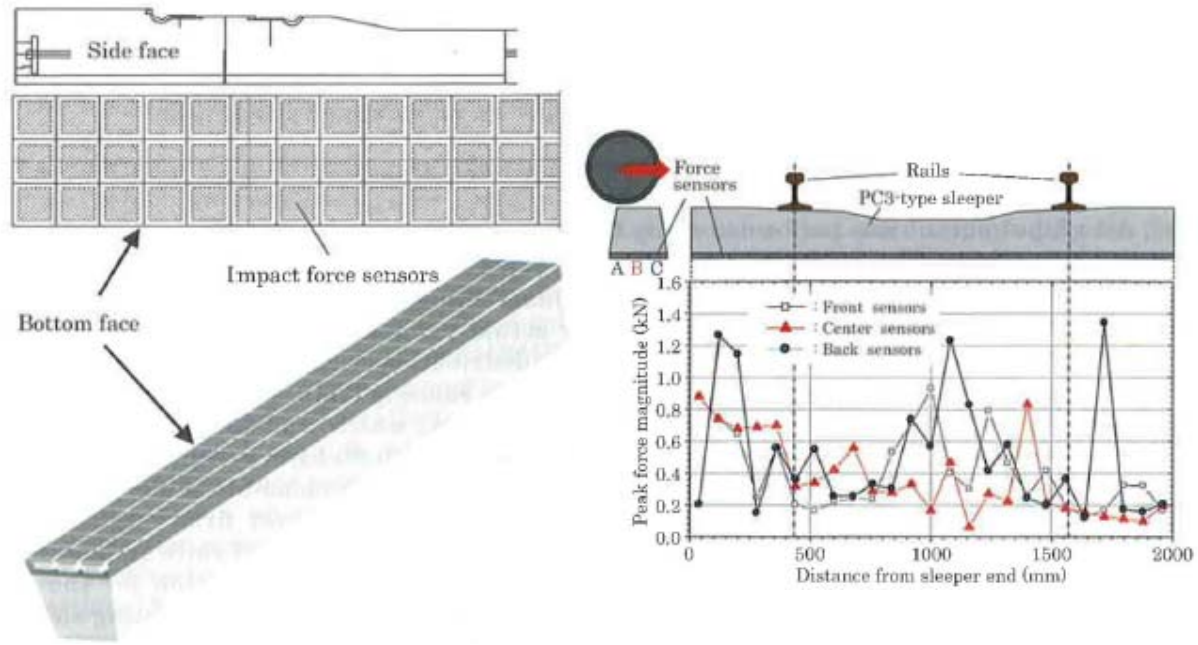

Fig. 4: layout of force sensors (left) and peak magnitude distribution at the time of axle passage (from Aikawa (2009))

Ballast layer thickness was 30 cm, the train speed was 90 km/h and axle load was 7.5 tons. The sum of all force sensor readings added up to 29 kN (i.e. 40% of the axle load, or 60 kPa for the mean compressive stress) and the maximum single value was about 1.4 kN (see Fig. 4 right), which is equal to 219 kPa. Fig. 4 also shows that the load distribution from the sleeper into the ballast layer is highly inhomogeneous. Only a few dozen ballast particles actually form the bedding and transmit the bulk of the sleeper load.

Loads and contact forces in the ballast layer

Knowledge of the velocity and of the axle-center distance allow one to calculate the frequency of the load impact induced by the passage of a bogie (Tab. 5).

			global		max to max	
axle load	axis-center dist.	velocity	frequency	ΔF	frequency	ΔF
[to]	[m]	[km/h]	[Hz]	[kN]	[Hz]	[kN]
12	2,4	80	3,70	51,9	9,26	43,9
18	2,4	80	3,70	55,4	9,26	47,0
18	2,4	140	6,48	72,4	16,20	61,8
25	1,8	80	4,12	152,2	12,35	72,7

Tab. 5: numerical simulation – passage of a bogie – frequencies and amplitudes

2.2 Stress level in the ballast layer

Fig. 5 depicts the compressive stress (top) and shear stress (bottom) in the ballast layer over the course of an axle/bogie passage for three measuring points. The points P1, P2 and P3 are located 1 cm, 10 cm and 35 cm below the sleeper. The compressive stress decreases with increasing distance to the sleeper. Near the bottom line of the ballast layer (P3) the load level is half of that found near the sleeper (P1). The area of influence is about three sleeper distances (i.e. 1.8 m) for all measuring points.

The shear stress values reach approx. 20% of the compressive stress values. They increase with increasing depth. Here, the readings for point P1 are about 50% of those of point P3. Maximum values are reached one sleeper distance before the passage of the 1st axle and one sleeper distance after the passage of the 2nd axle. For a single axle, one zero-crossing occurs at the moment when the axle passes the measuring section, whilst for a bogie, three such zero-crossings occur.

The results comply well with the respective values from an extensive study (Riessberger et al. 2007) aimed at the estimation of the impact of under ballast mats on load distribution and displacements in the ballast layer. The study used a three-dimensional finite-element model and applied material parameters similar to the present study (see Tab. 3). For a freight train (axle load 22.5 tonnes, axle-center distance 1.80 m) a maximum compressive stress of 99 kPa resulted at the level of the under ballast mat. For a passenger train (axle load 12 tonnes, axle-center distance 2.50 m), the respective value was 79 kPa. Maximum shear stresses were 9 and 5.5 kPa, respectively.

Loads and contact forces in the ballast layer

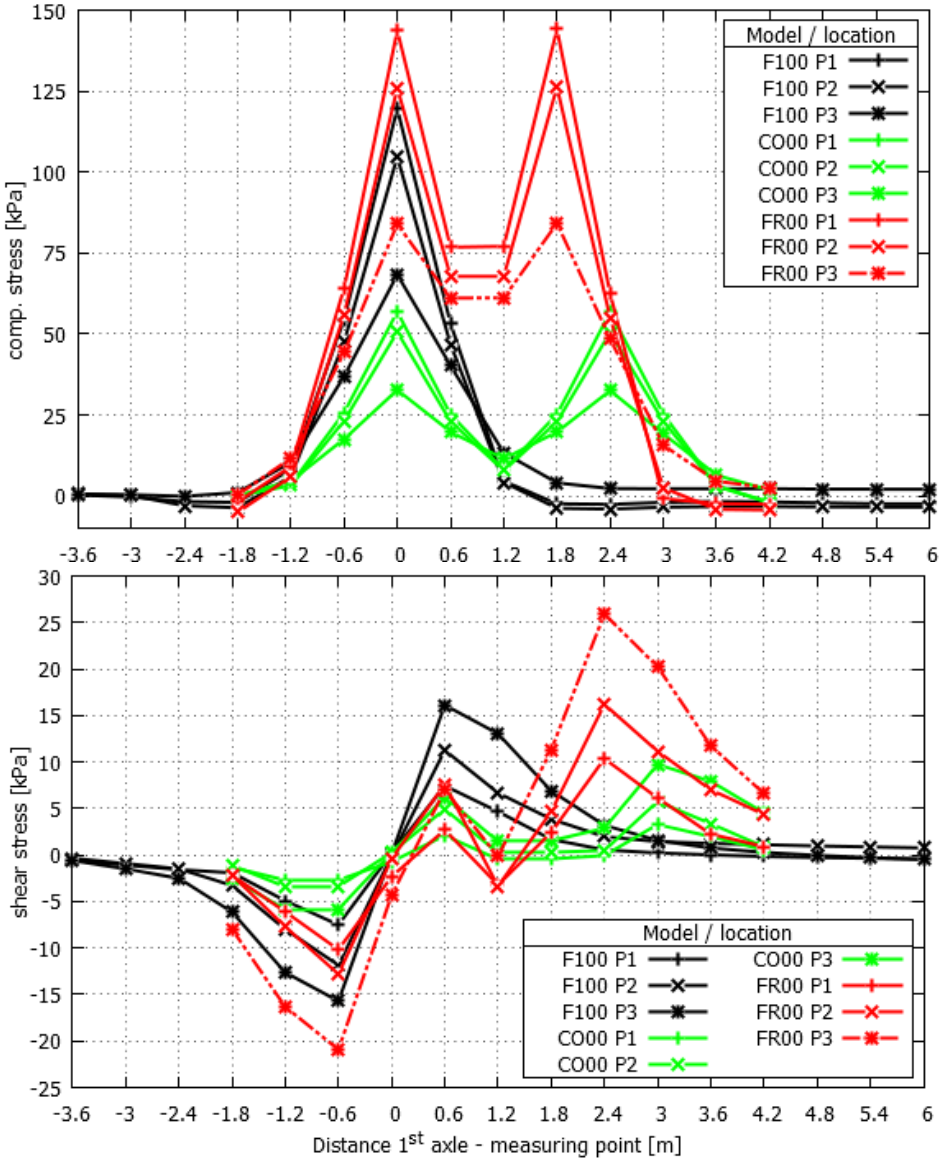

Fig. 5: numerical simulation – shear and compressive loads within ballast layer

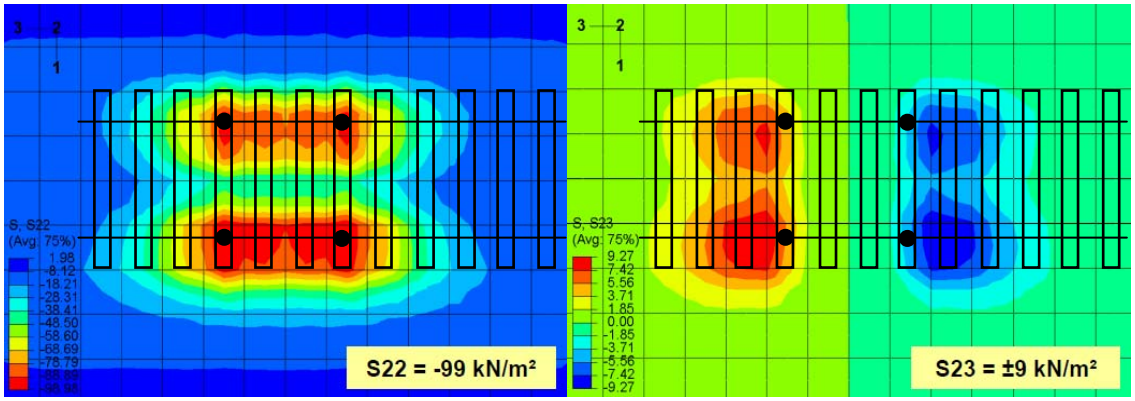

Fig. 6: compressive stresses (left) and shear stresses (right) at the level of the under-ballast mat (from (Riessberger et al. 2007)) for a freight train – direction "3" is longitudinal direction – grid dimension ca. 60 cm

Loads and contact forces in the ballast layer

The static finite-element model does not allow for an estimation of the displacement rates (velocities) and accelerations of the ballast particles. AIKAWA's above mentioned experimental work also included the placement of special sensoring stones in the ballast layer that measure the three-dimension motion of the ballast. The stones were located 15 cm below sleeper level, at the level of a rail weld, and measured accelerations during the passage of a two-axle bogie. The train speed was 78 km/h and axle load was 7.5 tonnes. Translational acceleration was up to 20 m/s². The time distance between the two peak values in (Fig. 8) is equivalent to the axle-center distance of the two-axle bogie. Rotational accelerations reached 12 m/s² peak values.

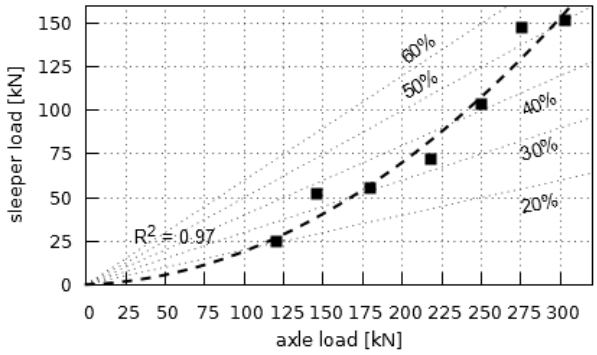

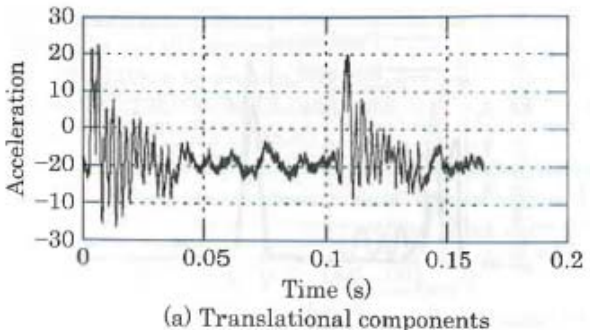

Fig. 7 (left): numerical simulation – axle load vs. sleeper load for models CO00, CO80, IC00, IC80, IC140, FR00 and FR80

Fig. 8 (right): translational acceleration of a ballast particle in the course of a bogie passage in [m/s²] (from Aikawa (2009))

2.3 Conversion into particle-to-particle loads

The granular structure, or grain skeleton, of the ballast layer transmits the sleeper load into the subsoil. The size of the ballast particles (typically 22 to 63 mm diameter) is relatively large compared to the ballast layer thickness below the sleeper (usually 30 to 35 cm). Thus, only some 8 to 15 particles make up the ballast layer thickness. The sleeper load is transferred via a few preferred load-chains that transmit the load from one ballast particle to another. This leads to high point-loads which may in turn cause particle fragmentation or chipping off of edges and corners and thus rounding. This can be verified by means of numerical particle models (see Lu, McDowell (2009) and Lobo-Guerrero, Vallejo (2006), for example).

The knowledge of the number of such contact points per volume unit or per particle and of the magnitudes of the point loads being transmitted along these points is essential for an estimation of a particle-based load level. Both values are governed by the particle size distribution and the particle geometry.

Loads and contact forces in the ballast layer

The number of contact points per particle is called the coordination number and can be estimated by means of numerical methods (discrete element method, for example) or by experiments.

FISCHER investigated the load transfer from the sleeper to the uppermost ballast layer using carbon-paper in order to estimate the contact area (Fischer 1983). A sample (gradation 22.4/63 mm) was placed in a 50 x 50 cm shear box (height 10 cm) and loaded with 200 kPa and a beech wood plate (d = 10 cm) or, alternatively, a concrete plate, was placed between sample and abutment. For the wooden plate, the contact area made up 24% of the plate area, whilst the respective value was 8% only for the concrete plate (Tab. 6, top).

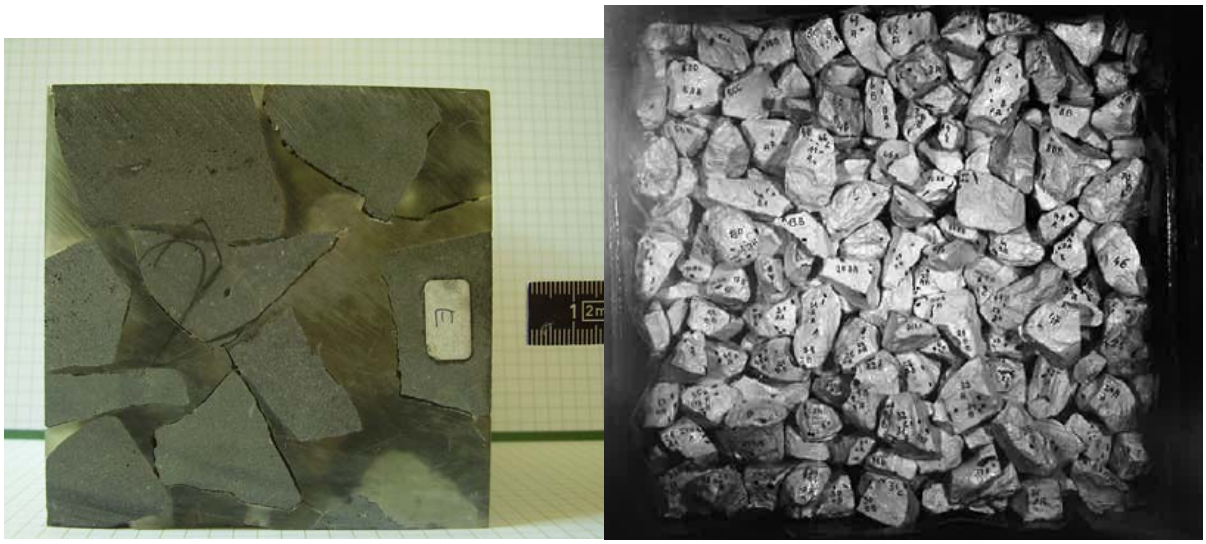

Fig. 9: ballast cube, fixed with resin (left) – contact points (dyed ballast particles in shear box A = 50 x 50 cm) (right; from Fischer (1983))

All ballast particles were dyed prior to the test, using a thin film of white lacquer. In the course of the test, lacquer chipped off at those areas at which a high load level occurred. Fischer counted these contact points and measured their area (Fig. 9, right). The coordination number was found to be 2.20 for the layer nearest to the "sleeper" plate and 4.06 for the layer nearest to the load application (Tab. 6, bottom). The average load level decreased with increasing distance from the "sleeper" plate and ranged between 0.35 and 0.14 kN per contact point for particle-to-particle contact, and was 0.68 kN for particle-to-sleeper contact. The contact point area turned out to be quite uniform with about 0.1 cm², regardless of the coordination number and the local load level.

It should be noted that the shear box does not allow for lateral expansion and that the load was applied from below and not via the "sleeper" plate.

Loads and contact forces in the ballast layer

method: carbon-paper	contact points (referred to A = 2,500 cm²; F = 50 kN)					...per contact point	
layer	particles	contact points	Σ area	Σ area	Area / CP	stress	load
	[-]	[-]	[cm²]	[%]	[cm²]	[kN/cm²]	[kN]
wooden sleeper	74	49	23.61	0.944	0.482	2.12	1.02
concrete sleeper	45	35	8.15	0.326	0.233	6.13	1.43
method: laquer	contact points (referred to A = 2,500 cm²; F = 50 kN)					...per contact point	
	particles	contact points	Σ area	Σ area	Area / CP	stress	load
concrete sleeper	45	74	8.54	0.342	0.115	5.85	0.68
1st ballast layer	64	141	12.36	0.494	0.088	4.05	0.35
2nd ballast layer	86	152	13.48	0.539	0.089	3.71	0.33
3rd ballast layer	89	361	39.32	1.573	0.109	1.27	0.14

Tab. 6: Fischer's study (Fischer 1983) – contact points

Another experiment aimed at estimating the void ratio of the ballast layer, and also yielded information on the coordination number. A ballast sample (gradation 22.4/63 mm) was put into a quadratic box (side length 19.45 cm) without compaction, and was subsequently filled with resin. The porosity n was also determined (n = 0.39, void ratio e = 0.64). This sealed block was then cut into eight equally dimensioned cubes (Fig. 9, left) and all contact points were counted and the number of contact points per unit volume and the coordination number was calculated based on the thickness of the saw blade (4.5 mm). (Tab. 7, top row).

A multitude of studies investigate the impact of the particle size distribution of a granular material on the respective coordination number. Most authors agree that there is no dependency between particle size distribution and mean coordination number, and that its deviation increases with increasing variation of the particle size within a sample, i.e. with an increasing coefficient of uniformity. This means that the number of contact points of a sample can be estimated if particle size distribution, unit weight of the particles, particle geometry and void ratio are known. For FISCHER's resin study, assuming one third of cuboidal, one third of brick-shaped and one third of tetrahedral particles, this leads to 11,156 particles per m³ and 29,000 to 53,000 contact points per m³ (Tab. 7, top row). The lacquer method also leads to 29,000 contact points per m³.

SCHARINGER compiled many theoretical and experimental studies that investigated the impact of relative density on the coordination number (Scharinger 2007). For a void ratio e of 0.64 (as in FISCHER's resin experiment) coordination numbers of 7.2 to 8.6 result (see Fig. 10, equ. 49 to 53 and Tab. 7).

Loads and contact forces in the ballast layer

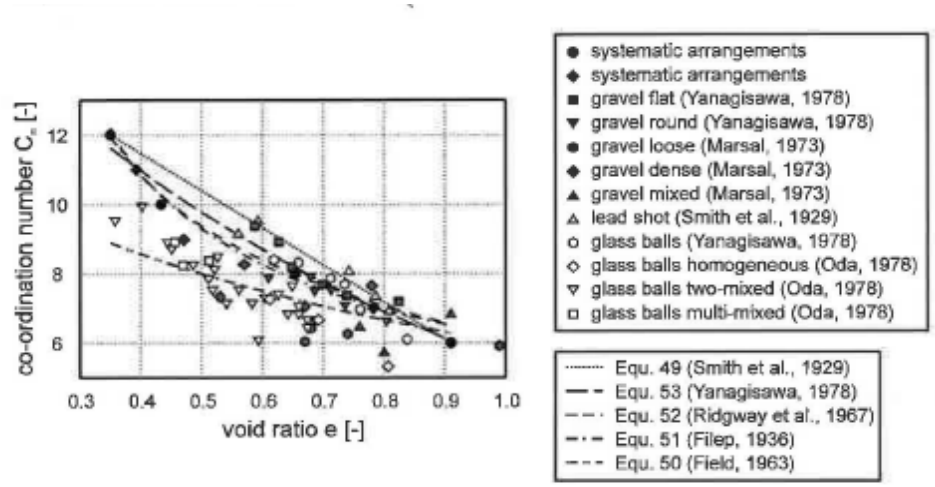

Fig. 10: coordination number – impact of void ratio - literature (from Scharinger (2007))

LU & MCDOWELL used the discrete element method code PFC3D for a back-analyses of box tests. The numerical model included the entire test arrangement (Fig. 11) at real scale. With box dimensions of 700 x 300 x 450 mm and a sleeper section measuring 250 x 150 x 150 mm, 1,936 particles were found, which is equal to a density of 1.41 to/m³ or 21,950 particles per m³ (porosity e = 0.458). The numerical model calculated 10,337 contact points (for a coordination number of 5.34). A mean contact force of 0.336 kN, and a maximum value of 4.05 kN were calculated, based on a sleeper load of 40 kN. Sleeper load is thus about 100 times greater than the mean contact force, and about 10 times greater than maximum contact force (which is presumably immediately below the sleeper (Lu, McDowell 2007).

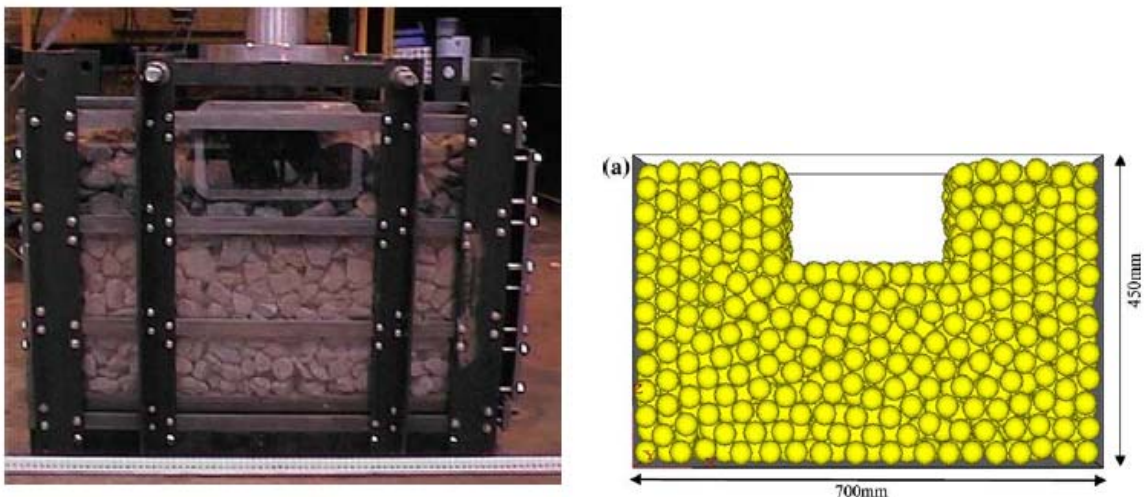

Fig. 11: particle model for back-analysis of box test (from Lu, McDowell (2007))

A similar model using angular particles led to similar maximum and mean contact forces, although the coordination number was found to be much higher. Thus, lots of contact points seem to transmit no or only very small loads.

Loads and contact forces in the ballast layer

The compilation of all results discussed in this section (in Tab. 7) makes clear that a large amount of uncertainty exists concerning the estimation of the coordination number and the number of contacts per unit volume. Clearly, one has to distinguish between the coordination number (which seems to increase with increasing angularity) and the number of particle-to-particle contact points that actually transmit substantial loads. As a result, estimation of particle-to-particle forces is difficult, even when the applied macroscopic stress (the sleeper load) is known.

source	porosity	spec weight	part./m³	contacts / m³	coord. number	ratio	ratio
	[-]	[kN/m³]				$F / F_{CP,Sleeper}$	$F / F_{CP,Ballast}$
Fischer (resin method)	0.39		11,156	29,333 - 52,889	2.60 - 4.70		
Fischer (lacquer method)			11,156	29,120	2.60	50	142 - 357
Smith et. al.	0.39		11,156	96,053	8.61		
Yanagisawa	0.39		11,156	89,917	8.06		
Ridgway	0.39		11,156	88,244	7.91		
Filep	0.39		11,156	86,459	7.75		
Field	0.39		11,156	80,323	7.20		
Lu & McDowell		1.41	21,950	117,213	5.34	10 (?)	100

Tab. 7: coordination numbers derived from Fischer and other studies (Fischer (1983), Smith, Foote & Busang (1929), Yanagisawa (1978), Ridgeway & Tarbuck (1967), Filep (1936), Fiels (1963), Lu & McDowell (2007))

Please note that none of the results compiled in Tab. 7 takes fragmentation into account. Fragmentation will increase the number of loads chains per unit volume and will thus decrease maximum and mean particle-to-particle force level.

For a given particle size and shape, an increase in the coordination number results in a smaller fracture probability, as more contacts almost inevitably decrease the induced tensile stress in the particle (McDowell, Bolton & Robertson 1996).

3 Ballast attrition

3.1 Attrition typology

Attrition of railway ballast can be subdivided into fragmentation of grains, rounding (or "chipping"), and abrasion (or "polishing").

Fragmentation (Fig. 12, A), means that due to a high point load of a large impact momentum acting on a particle, the particle breaks into a few medium-sized fragments. Depending on the rock type, a certain degree of fines may also be generated.

Fragmentation occurs in track chiefly below the sleeper. In the course of an axle passage, the sleeper is first lifted up from its bedding due to the deflection curve of the rail and is then forced down whilst the wheel contact point approaches the particular sleeper. The fast downward movement and the large axle load exert a large impact momentum and induces high point loads.

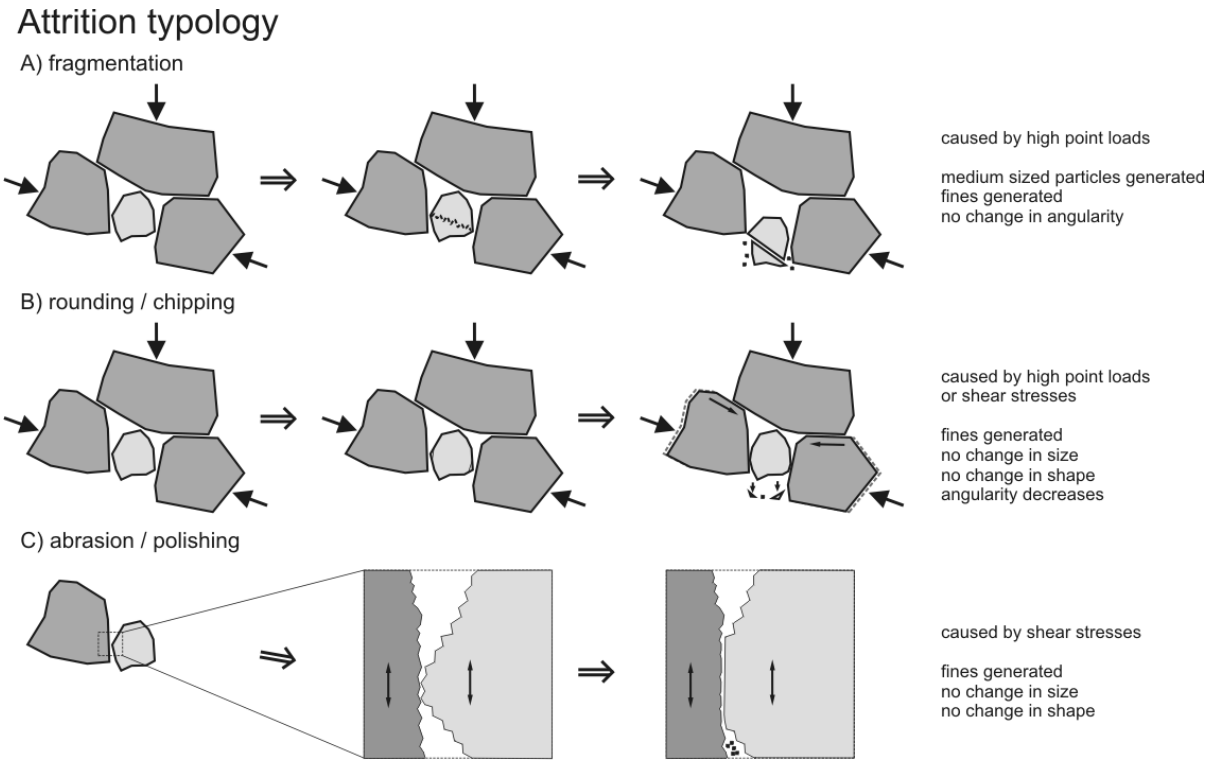

Fig. 12: attrition typology

Rounding, or "chipping", refers to the breaking off of exposed edges and corners due to high point loads (Fig. 12, B), or, alternatively, due to high shear loads. Thus, the angularity of the original particle decreases, while its size and shape (i.e. the relation of its main axes) will stay almost the same.

Ballast attrition

Rounding occurs in track once more below the sleeper – similar to fragmentation – and also below the edges of the sleepers. This is where the largest shear stresses are induced (see also Fig. 6, p. 16).

Abrasion, or "polishing" (Fig. 12, C), refers to a decrease in surface roughness (but not necessarily in angularity), caused by repeated relative movements of two neighbouring particles inducing shear stresses. Shear stresses are induced where large relative displacements take place. This is likely to be the case in track below the edges of the sleepers.

Obviously, there is a relatively smooth transition between the phenomena "rounding" and "polishing". For example, the change in the shape of the particle on the right in Fig. 12, C) could also be interpreted as rounding. In the present study, the term 'abrasion' is used to refer to a mass loss of a particle due to shear forces, with no decrease in angularity.

Strictly speaking, particle rearrangement cannot be ranked among the attrition types, as all particles stay intact, but it undeniably contributes to track settlement and causes waves and troughs in the track bed.

Heineke (2001), Katzenbach & Heineke (2003), Augustin (2002), Augustin et al. (2003), Holtzendorff (2003) and Baeßler & Ruecker (2003) investigated the impact of sleeper load characteristics on the degree of particle rearrangement, using both scale models and numerical simulations. They proved that the establishment of track bed waves and troughs in the course of the operation time is decisively influenced by the stress minimum. Small stress minimums, or, worse, a stress minimum of zero, enable rearrangement of ballast particles.

This is in fact the case when the sleeper is lifted up immediately before the axle passage. Additionally, an insufficient lateral confinement may cause small lateral minimum stresses and create a dilatant, unstable degradation zone (Indraratna, Lackenby & Christie 2005).

The contribution of the three attrition types, described above, to track quality, varies over time as cumulated traffic increases. The service life of the track can roughly be divided into two phases:

- During the first phase (< ca. 100,000 GMT) extensive fragmentation and particle rearrangement causes high settlement rates or a rapid decrease in track quality (see Fig. 13). Initial settlement magnitudes typically reach 10mm to 15 mm. The contribution of abrasion and chipping to such settlement is comparatively low. As

the coordination number and the number of load chains increase in the course of the fragmentation and particle rearrangement process, maximum and mean particle-to-particle loads are reduced until an almost stable configuration is established.

- Track quality still decreases in phase II (> 100,000 GMT), but at a much lower rate. The contribution of particle rearrangement and fragmentation is small. Abrasion and chipping cause the main part of track settlement during this phase.

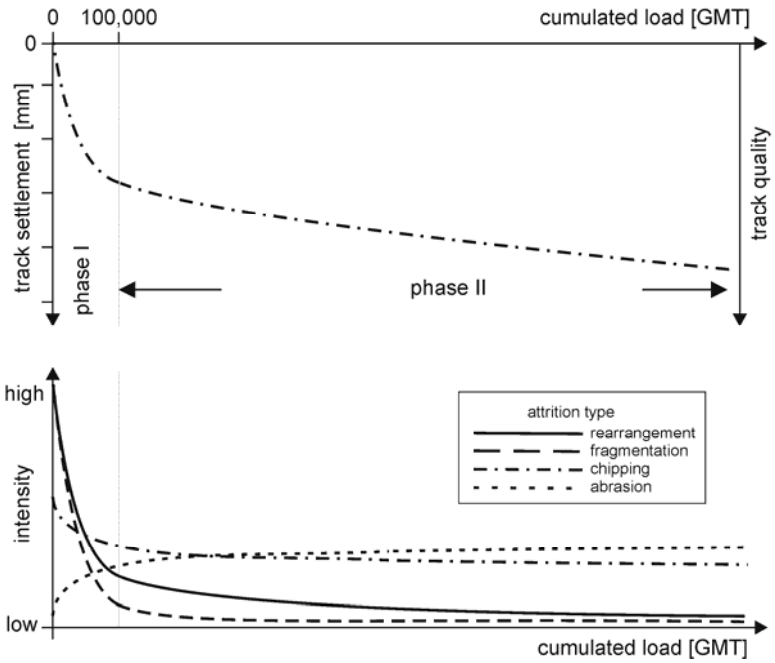

Fig. 13: track quality and contribution of attrition types (schematic)

3.2 Particle geometry - methods of description and measurement

The main properties of particle geometry in coarse granular media are the particle shape and its angularity. Particle shape influences mechanical properties, chiefly those such as shear strength, compressive strength and tensile strength, and thus has an impact on the degree of fragmentation. One would expect that a flat or an elongated particle is more subject to fragmentation than a compact one, as macroscopic loads induce larger stresses in the particle (see Röthlisberger et al. (2005) for example). Angularity has an impact on the degree of rounding and abrasion. For a given load regime, angular particles will produce more fines due to rounding and polishing than already rounded ones.

3.2.1 Shape

One of the earliest classification schemes for particle shape relates to ZINGG's flatness and elongation ratios (Zingg 1935). The length L, breadth I and thickness S of a particle

are all measured. All three dimensions are taken to be perpendicular to each other and the product of L, I and S (i.e. the volume of the enclosing cuboid) is assumed to be at a minimum (see also Fig. 14 left). The elongation ratio ER is then defined as

$$ER = \frac{I}{L} \tag{1}$$

For an elongation ratio ER < 0.67, ZINGG called the particle "elongated". The flatness ratio is similarly defined:

$$FR = \frac{S}{I} \tag{2}$$

Particles with a flatness ratio FR < 0.67 are called "flat". If both ER and FR surpass 0.67, the particle is called "cuboidal".

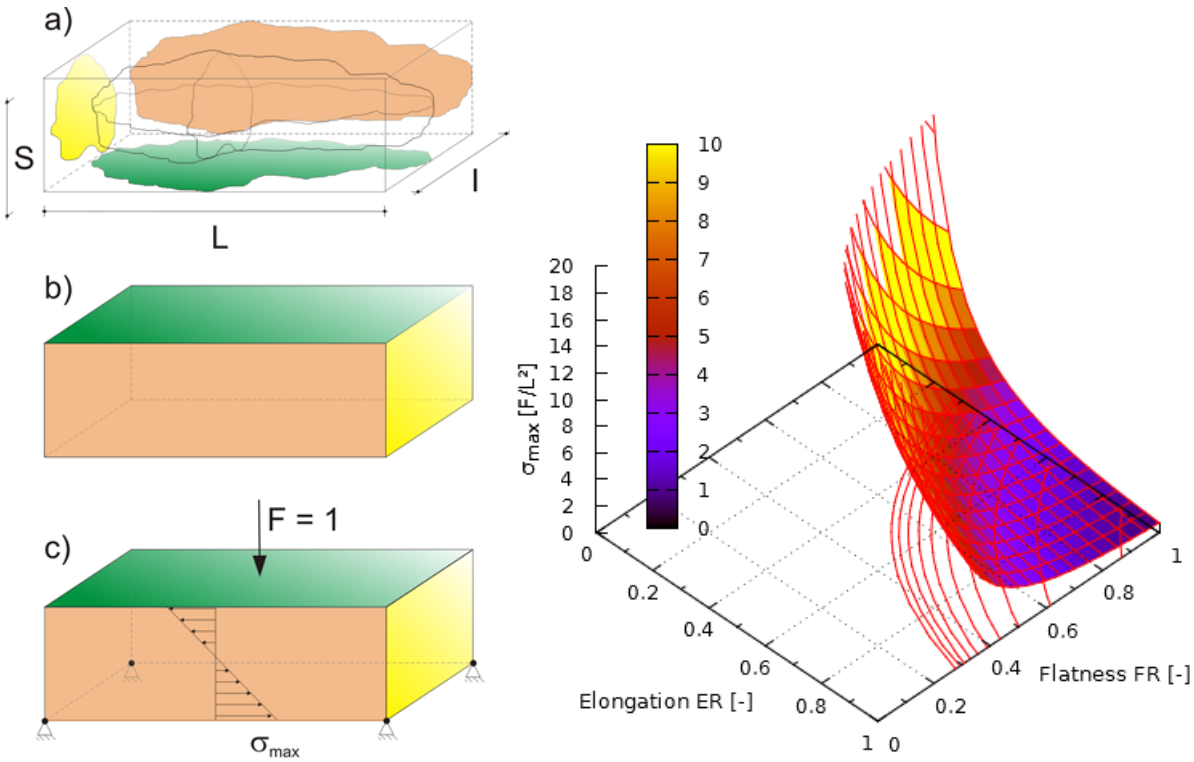

Fig. 14: protocol for measuring L, I and S (left) - σ_{max} – impact of particle geometry (σ_{max} =! 1 for ER = FR = 1) (right)

Fig. 14 illustrates the connection between shape and maximum tensile stress in a Bernoulli beam with dimensions L, I and S. We have

$$\sigma_{max} = \frac{M}{W}, \quad \text{where} \quad M = \frac{FL}{4} \quad \text{and} \quad W = \frac{IS^2}{6} \tag{3}$$

M denotes the bending moment, W is the section modulus of the beam and F is a single load of magnitude 1 acting at $^{L}/_{2}$. Even a small decrease in elongation and / or flatness leads to significantly higher tensile stresses and will thus induce breakage.

Several alternative methods for describing shape exist, most of them are based on L, I and S (see Blott & Pye (2008) for an extensive compilation). However, only a few characterization methods manage to put all three shape dimensions into one characteristic factor. ASCHENBRENNER's "working sphericity" ψ' is based on a scaled tetrakaidekahedron (Fig. 15, left), which ASCHENBRENNER chose since "[…] it is easily handled mathematically and smooth enough for approximating rounded forms. It is thought to be superior to the triaxial ellipsoid [...] because sedimentary particles, especially sand grains, as a rule do not have perfectly smooth surfaces." (Aschenbrenner (1956), p.16). The working sphericity is defined as

$$\psi' = \frac{12.8\sqrt[3]{FR^2 ER}}{1 + FR(1+ER) + 6\sqrt{1+FR^2(1+ER^2)}}, \qquad \text{with} \qquad \psi' \in [0,0.96] \tag{4}$$

For a sphericity close to 1.0, the tetrakaidekahedron approximates a cuboidal, angular ballast particle. The connection between working sphericity ψ' and induced tensile stress σ_{max} is illustrated in Fig. 15 (right) for typical ballast particle samples (see section 5.1 for a description of the rock types).

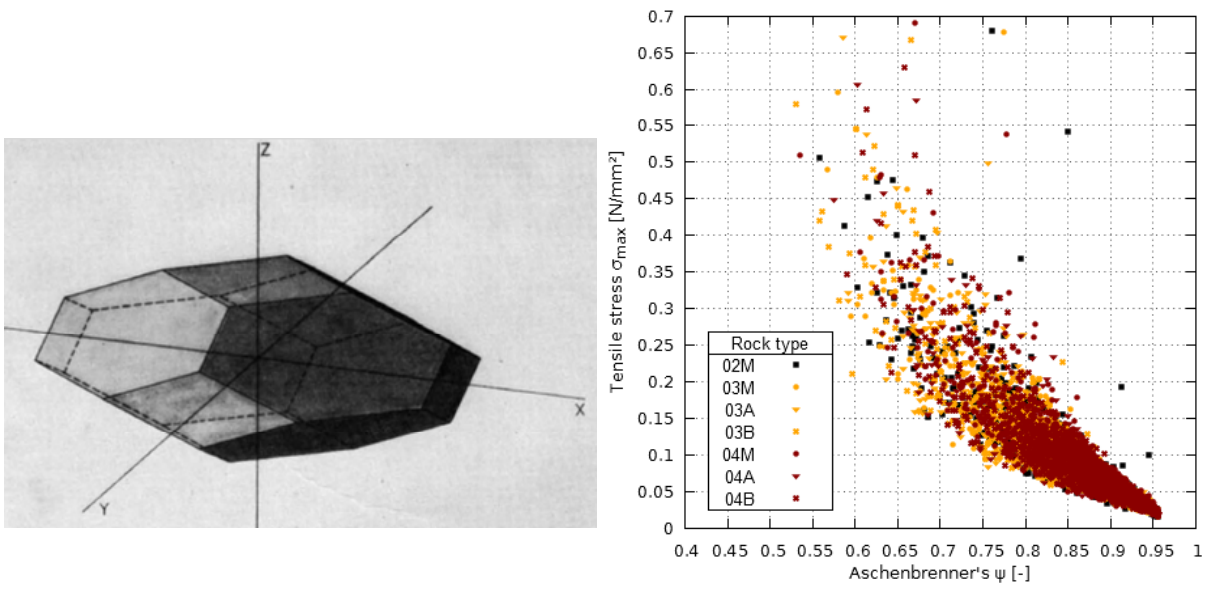

Fig. 15: tetrakaidekahedron (left) - Aschenbrenner's form factor ψ' and corresponding σ_{max} for typical ballast particle samples (crushed rock with gradation 31.5/50 mm; see section 5.1 for details) (right)

3.2.2 Angularity

The angularity of a particle depends on the sharpness of its edges and corners relative to its overall size and is independent of its shape. Wadell (1935) introduced the concept of the ratio of the average radii of the corners to the radius of the maximum inscribed circle. POWERS' scale (Powers 1953) is based on this concept and constitutes the most widely used method today. POWERS defined six angularity classes in sediments (see Fig. 16), and included classes for rounded and well-rounded particles. In Fig. 16, r_2 defines the radii of the corners and r_1 the radius of the maximum inscribed circle.

Classification is done either manually, using models for comparison (see Fig. 16 bottom), which is both arduous and error-prone, especially for angular particles (Lee et al. 2005), or is computer-aided, using image recognition techniques.

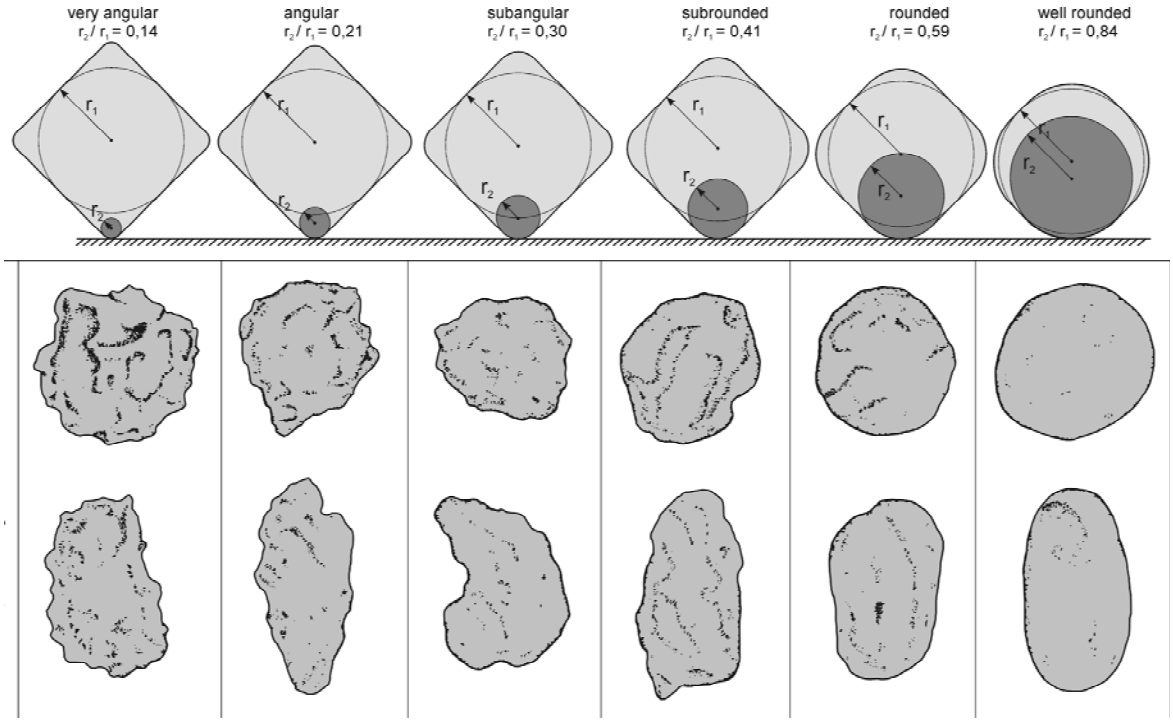

Fig. 16: roundness scale and classes according to (Powers 1953) (top) –typical particles with high (middle) and low sphericity (bottom)

The interval of the ratio r_2/r_1 from 1.00 to 0.12 has been divided into six intervals in such a way that the ratio of the upper limit to the lower limit of any interval is 0.7. The characteristic point of each interval is the geometry mean of the class limits. The values given have been rounded off to the nearest hundredth.

As Fig. 17 shows, the specific loss of mass of a particle subject to rounding differs depending on particle shape. Cuboidal particles experience a larger mass loss than flat and elongated ones. Furthermore, POWERS's class intervals do not evidence a linear

relationship with mass loss. Measuring the loss of mass directly (i.e. in terms of volume) thus appears to be a more promising approach.

Based on POWERS's concept, LEE developed an improved algorithm (Lee et al. (2005); Lee, Smith & Smith (2007)). In order to overcome the impact of shape, the structural element used here is not a sphere, but an ellipsoid exhibiting the same aspect ratios L/I and I/S as in the particle examined, but scaled down to one third of its size. The ellipsoid's principal axes remain aligned with those of the particle. The volume of those regions that are inaccessible by the ellipsoid (i.e. regions close to sharp edges and corners) is measured and and expressed as a proportion of the particle volume. Lee calls this proportion "volume loss".

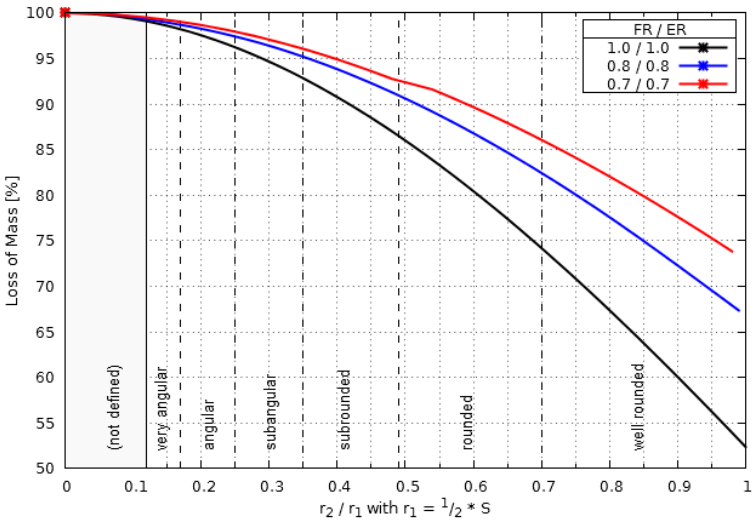

Fig. 17: connection between r_2/r_1 and mass loss of a brick-shaped object due to rounding for three shape characteristics (POWERS's roundness classes added)

It should be noted that this approach cannot access concavities, as only convex features lead to an increase in the measured volume loss.

3.2.3 Measuring shape and angularity – machine vision

In order to measure both shape and angularity of large ballast samples with high precision and efficiency, an automated technique is necessary. Maerz & Zhou (1999) describe a device, consisting of a hopper, i.e. a feeding mechanism placing the grains onto a belt, an "orientor" aligning them, and two orthogonal cameras that allow for a quasi-3D-measurement of the particle shape. Software determines the sieve size of each particle and its respective elongation and flatness ratios, using digital image analysis. Angularity, however, is not evaluated. The speed of the process is described as 'developable'.

Ballast attrition

TOLPPANEN developed a 3D-laser scanner with a resolution of 10µm and an accuracy of 20 µm, scanning one particle at a time. For a full 3D measurement, the particle has to be turned around manually and a second measuring session follows. Processing capacity is thus quite low. However, the high accuracy does allow for estimation of the surface roughness. Particle size was calculated for a few particles, whilst particle shape and angularity was not (Tolppanen (2001), Lanaro & Tolppanen (2001) and Tolppanen, Stephansson & Stenlid (2002))

The device developed by DESCANTES uses the shadowgraph principle to capture images of aggregate particles. This consists of extracting the silhouette of an object that is located between a light source and a camera, and the contrast between background and object is then sufficient to produce a defined resulting silhouette (i.e. a 2D image). Resolution is 0.2 mm and minimum particle size 1 mm. Capacity is about 120 kg per hour for typical railway ballast gradation (Descantes, Fosse & Milcent (2006) and Pham, Descantes & Larrard (2010)).

The device used for data collection in the present study, Petroscope 4D® (Fig. 18), was developed in the EUREKA projects No. 2569 (EUREKA 2001) and No. 3665 (EUREKA 2005) for the purpose of rock aggregate analysis. The device uses machine vision – a combination of digital photo imagery and software analysis – details on the project can be found in (Hofer, Pilz & Helgason 2006).

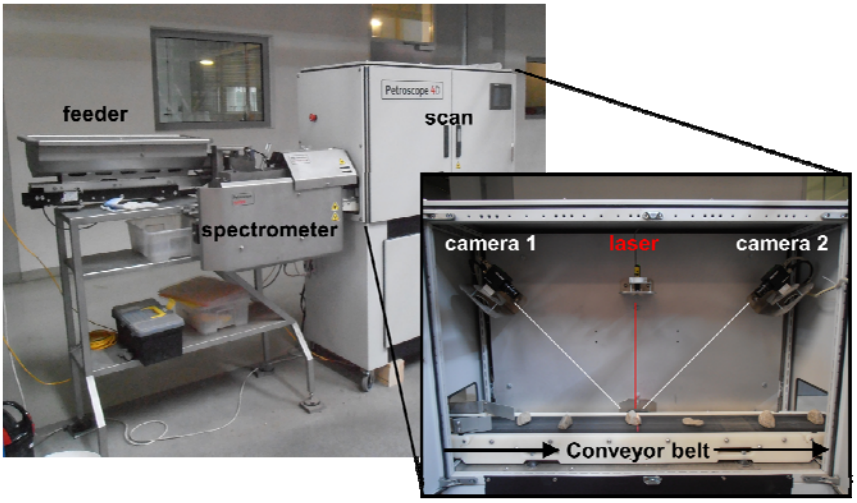

Fig. 18: Petroscope© - overview and detail of scan unit

For each particle of a sample the Petroscope 4D® determines the following geometric properties:

- the size of the three particle axes (L, I, S)
- elongation ratio and flatness ratio according to Zingg (1935) (see also section 3.2.1)

- sieve size
- angularity, using LEE's approach (see section 3.2.2). Henceforth, Lee's 'volume loss' (in [Volume-%]) is called "proportion of angles" (PropA) [%].
- volume and sphericity

Resolution and accuracy are both about 0.15 mm, capacity is 300 to 600 particles per hour, and minimum particle size is 4 mm. Due to the camera position above the sample, only the upper hemisphere is measured correctly. The particle volume is thus overestimated (Fig. 19).

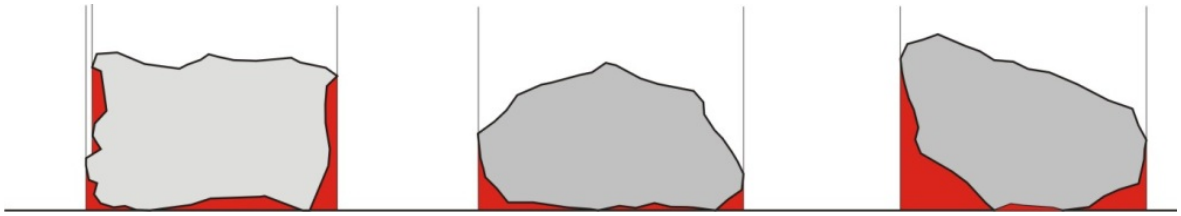

Fig. 19: Petroscope© - overestimation of particle volume – impact of particle shape and position

The estimation of angularity and shape is not affected by these limitations, as L, I and S are still measured correctly, according to the procedure described in section 3.2.1, and angularity is not dependant of the particle face. Sieve size is calculated using a virtual (computer-generated) particle with the same aspect ratios and the same angularity as the measured particle. An extensive evaluation report (Daniel, Lowe 2011) asserts that Petroscope performs within "single operator precision" limits as defined in ASTM C 136-06, and as compared with manual sieving.

Petroscope also measures reflectance spectra particle-wise, mainly in the visible light range.

3.3 Fragmentation – methods of description and measurement

Fragmentation results in a change in particle size distribution. The breakage of a large particle may produce only a few medium-sized particles (Fig. 20 left), or many fines (Fig. 20 right).

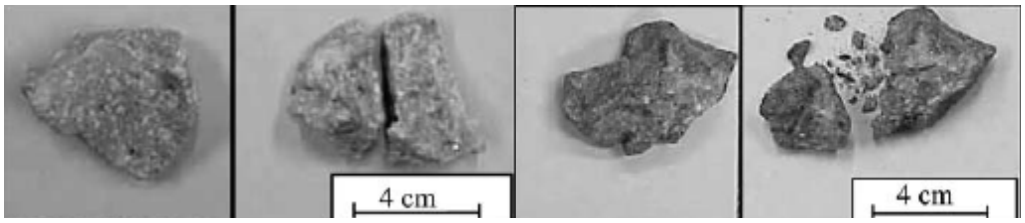

Fig. 20: breakage characteristics of quartzite (left) and biotite-gneiss (right) in point load test (from Lobo-Guerrero & Vallejo (2006))

Ballast attrition

Rittinger (1867) stated that the energy required for the change in particle size distribution is proportional to the newly generated surface area of the particles involved. Based on this, Kick (1883) postulated that equivalent size reductions require equal energy:

$$E = K_1 \cdot \ln\left(\frac{x_f}{x_p}\right) = K_1\left(\ln\left(x_f\right) - \ln\left(x_p\right)\right) \tag{5}$$

where K_1 is a material constant and x_f and x_p are the particle sizes prior to, and after fragmentation, respectively. BOND proposed a comminution law ("third law of grinding") that states that the energy required for fragmentation is proportional to the total length of the newly formed cracks (Bond 1952), which leads to:

$$E = K_2 \cdot \left(\frac{1}{\sqrt{x_p}} - \frac{1}{\sqrt{x_f}}\right) \tag{6}$$

BOND's law is most widely used for the sizing of ball and rod mills, which operate in a fashion similar to that of the Los-Angeles test device (Jankovic, Dundar & Metha 2010).

Whilst all above mentioned approaches are intended to estimate the amount of energy needed to create a given particle size, a common task in mineral engineering or materials preparation technology, HARDIN used a similar approach as a means of quantifying the degree of fragmentation (Hardin 1985). Thus, the potential for breakage b_p of a particle with size D is then

$$b_p = \log_{10}\frac{D[mm]}{0.074mm} \qquad \text{for } D \geq 0.074mm \tag{7}$$

HARDIN follows KICK here. The largest silt size, 0.074 mm, was chosen because breakage of very small particles is usually of little interest when the mechanical behaviour of aggregates is being examined (i.e b_p = 0 for D < 0.074 mm). Where an aggregate sample is being considered, rather than a single particle,

$$B_P = \int_0^1 b_p df \tag{8}$$

holds. B_p is called breakage potential (see Fig. 21 left).

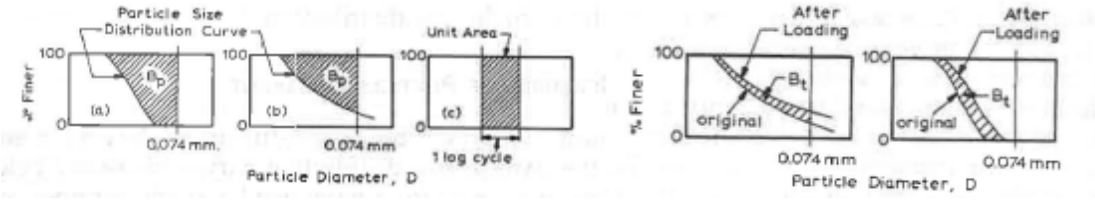

Fig. 21: Breakage potential B_p for two different particle size distributions (left), definition of unit area (center) and total breakage B_t for two different particle size distributions (right) (Hardin 1985)

The breakage that actually occurs in the course of a macroscopic load may then be written as

$$B_t = \int_0^1 (b_{p0} - b_{pl})df \tag{9}$$

b_{p0} and b_{pl} are the respective values for b_p prior to and after loading. B_t is called total breakage (see Fig. 21 right). The relative breakage B_r is then a utilization factor with respect to the breakage potential.

$$B_r = \frac{B_t}{B_p} \qquad \text{with } B_r \in [0,1] \tag{10}$$

Where the initial particle size distribution is defined, as is the case for virtually all ballast attrition tests, B_t is then proportional to B_r.

The Swiss Federal Laboratories for Materials Science and Technology, EMPA, developed a very similar method for analysing their aggregate crushing test. The method is described in (Wieden 1969). The degree of fragmentation Z *("Zertrümmerungsgrad")* is defined as

$$Z = 100 \cdot \frac{F_v - F_n}{F_V}[\%] = 100 \cdot \frac{"I" - "II"}{"I"}[\%] \qquad \text{with } Z \in [0,100] \tag{11}$$

using a log scale for the hatched areas "I", "II" and "III" in Fig. 22 ("I" = "II" + "III") . The minimum particle size is 1/32 of the maximum particle size prior to loading.

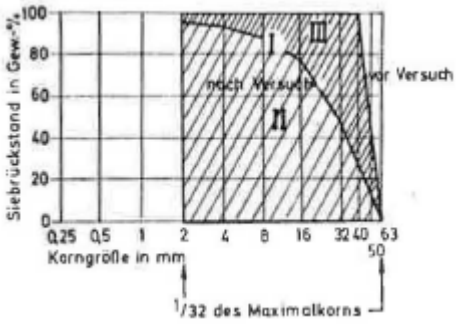

Fig. 22: Degree of fragmentation Z according to EMPA (cited in Wieden (1969))

The present study uses Z, the EMPA degree of fragmentation throughout. It should be noted that changes in particle size distribution do not result from fragmentation processes only, but also from rounding and abrasion (see section 3.1). This implies that the degree of fragmentation, Z, may include phenomena other than fragmentation, depending on the load regime of the respective test method.

4 Ballast index tests - testing procedures

4.1 Los-Angeles Test

The Los-Angeles test was originally developed to determine the toughness and abrasion of aggregates for asphalt concrete and other road surface material. As a consequence, a sample with a gradation of 10/14 mm is used (Österreichisches Normungsinstitut 2006). The repeatability limit is given in EN 1097-2, based on an interlaboratory comparison (28 labs, three aggregate types), as

r_1 = 0,06 X (repeatability)

R_1 = 0,17 X (reproducibility)

EN 1097-2 refers to the test as a "method for the determination of resistance to fragmentation". The adaptation for railway ballast defined in EN 13450 (Österreichisches Normungsinstitut 2004a) uses the same test drum, 12 (instead of 11) steel spheres, 10 kg of aggregate 31.5/50 mm (instead of 5 kg), and calls for 1,000 (rather than 500) revolutions of the test drum (Fig. 23).

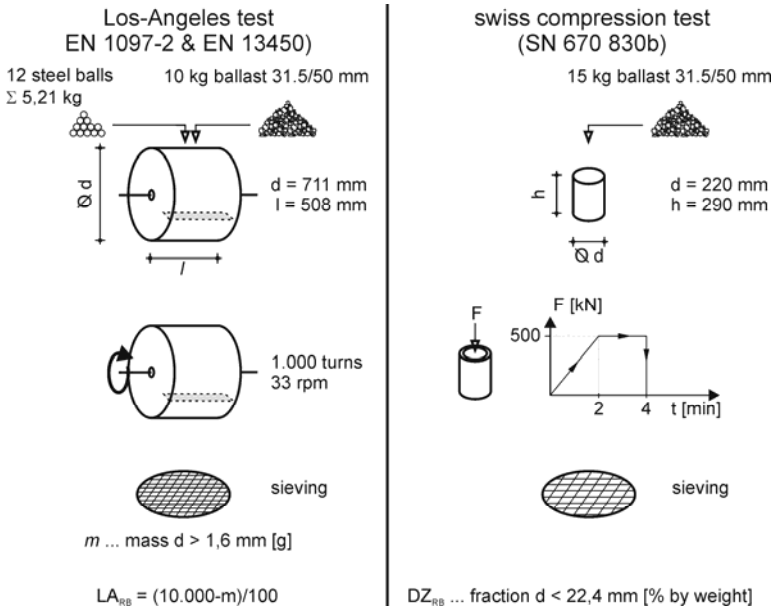

Fig. 23: testing procedures – Los-Angeles test (this section) and Swiss compression test (see section 4.2)

Fig. 24 depicts a cross section of the test drum. The sample (including the steel spheres) fills some 3.6% of the drum volume (Fig. 24, I). The turning of the sample starts as soon as the shelf (height 90 mm) has lifted up the sample by approx. 35° (Fig. 24, II). The whole sample is turned over when 90° (or a quarter-turn) is reached (Fig. 24, III). After a free fall of approx. 150 to 300 mm height, the particles either hit the cylinder wall or other particles. Additionally, one of the steel spheres may hit a particle.

Ballast index tests - testing procedures

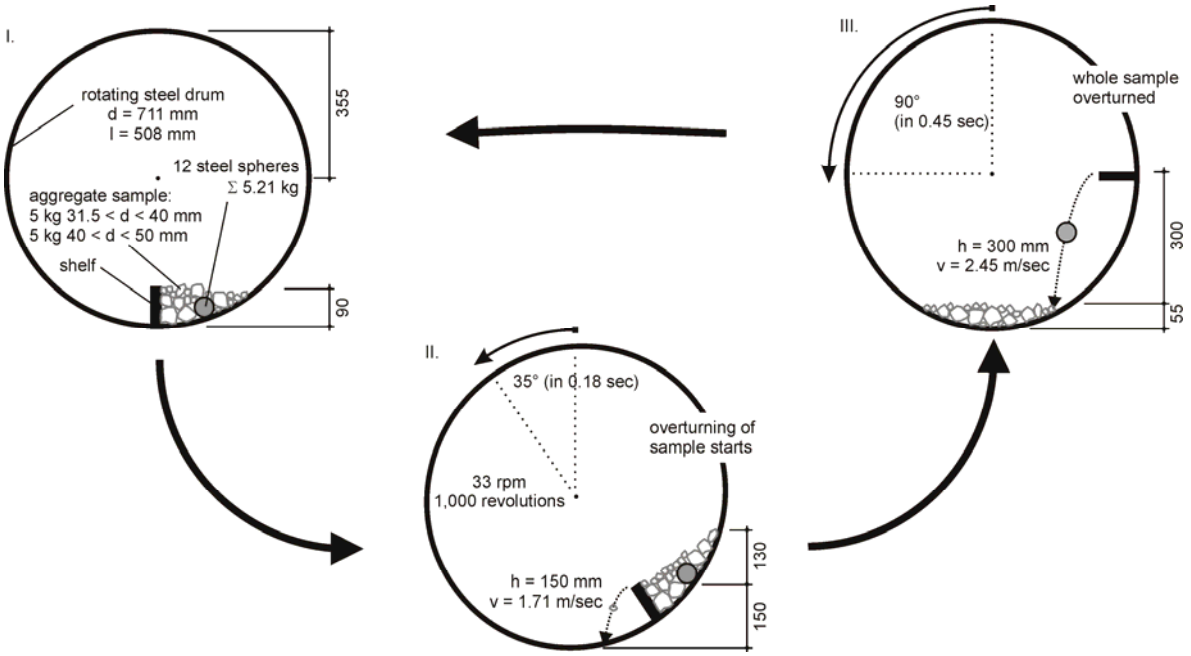

Fig. 24: testing procedures – Los-Angeles Test – test kinematics

Knowledge of the free-fall height and the weight of the object enable one to calculate the impact momentums or, alternatively, the performed work (Tab. 8).

object	fall height	mass	impact velocity	momentum	work
	h	m	v	p	w
	[mm]	[g]	[m/s]	[kg m/s]	[kg m²/s²]
ballast d 31.5 mm	150	81	1,72	0,139	0,120
ballast d 31.5 mm	300	81	2,43	0,197	0,239
ballast d 50 mm	150	325	1,72	0,558	0,478
ballast d 50 mm	300	325	2,43	0,788	0,956
steel sphere	150	434	1,72	0,745	0,639
steel sphere	300	434	2,43	1,053	1,278

Tab. 8: testing procedures – Los-Angeles Test – momentums and performed work

If no fragmentation occurred, every particle would experience two impacts per revolution: the impact of the given particle itself on either the test drum wall, another particle, or a steel sphere; and the impact of a separate particle (or one of the steel spheres) on the given particle. With approx. 100 particles per sample and 12 steel spheres, for a given particle, this would result in 194 collisions of a steel sphere with this particle and 1806 collisions with no steel sphere involved.

However, as fragmentation does occur in reality, the number of particles increases and mean diameter (and weight) decreases. This inevitably leads to a decrease in load level over the course of the test. Additionally, the increasing share of small and very small particles vastly increases the coordination number (see section 2.2) and thus further

reduces load peaks or point-to-point-loads. To illustrate the discussed process, an example is given, taking two samples with a differing degree of fragmentation. The mean impact momentum at test start is 0.367 kg m/s. For sample #1, the mean decreases to 0.246 kg m/s (i.e. 67% of the initial value). For sample #2, the respective value is 0.268 (73%).

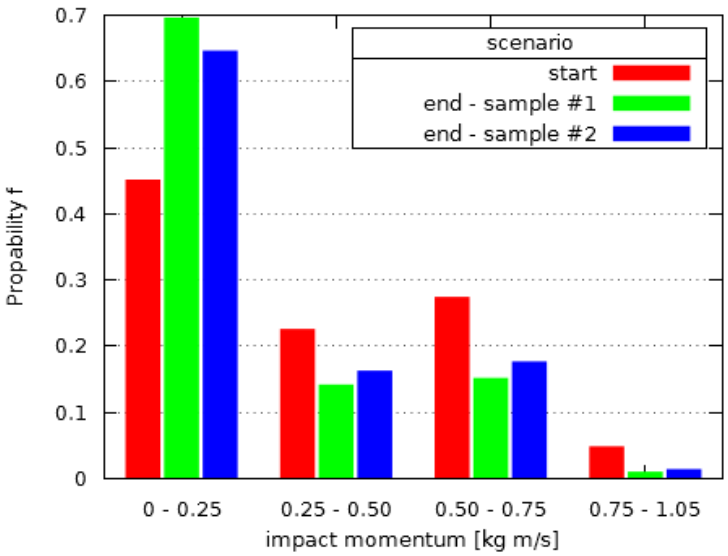

Fig. 25: testing procedures – Los-Angeles Test – impact momentums at start and at end of test duration for two samples with a differing degree of fragmentation

For about three quarters of a turn (or 1.8 sec), the sample is located at or near the lowest point of the rotating test drum and is thus subject to abrasion. The accumulated relative displacement (between test drum wall and a ballast particle) adds up to 1,276 to 1,702 meters, depending on the location of the particle in the heap.

4.2 Compression test (SN 670 830b)

The Swiss compression test for railway ballast (Schweizerischer Verband der Strassen- und Verkehrsfachleute 2007), titled "Compressive Strength on the Stack", was originally developed by the Swiss Federal Laboratories for Material Sciences and Technology for the testing of crushed stones (described in Wieden (1969)). The railway ballast variant makes use of the same identical test cylinder dimensions and applies an identical load regime, but uses a larger sample grading (see Fig. 23 on page 34).

The test resembles the ACV test (British Standards Institution 1990), but differs in terms of sample grading (31.5/50 mm instead of 10/14 mm), test cylinder geometry (D:H = 290:220 mm instead of 150:100 mm), and loading rate (500 kN in 2 min rather than 400 kN in 10 min).

LIM and MCDOWELL proposed and constructed a test cylinder with D = 300 mm and H = 150 mm (i.e. an aspect ratio approximately similar to that of an oedometer) and applied

a path-controlled axial load of 1600 kN (or 22.6 MPa), with 1 mm/min, rather than the force-controlled Swiss test (250 kN/min) (McDowell, Lim & Collop (2003) and McDowell et al. (2004)). Six ballast types were tested and results were compared to those from standard aggregate crushing value (ACV) tests (British Standards Institution (1990), Lim, McDowell & Collop (2005)) and from box tests. The values of Hardin's Total Breakage beneath the sleeper in the box tests were found to correlate much better with the respective values in the self-designed large oedometer tests than those obtained with the standard ACV tests.

As shown in McDowell & Bolton (1998) yielding occurs due to the onset of particle breakage. Based on this, and using a 3D-discrete-element model, McDowell & Harireche were able to demonstrate that yielding coincides with bond fracture at a strain of approx. 30% (McDowell, Harireche 2002). The corresponding yield stress is proportional to the 37% tensile strength of the particles involved. For railway ballast, the constant of proportionality is given as 0.14 to 0.17 (McDowell, Lim & Collop 2003). In order to obtain a precise measure of yield stress, the axial stress σ is plotted on a log scale against strain (or void ratio). The point of maximum curvature may then be located (Fig. 26).

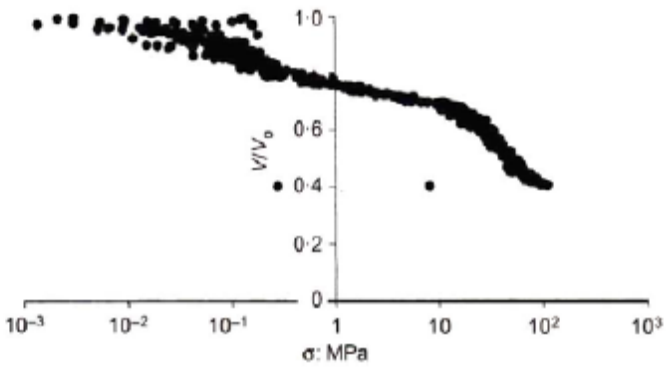

Fig. 26: Compression test – Compression curve from numerical analysis ((McDowell, Harireche 2002))

As the yielding process occurs gradually, this turns out to be rather difficult. As the title of the standard suggests, a mechanical parameter (compressive strength) is derived on the basis of a geometric parameter (sieve size or particle size distribution). If the amount of fines (ACV value or DZ_{RB}) shows a correlation with yield stress, the test may be considered useful as a means for determining the resistance to fragmentation.

Lim (2004) carried out a multitude of compression tests on six ballast types, using both the standard ACV test equipment, a large oedometer device, and an initial grading of 37.5/50 mm. Among his findings for the latter test variant was a very strong correlation between the degree of fragmentation, stated as B_t, and ACV (R^2 = 96%) and also a

strong correlation between B_t and tensile strength σ_0, as determined with single particle crushing tests (R^2 = 71%). This suggests that the above mentioned hypothesis concerning the correlation between fines and stress seems to hold.

4.3 Deval Attrition Test

The Deval Attrition Test according to BS812:1951 (British Standards Institution 1951) is a test for determining the resistance to abrasion (Fig. 27). The test method was included in Austrian Railways' engineering specification for railway ballast up to the 1960s (Österreichische Bundesbahnen (ÖBB) 1962), but was then eventually replaced by the Micro-Deval test (Österreichisches Normungsinstitut (2004b) and Österreichisches Normungsinstitut (2004a)).

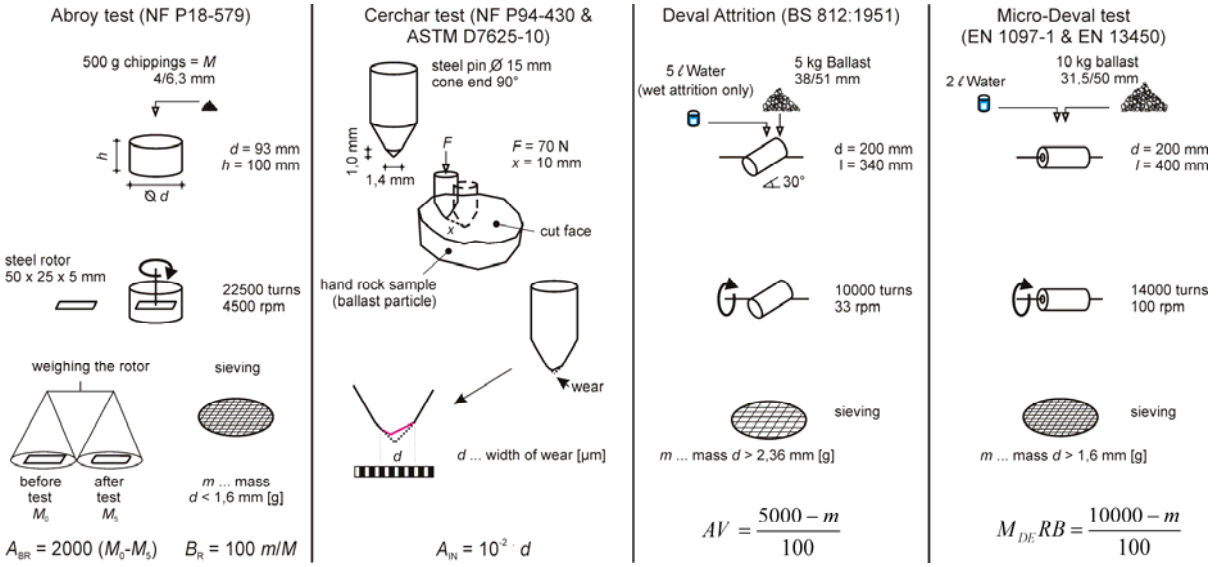

Fig. 27: testing procedures – LCPC Abroy test, Cerchar test (see section 4.4), Deval Attrition test & Micro-Deval test (this section)

Two alternative test variants exist with almost identical test procedures. The Wet Attrition Test (WAT), in which water is added, and the Dry Attrition Test (DAT) in which no water is added. There is hardly any fragmentation, as the impact momentums are small due to the small dimension of the test drum. The high number of revolutions, and – in the case of the WAT – the added water, result in a high abrasion load. The sample weight of 5 kg typically results in 32 to 40 particles. The level of filling is about 16% to 18%, based on grain density, or 30% to 33%, based on bulk density.

Due to the test drum's inclined mounting, 10,000 revolutions are equal to 20,000 load cycles (Fig. 28). We assume that the sample may be represented by its centre of mass, which is located at a distance of approx. 6 cm from the left wall of the test drum. This implies a maximum possible displacement of the sample in longitudinal direction of 0.23 m. The following assumptions are also made:

- The sample will not start sliding in longitudinal direction until the orientation of the test drum axle is > 0° (we assume that the rotational movement of the sample has already overcome the static friction during the first quarter rotation)
- Sliding occurs with a continuously rising velocity (due to the rising inclination of the drum) until the sample hits the right end wall shortly after the maximum inclination of the test drum axle is reached (i.e. after 95.5° or 0.51 sec). Velocity is approx. 1.33 m/s at this point.
- There is no displacement in a negative direction until the inclination of the test drum axle turns negative (i.e. after 180° or 0.95 sec)
- The sample starts sliding again, once more with rising velocity, until it hits the left end wall (after 275.5° or 1.46 sec) with a velocity of 1.33 m/s.
- Again, there is no displacement in longitudinal direction until the turn of the test drum is completed (360°).

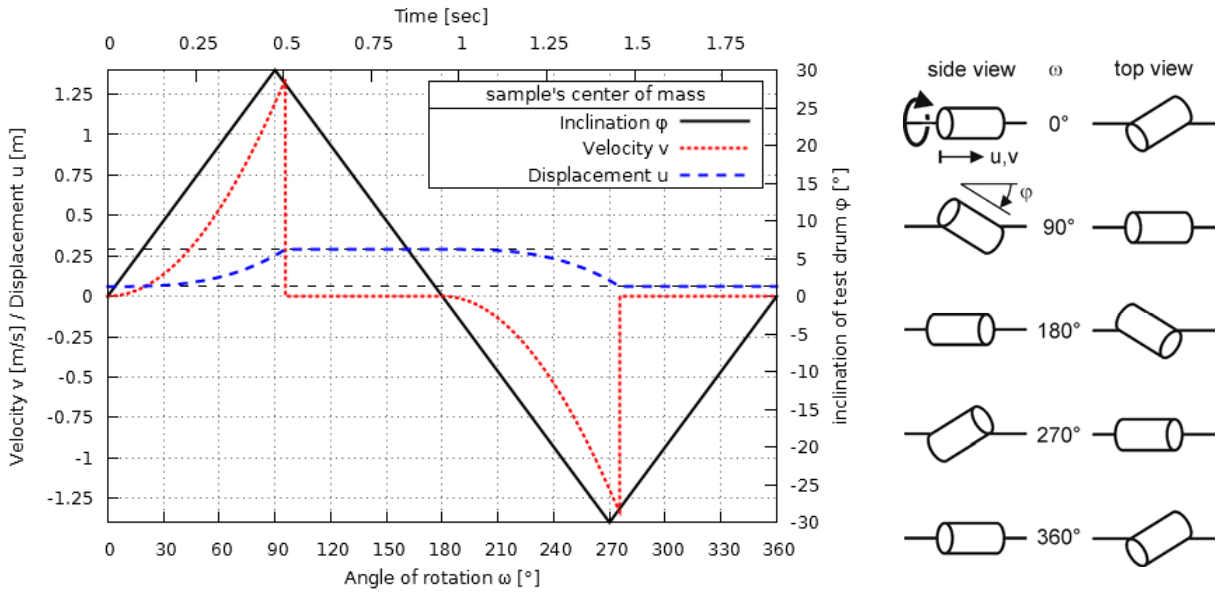

Fig. 28: Deval test – velocity and longitudinal movement of the sample's centre of mass in the course of one revolution (left) and respective inclination of test drum (right)

This longitudinal sliding movement (0.46 m per turn) is accompanied by a rotational component (0.63 m per turn with a velocity of 0.33 m/s). The accumulated displacement adds up to 10,883 meters.

In the course of each load cycle, the particles are subject to several collisions with other particles and with the wall of the test drum, resulting in rounding and polishing.

As shown in section 3, rounding is caused by shear or compressive loads, whilst abrasion occurs due to shear only. The impact momentums and point loads generated from particle collisions and collisions of particles with the wall of the test drum ought to have a

similar range for the wet and the dry test. The wet test may exhibit slightly smaller load levels due to the highly turbulent flow conditions. The same holds for the shear loads generated by the relative movements of the particles ("polishing"). Fines are generated, which, in the case of the dry test, cling to the ballast grains. For the wet test, these fines are washed away by the water. Thus, for the wet test, the particle surface lies open and is subject to polishing. In the case of the dry test, the fines form a kind of protective layer and prevent polishing after only relatively few rotations (see also (Heibaum, Warnecke 2012) and (Salas Cazón, Milton Antonio 2002)).

4.4 Abrasion tests for tool wear estimation (LCPC Abroy test and Cerchar test)

The comparison of the traditional tests for railway ballast for resistance to abrasion with two alternative tests, the LCPC Abroy abrasivity test according to (Association française de normalisation (afnor) 1990) and the Cerchar test according to (Association française de normalisation (afnor) 2006), is designed to provide information on the suitability and applicability of these standard testing procedures for mining and tunnelling in quality control for railway ballast. At the same time, they may also serve as an evaluation method for similar attrition tests such as the Deval test and the Micro-Deval test.

Both tests are well established in geotechnics and tunnelling. They are used to estimate the wear of metal cutting tools such as drill bits, cutting blades and cutter rolls in tunnelling, drilling and excavating.. Tool wear constitutes an important factor when estimating cutting performance and penetration rates in underground engineering. Consequently, the impact of abrasivity on tool wear and performance rates in tunnelling and underground engineering, as well as the search for adequate testing methods are areas of intense research (see Köhler, Maidl & Martak (2011), Drucker (2011), Thuro & Käsling (2009), Plinninger & Restner (2008), Lassnig, Latal & Klima (2008), Käsling, Thiele & Thuro (2007) and Thuro et al. (2006) for example).

Test results exist for almost all imaginable rock types, including many rock types which are not suitable for use as railway ballast (due to their low resistance to wear and fragmentation). This thus allows for a realistic estimation of maximum permissible values for purposes of aggregate quality.

Ballast index tests - testing procedures

left: 1 motor, 2 metal impeller, 3 sample container, 4 funnel tube

below: 1 unused impeller 2 limestone (not abrasive) 3 quartzitic sandstone (abrasive to very abrasive) 4 diorite (very abrasive) 5 vein quartz (extremely abrasive)

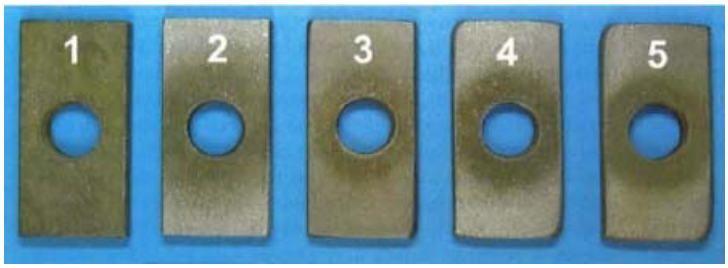

Fig. 29: Abroy test – abrasimeter (left) – impeller before and after test (right) (from Thuro et al. (2006))

Fig. 30: Cerchar test – test device according to West (1989) (left) – rock sample with testing pin (from Plinninger (2007))

The test procedures of the two tool wear tests are depicted in Fig. 27 (page 38). Fig. 29 depicts an Abroy abrasimeter and abraded impellers (rotors). The Cerchar test device is shown in Fig. 30.

Both tests are not limited to a specific particle size, angularity, or shape. For the Abroy test, an initial gradation of 4/6.3 mm is used, and this is obtained by means of grinding, regardless of the particle size distribution of the raw material. Information on the raw material's angularity and particle shape is thus inevitably lost. However, the grinding process influences the angularity and particle shape of the 4/6.3 gradation (see Tab. 9). Sieving may be used if soil or aggregate is being tested, but studies show size dependency with respect to particle geometry, angularity and the resulting abrasivity (see Lim (2004), Lim, McDowell & Collop (2005), McDowell & Amon (2000) and Weiher

(2009) for example). For the study presented here, ground material was used throughout.

The Cerchar test uses one hand rock sample with a minimum size of approx. 30 mm. As a cut surface is used for the determination of tool wear, particle geometry and angularity do not influence the test result (Tab. 9).

test method	angularity	particle size distribution	particle geometry	particle size
Abroy test	+	-	+	-
Cerchar test	-	-	-	-

Tab. 9: Abroy- and Cerchar test – factors of influence on test result

Both testing methods estimate tool wear. The estimation of the breakability and the abrasion of the respective rock mass is not the prime target. However, one may assume that rock types with high abrasivity show low grain-to-grain wear in track.

The classification schemes of Thuro et al. (2006) and Cerchar (1986) (see Tab. 10) have become a quasi-standard and are used throughout the present document.

Abroy test		Cerchar Test	
A_{BR} [g/t]	Classification	A_{IN} [-]	Classification
0 – 50	not abrasive	0.3 – 0.5	not very abrasive
50 – 100	slightly abrasive	0.5 – 1.0	slightly abrasive
100 – 250	low abrasiveness	1.0 – 2.0	medium abrasiveness to abrasive
250 -500	abrasive	2.0 – 4.0	very abrasive
500 – 1,250	very abrasive	4.0 - 6.0	extremely abrasive
1,250 – 2,000	extremely abrasive		

Tab. 10: Abroy- and Cerchar test – classification scheme based on Thuro et al. (2006) and Cerchar (1986)

5 Evaluation of tests

5.1 Ballast used for test series - deviation of particle geometry and petrography

As of 2011, eleven producers accounted for some 96% of Austrian Railways' ballast demand (Kuttelwascher 2011). 55% of the ballast is of igneous origin (granite, granite porphyry, dunite and basalt), another 37% is metamorphic rock (granulite, diabase), and a small share of 4% consists of dolomite (Tab. 11). The test series presented here make use of all eleven rock types and can thus be called a representative selection for the conditions in Austria.

Ballast samples from four of these quarries (basalt (02), granitic porphyry (03), dunite (04) and granulite (10)) were studied in detail (see sections 5.2 and 5.5). Rock type 02 (basalt) was chosen as it appeared to be comparably homogeneous in terms of petrography and particle shape. In addition, basalt rock has the advantage that it is widely used internationally as railway ballast. Similarly, rock type 10 was chosen as representative of the granitoids, since these also form a large source for railway ballast. Rock type 04 is typical for ballast provided by Austrian Railways' largest supplier (Kuttelwascher 2011). Rock type 03 exhibited two clearly distinguishable subclasses.

The samples analysed originate from a single day's production. Based on simple macroscopic characteristics, two subclasses (A and B) were defined for granitic porphyry (03), dunite (04) and granulite (10). Macroscopic characteristics include the main petrographic features such as colour, texture, particle shape and angularity of each grain. In order to separate subclass A and B some 500 kilos of washed sample material were sorted grain by grain by hand (Neubauer 2013). Subclass A represents the main rock type of each quarry. A suffix 'M" indicates a randomly taken sample, consisting of a mixture of subclass "A" and "B".

For granitic porphyry and dunite rock fabric, mineralogical composition and colour allow for a clear distinction to be made between subclass A and B – subclass A of granitic porphyry (03) can easily be distinguished from subclass B by its prominent foliation and high amount of large biotite – subclass A of dunite (04) is a greenish, very fine-grained rock, while subclass B represents a coarse-grained, brownish altered variety.

The difference in subclass A and B of granulite is only due to small variations in the amount of biotite. Subclass A and B are characterised by similar rock fabric (slight foliation and grain size) and by the same colour.

Evaluation of tests

rock type		rock class	colour	rock fabric	main mineral components	equivalent quartz content
granite	01	igneous	light grey	non-oriented, macrocrystalline	quartz, feldspar, biotite, garnet	53.4
basalt	02	igneous	dark grey	non-oriented, microcrystalline	pyroxene, foids, magnetite	29.4
granitic porphyry	03	igneous			quartz, feldspar, amphibole, biotite	52.5
	03A	igneous	dark grey with white layers	preferred orientation (foliated), macrocrystalline	quartz, feldspar, amphibole, biotite, garnet	60.0
	03B	igneous	dark grey	porphyritic (microcrystalline)	quartz, feldspar, amphibole, biotite	40.7
dunite	04	igneous (modified by metasomatosis)			serpentine, olivine, amphibole, chlorite ± talc	39.9
	04A	igneous (modified by metasomatosis)	greenish	non-oriented, microcrystalline	serpentine, olivine, amphibole, ± magnetite, talc	42.7
	04B	igneous (modified by metasomatosis)	grey with brownish parts	slight preferred orientation, macrocrystalline	serpentine, olivine, amphibole, chlorite, ± talc	24.6
diabase	05	metamorphic	grey-green-red	brecciated, microcrystalline	feldspar, amphiboles, quartz, chlorite	36.5
granulite	06	metamorphic	white to light grey	preferred orientation (foliated),	quartz, feldspar, biotite, chlorite, garnet	63.4
diabase	07	metamorphic	greenish-grey	non-oriented, microcrystalline	feldspar, chlorite, quartz, carbonates, biotite	32.1
diabase	08	metamorphic	greenish-grey	non-oriented, microcrystalline	feldspar, chlorite, quartz,	31.3
granite	09	igneous	light grey	non-oriented, macrocrystalline	quartz, feldspar, biotite, chlorite	49.3
granulite	10	metamorphic			quartz, feldspar, biotite, garnet	60.0
	10A	metamorphic	white to light grey	preferred orientation (foliated), phaneritic	quartz, feldspar, biotite, garnet	66.5
	10B	metamorphic	light grey	preferred orientation (foliated), phaneritic	quartz, feldspar, biotite, garnet	63.9
dolomite	11	sedimentary	light grey	brecciated, microcrystalline	dolomite, calcite	30.0

Tab. 11: rock types used in test series

Evaluation of tests

In order to carry out X-ray diffraction analysis a small portion of material was milled. Samples were measured with a Panalytical X`Pert Pro (Co-tube) in the range of 4° to 85° 2 Q. Semiquantitative calculations were carried out by comparing characteristic x-ray reflection intensities with calibration diffractograms.

For semiquantitative calculations, calibration diffractograms of minerals with an average chemical composition were used. Thus, greater inaccuracies in the calculations occur when minerals with a great chemical variability (e.g. feldspars, amphiboles, pyroxene, garnet etc.) are present.

Equivalent quartz content E_{Qu} [%] (Thuro (1996) based on Rosival (1986) and Rosival (1916)'s mineral hardness classification) is traditionally estimated using the mineralogical composition of a thin section and follows:

$$E_{Qu} = \sum_{i=1}^{n} A_i R_i \tag{12}$$

with A_i fraction of mineral type

R_i mineral hardness based on (Rosival 1896) and (Rosival 1916)

n mineral count

However, in the course of the present study, the alternative method based on X-ray diffraction analysis was used, which combines the identification of the mineral types with a quantification of their fraction.

The values applied for ROSIVAL's mineral hardness are listed in Tab. 12.

Mineral	hardness	Mineral	hardness
quartz	100.0	pyroxene	30.0
garnet	100.0	amphiboles	16.0
olivine	80.0	apatite	5.5
hematite	55.0	micas/clay minerals	4.0
pyrite	55.0	serpentine	3.0
foids	31.0	carbonates	3.0
magnetite	31.0	talc	2.0
Feldspars	30.0		

Tab. 12: Rock types used in test series - values for ROSIVAL's mineral hardness for the evaluation of equivalent quartz content

Evaluation of tests

PLINNINGER introduced the Rock Abrasivity Index RAI (Plinninger 2002). Thus:

$$RAI = \sum_{i=1}^{n} A_i \cdot R_i \cdot UCS \tag{13}$$

with UCS unconfined compressive strength of rock [MPa].

The RAI is equal to the product of E_{Qu} and UCS and thus takes two core parameters into account: the content of abrasive minerals, and the rock strength. It constitutes a simplification of SCHIMAZEK's earlier concept of a wear index which also included quartz content and rock strength, as well as the grain size of the quartz minerals (Schimazek, Knatz 1976). Grain size was omitted by PLINNINGER due to its complicated and error-prone method of determination. Today, the RAI is a widely-used characterization parameter for tool wear in drilling.

Evaluation of tests

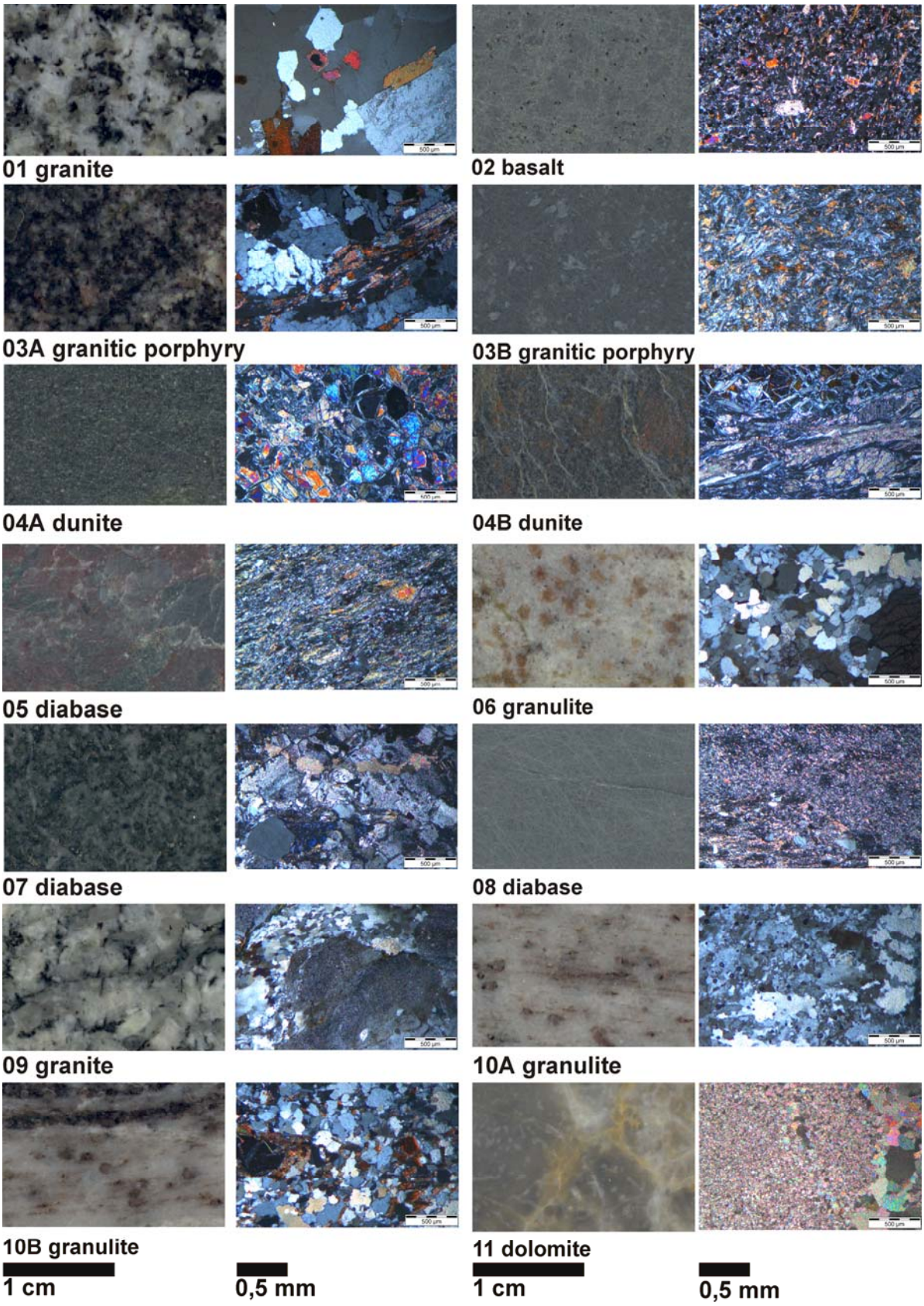

Fig. 31: Rock types and subclasses used for test series – polished sections and thin sections

Evaluation of tests

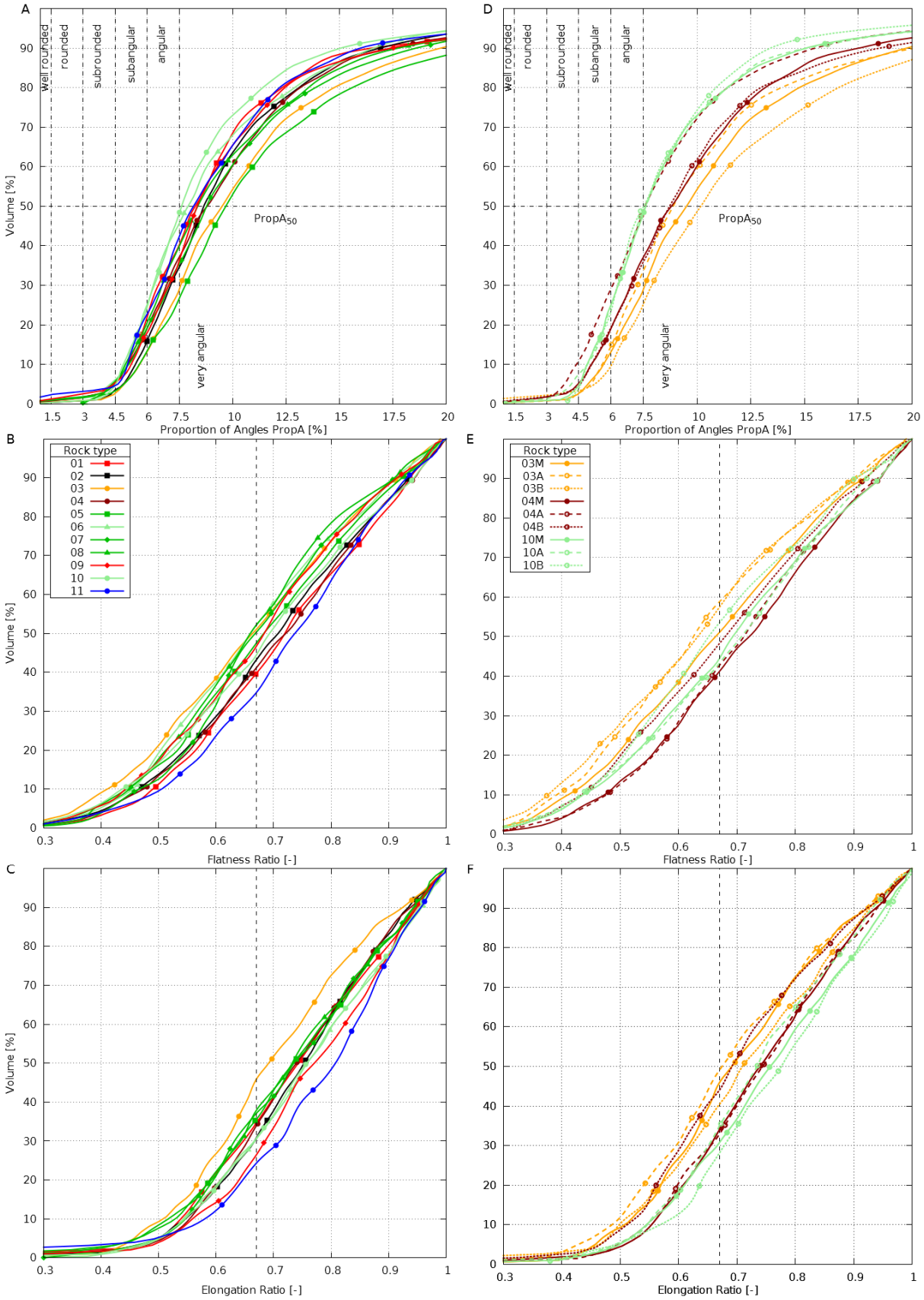

Fig. 32: Angularity PropA, Flatness ratio and Elongation ratio for rock types 01 to 11 (left) and for subclasses 03A, 03B, 04A, 04B, 10A and 10B (right) Petroscope® scans with ballast type I (Österreichische Bundesbahnen (ÖBB) 2007) (smoothed)

Evaluation of tests

All rock types and subclasses were analysed by means of the Petroscope® device with respect to their angularity (Fig. 32 left) and particle shape (Fig. 32 center and right). Sample size was 300 to 500 particles each for rock types 01, 05 to 09 and 11 and well over 1000 particles each for rock types 02 to 04 and 10.

The distribution of the angularity, expressed as the proportion of angles PropA (see section 3), shows a similar shape for all rock types. There are almost no "rounded" and "well-rounded" particles (<5 Volume-%) and a linear slope exists between 5 and 10% of PropA. The mean angularity varies between 7.5 and 9.5% PropA (i.e. "very angular" in terms of POWERS' scheme). 75 to 85% Volume-% are "angular" or "very angular". The share of particles with PropA >15% is 10 to 25%, with illustrates that POWERS' roundness class scheme is not suitable as a means of description for very angular particles. The subclasses of rock types 03 and 04 vary noticeably in terms of their angularity.

There is an almost uniform distribution of the flatness ratio between 0.4 and 1.0 and, similarly, for the elongation ratio (between 0.55 and 1.0). The mean flatness ratio varies between 0.62 to 0.69 and the mean elongation ratio between 0.73 – 0.78 (outliers are rock type 03 and 11), i.e. there are less elongated particles than there are flat ones. Less than 5 Volume-% have a FR of less than 0.35 and an ER of less than 0.45 (ratio of longest to intermediate axis of 1 : 2.22). Again, the subclasses of rock types 03 and 04 vary noticeably in terms of particle shape.

Particle shape and angularity seem to be heavily influenced by man-made factors:

- blasting technique used at the respective quarry
- local crusher (its type and its calibration)
- transport-related issues such as repeated relocation of heaps or transhipping between rail and road etc.

Geological factors such as mineral content, mineral size, parameter length, texture and foliation, which determine particle shape in the course of natural processes such as erosion and frost weathering, are apparently overridden by those originating from processing techniques.

Fig. 32 and Fig. 33 also illustrate that a discrimination of different rock types on the base of particle geometry and angularity is difficult, even if large sample sizes are available. A particle-based classification test, based on a combined examination of ER, FR and PropA, using statistical methods, yielded a hit rate of 65% (Hofer et al. 2012).

BREYMANN carried out point load tests on samples from all rock types (Breymann et al. 2011). Cuboidal particles with sieve sizes between 31.5 and 50 mm were used in order to minimize the impact of size and shape. Load was applied in a strain-controlled fashion, with a strain rate of 4 mm/min. Fig. 34 (left) gives the results. Mean values vary

between 9.6 MPa and 22.2 MPa. The coefficient of variation $v = s / \bar{x}$ is typically 32% to 40%. Rock type 04 exhibits the lowest point load index and the largest coefficient of variation (50%).

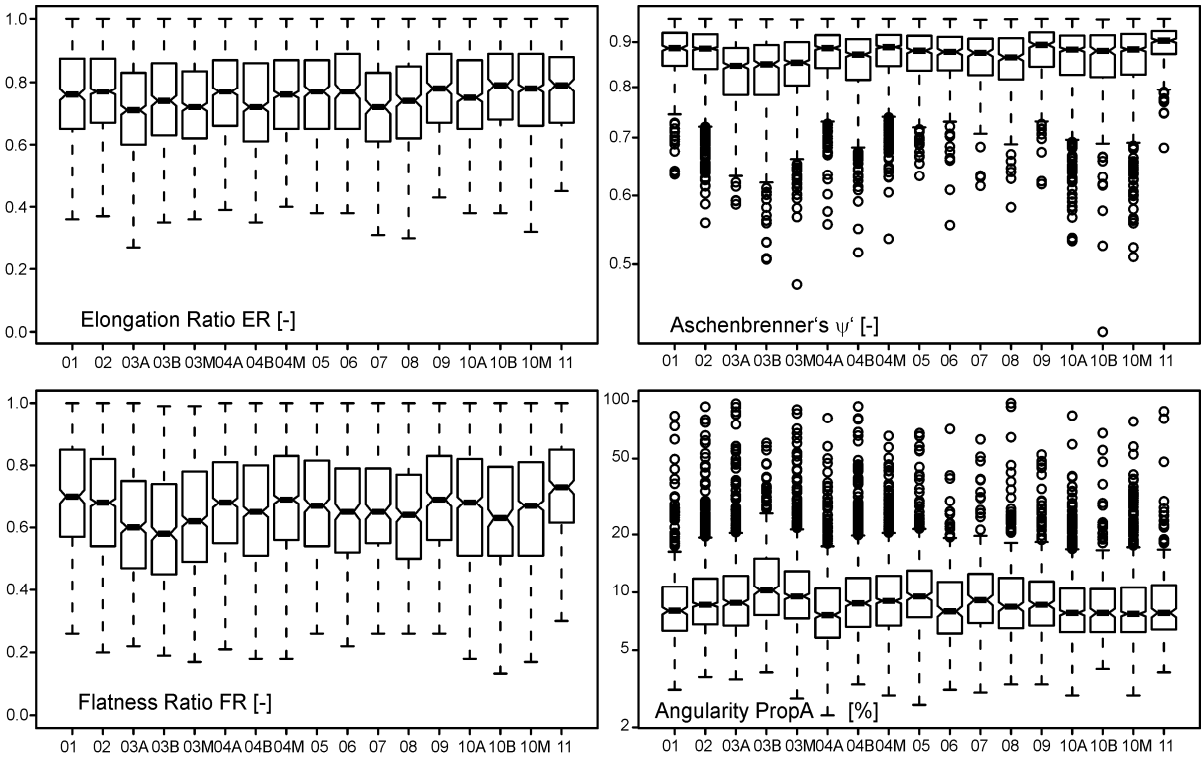

Fig. 33: Boxplots for geometric features (elongation ER, flatness FR, Aschenbrenner's working sphericity ψ' and angularity PropA) of all rock types and subclasses (from Hofer et al. (2012))

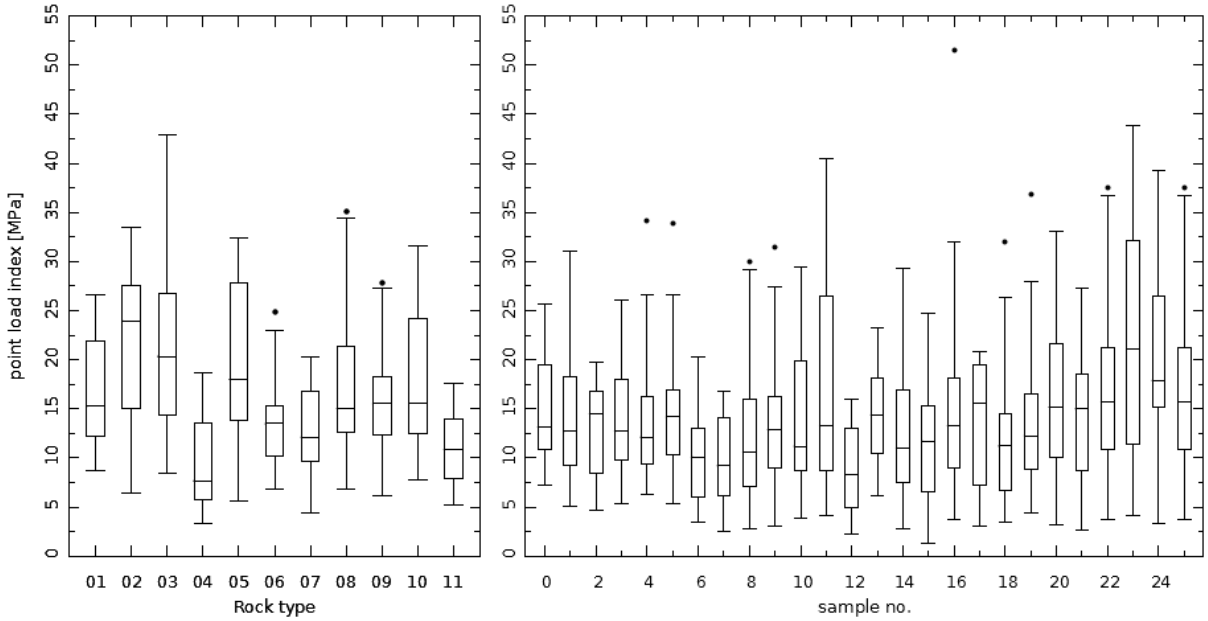

Fig. 34: Boxplots for point load index test results (n = 30) of rock types 01 to 11 (left; from (Breymann et al. 2011)) and of 26 samples from rock type 08 (n =30), drawn weekly (right) (from Breymann, Nindl & Scharler (2012))

Evaluation of tests

Additionally, samples taken in weekly intervals from the output of quarry 08 (rock type 08) were investigated over a period of half a year (Breymann, Nindl & Scharler (2012); Fig. 34 right). Mean values and deviation of results show strong time-dependency, indicating heterogeneous output for the respective quarry (or, alternatively, an insufficient sample size).

Tab. 13 gives a compilation of all ballast attrition tests carried out in the course of this study. Test results are given in sections 5.2 to 5.5.

Rock type	LA	Compression	Wet attrition	Dry attrition	Abroy	Cerchar
	(sec. 5.2)	(sec. 5.3)	(sec. 5.4)		(sec. 5.5)	
01	-	2	-	-	5	7
02	15	12	2	4	9	12
03M	9	2	2	4	9	7
03A	8	-	-	-	4	5
03B	5	-	-	-	4	5
04M	11	2	2	4	9	7
04A	8	-	-	-	4	5
04B	8	-	-	-	4	5
05	-	2	-	4	5	7
06	-	2	2	4	5	7
07	-	2	2	4	5	7
08	-	2	2	4	5	7
09	-	2	-	4	5	7
10M	10	2	2	4	9	7
10A	8	-	-	-	4	5
10B	3	-	-	-	4	5
11	-	4	2	4	5	7

Tab. 13: overview of attrition test series

5.2 Los-Angeles test

An extensive test series of 85 LA-tests (Fig. 35) was carried out by the author (Bach, Latal 2013). After measuring the sample with Petroscope®, the standard LA-test was performed and LA_{RB} was determined. The sample was then measured again with Petroscope®.

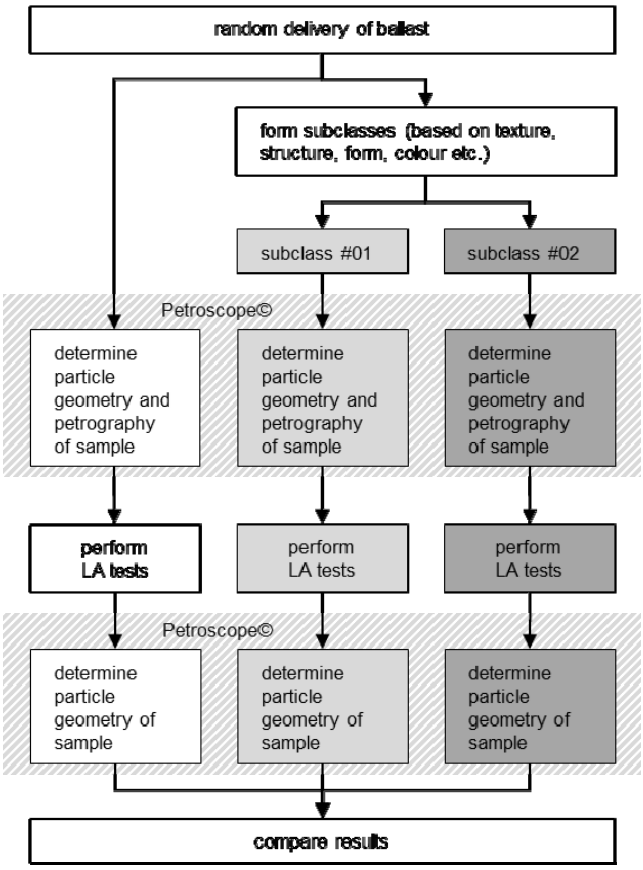

Fig. 35: LA tests – performed test series

5.2.1 LA_{RB} and Particle Size Distribution

Fig. 36C and D show that average LA_{RB} values are approx. 25% for rock type 04 (dunite) and 15% for rock type 10 (granulite). The results for subclass "A" differ very little from those of subclass "B" and those of the random samples "M". Rock type 02 (basalt) (Fig. 36A), which was considered to be comparatively homogeneous in terms of its petrographic composition, exhibits a fairly large deviation. Both subclasses of rock type 03 (granite porphyry, Fig. 36B) show large variations in LA_{RB}. Values for subclass 03B average out at 12%, while subclass 03A produces almost twice as many fines (approx. 20%)

Evaluation of tests

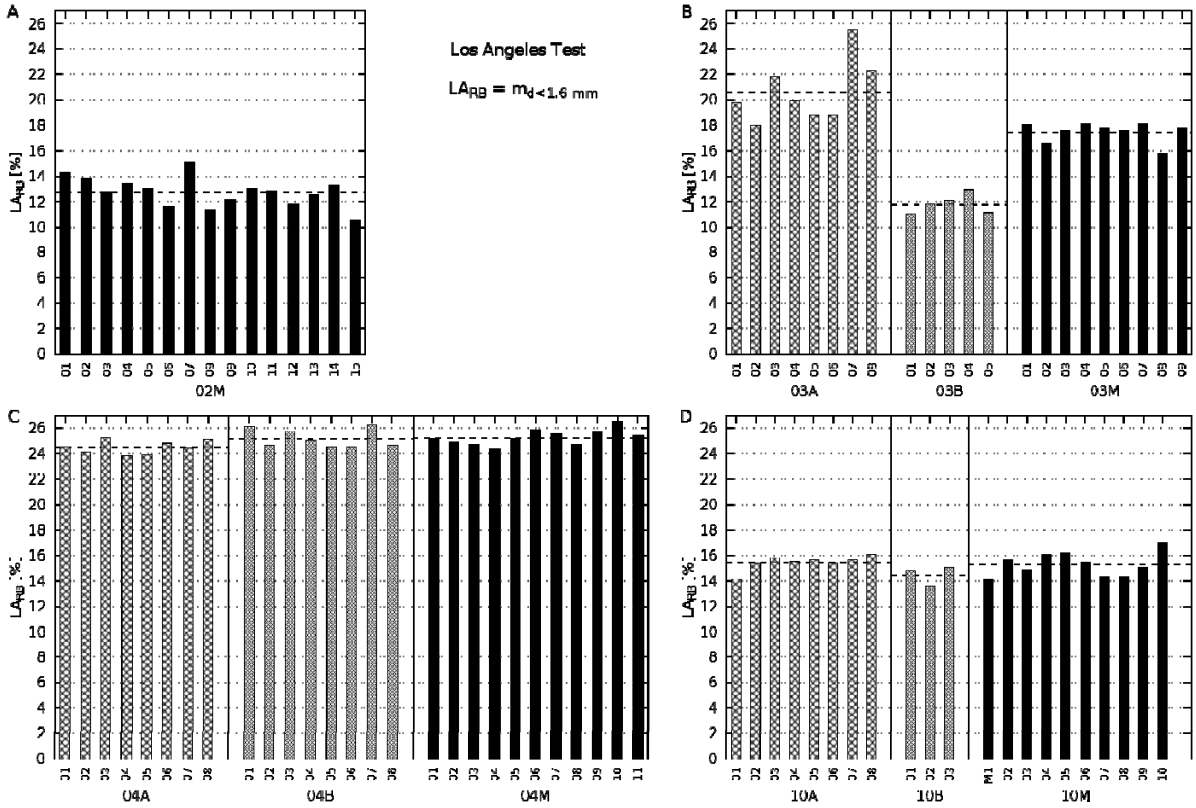

Fig. 36: LA tests – test result $LA_{RB} = m_{d<1.6\ mm}$

Tab. 14 gives the mean values for all rock types and subclasses, the standard deviations, based on number of tests and a student's t-distribution, and the respective confidence intervals, based on a confidence level of 95%. To ensure a confidence interval smaller than 5% of LA_{RB}, 16 tests needed to be performed in the case of rock type 02M, and 25 tests for rock type 03A. To achieve a confidence interval of 0.5%– regardless of the magnitude of LA_{RB} – some 25 (02M) or 100 tests (03A) would be necessary.

rock type	mean	No. Tests	Std. Dev.	Confidence	min No. Tests	min No. Tests
	LA_{RB}	n	s	interval $CI_{0.95}$	for $CI_{0.95} < 0.05\ LA_{RB}$	for $CI_{0.95} < 0.5\%$
	[%]	[-]	[%]	[%]	[-]	[-]
02M	12,75	15	1,20	0,66	16	25
03A	20,61	8	2,50	2,09	25	99
03B	11,78	5	0,76	0,94	9	12
03M	17,48	9	0,80	0,61	6	13
04A	24,51	8	0,54	0,45	4	7
04B	25,19	8	0,74	0,62	4	11
04M	25,29	11	0,62	0,42	4	9
10A	15,44	8	0,59	0,49	5	8
10B	14,45	3				
10M	15,29	10	0,94	0,67	9	16

Tab. 14: LA tests – deviation of results and confidence intervals

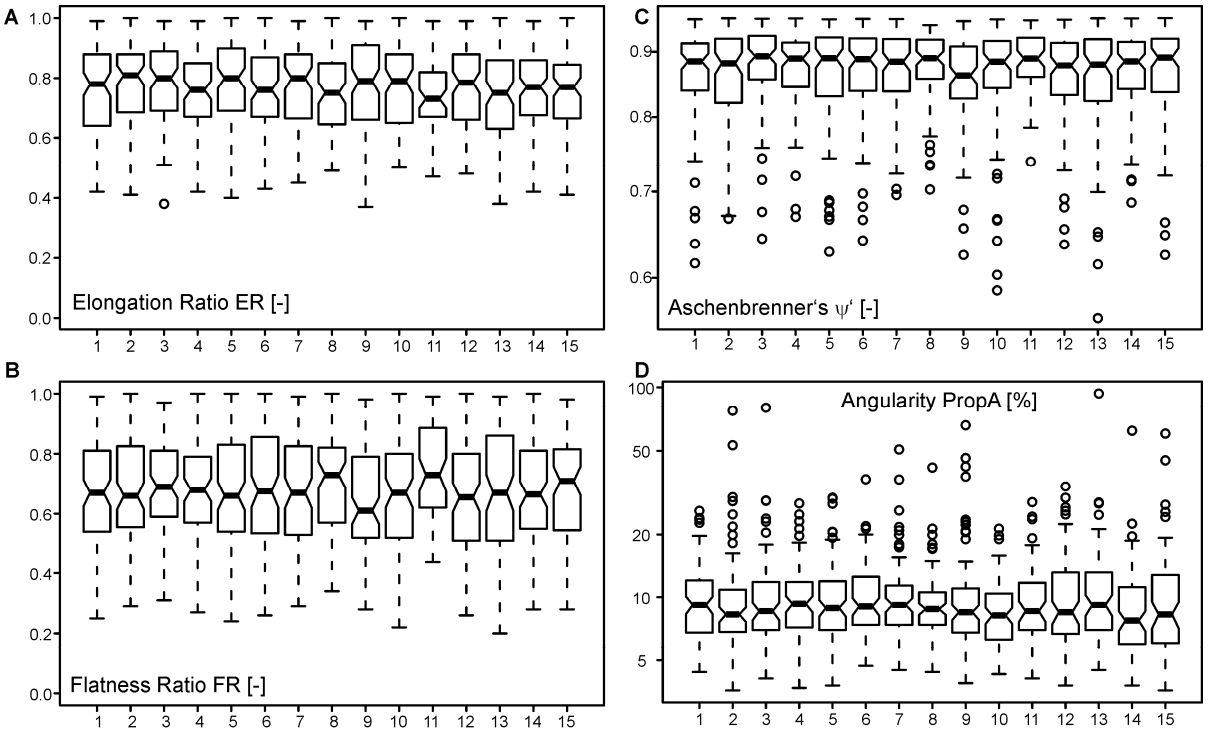

Fig. 37: LA tests – Boxplots for geometric features (elongation ER, flatness FR, Aschenbrenner's working sphericity ψ' and angularity PropA) of 15 samples of rock type 02M (from Hofer et al. (2012))

If mechanical properties differ samplewise (see also Hofer & Bach (2012)), this raises the question as to what extent geometric properties also vary samplewise. The boxplots in Fig. 37 show a large variation of the geometric properties of 15 samples for rock type 02M (10 kg per sample). Thus, even when samples are considered to be homogeneous with regard to rock type (i.e. same rock type and same subclass), the distribution of the geometric properties differs significantly between samples.

The unfavourable relation between gradation (31.5 mm– 50 mm) and sample mass (10 kg), resulting in a comparatively low number of particles in one sample (typically 87 – 100), implies that even a very small number of particles differing in terms of shape, angularity or petrographic composition can have a relatively strong impact. The work of (Hofer et al. 2012) deals with matters concerning the accuracy of the test results.

Fig. 38 depicts the particle size distribution for the LA-tests as described in section 4.1. The test criteria of the LA test (d < 1.6 mm) is highlighted, as is the grading prior to test.

Evaluation of tests

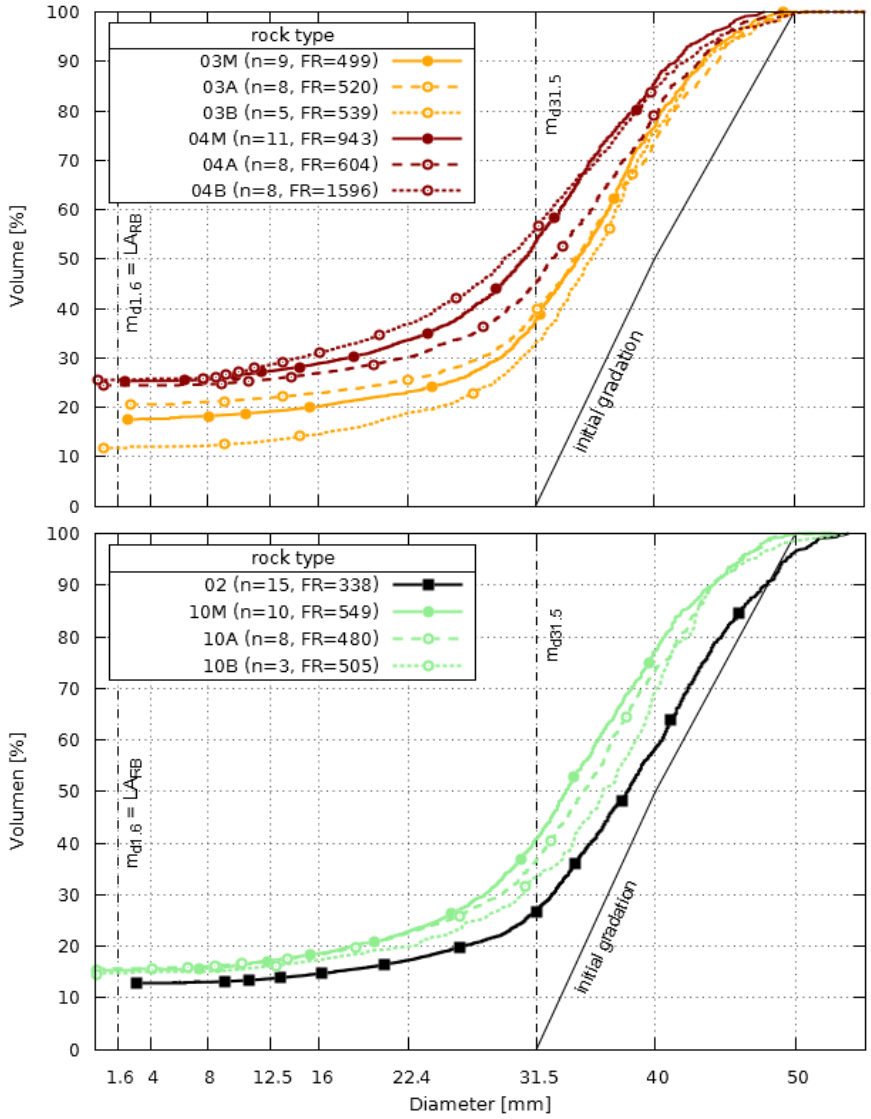

Fig. 38: LA tests - particle size distributions for rock types 03A, 03B, 04A and 04B (top) and 02, 10A, 10B and 10M (bottom)

All LA tests result in high $m_{d31.5}$ values (27% < $m_{d31.5}$ < 52%). However, $m_{d1.6}$ values range from 11% to 25 %, thus indicating that fragmentation and rounding must have occurred. For rock type 03, the LA-values (= $m_{d1.6}$) differ considerably for subclass "A" (approx. 11 %) and "B" (approx. 20%). The values for the random samples lie in between. $m_{d31.5}$ values vary by approx. 8% (40% vs. 32%).

This relatively diverse behaviour of the subclasses A and B of rock type 03 may be explained by their characteristic rock properties. In general, subclass A yields larger mineral size and shows prominent foliation (Fig. 31). In contrast, the rock fabric of subclass B can be described as microcrystalline to porphyritic, with no preferred orientation (Fig. 31) Liu et al. (2005) presents a correlation between average grain size of rock and LA value. An increase of average grain size leads to an increase in LA values.

Rock type 04 also exhibits noticeably different particle size distribution curves for both subclasses. However, the LA-values are very similar (all approx. 25%). Thus, the observed test value does not reflect the amount of fragmentation. These observations raise the question as to what extent the measured LA-values derive from fragmentation and from rounding.

For rock type 04, differences in mineral size, mineral spatial arrangement, and mineral composition between subclass A and B, might also account for the diverse results in particle size distribution. In contrast to rock type 03, subclass 04B exhibits slightly larger minerals and a slight preference with respect to orientation.

5.2.2 Rounding – Global View

The diagrams in Fig. 39 and Fig. 41 show cumulative frequency curves for angularity, stated as proportion of angles, PropA, relating to particle size, and using a log-scale. Powers' angularity classes (Powers 1953) are added for purposes of orientation.

Prior to the test (Fig. 39 top), for all rock types, angular and very angular particles prevail (> 90% sub-angular to very angular particles). The cumulative frequency curves show very similar gradients (slopes) while the mean (taken as $PropA_{50,P}$) ranges between 7.5% and 10%. Rock type 03 is most angular. The "A" and "B" subclasses of rock type 03 differ considerably in terms of angularity.

After the test, the occurrence of rounding is clearly apparent for all rock types (Fig. 39 bottom). The range between the roundest and the most angular rock type has increased ($3\% < PropA_{50,A} < 6.5\%$), and the slope values have also decreased. Thus, the range between the roundest and the most angular particles within one sample has increased. This effect is least pronounced for rock type 10. Rock type 04 exhibits the largest decrease in angularity as well as the roundest post-test configuration (see also Fig. 40). Here, for both subclasses, the mean post-test angularity, $PropA_{50,A}$, corresponds to the respective pre-test value, $PropA_{50,P}$. This is also the case for rock types 03A and 03B, and for 10A and 10B. Thus, no correlation between initial angularity and the degree of rounding was found.

Evaluation of tests

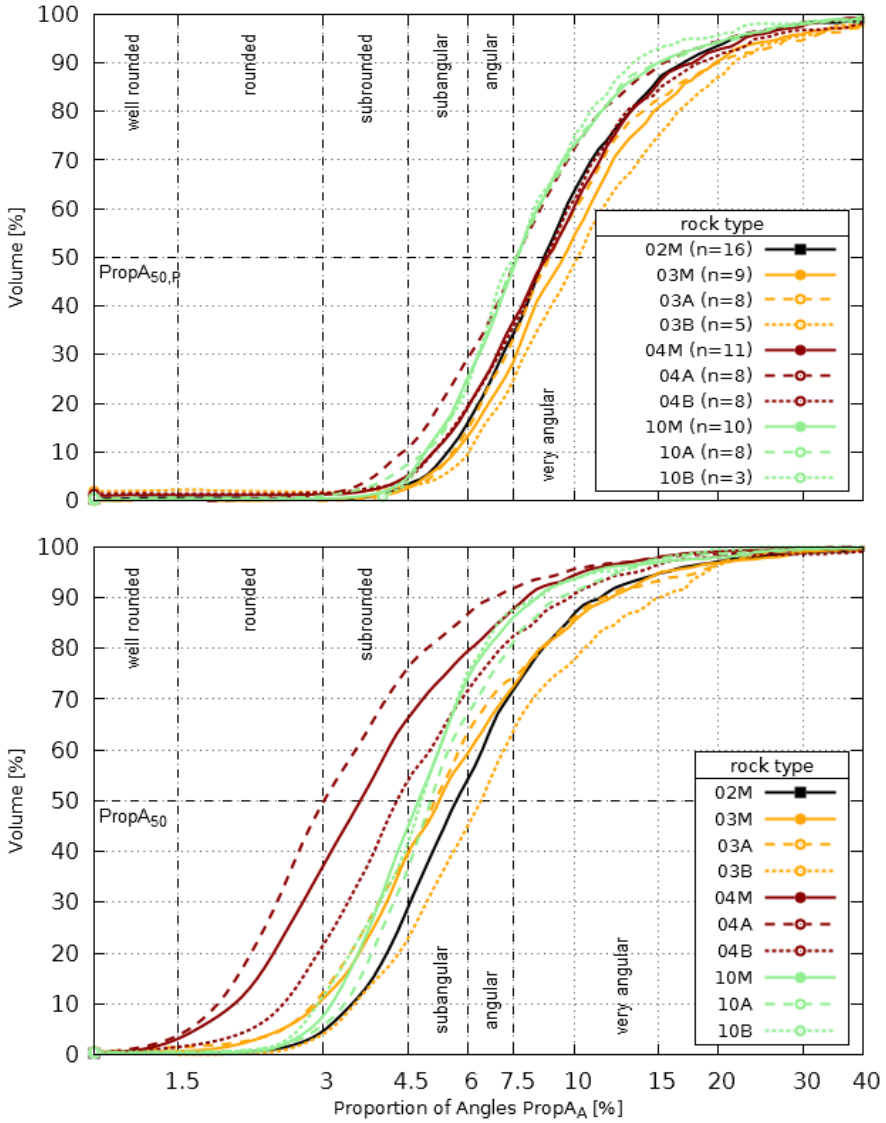

Fig. 39: LA tests – Angularity prior to test (top) and after test (bottom)

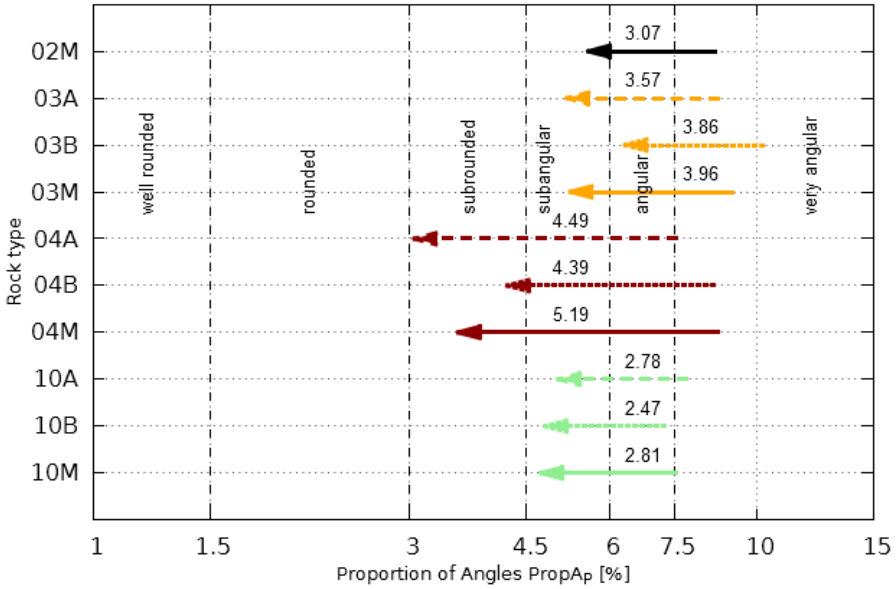

Fig. 40: LA tests - Decrease in angularity

5.2.3 Rounding by particle size

The gradations 31.5/50 ("coarse"), 16/31.5 ("medium") und 4/16 ("fine") are now analysed separately in terms of their angularity. Fig. 41 depicts the cumulative frequency curves with respect to angularity, stated as proportion of angles, PropA, for the three above mentioned gradations, together with the initial distribution of angularity (31.5 to 50 mm grains only).

Rock types 02M, 03A and 03B all reveal similar behaviour: the gradations 31.5/50 and 16/32 show an approximately similar degree of rounding. Compared to the initial configuration, the slope values haven't changed much. The gradation 4/16 exhibits a less inclined slope and a considerable degree of rounded and well-rounded grains. There are fewer particles, and the angularity is similar to that found in the initial configuration.

Rock types 04A, 04B and 10M yield a different result: the medium sized grains are rounder than the coarse sized ones, which are in turn rounder than those in the initial configuration. For the fine gradation, a wide range of angularity exists. About half of the gradation is about as angular as in the initial configuration.

An overview of gradation characteristics is given in Tab. 15.

Rock type	4/16 ("fine") contains angular grains?	angularity of 16/31.5 ("medium") similar to 31.5/50 ("coarse")?
02M	no	yes
03A	no	yes
03B	no	yes
04A	yes	no
04B	yes	no
10M	yes	no

Tab. 15: LA tests - Characteristics of rounding behaviour

As the load regimen of the LA-test obviously does not change during the test (i.e. 1,000 identical load cycles), we can assume that all grains are subject to rounding to an equal degree, regardless of their size. We may then conclude that for gradations smaller than 31.5 mm, angular grains must have been generated during the last revolutions of the test drum, while rounded particles must have been generated at or near the beginning of the test. A narrow range – or steep slope - of the angularity distribution thus indicates a small time span within which the respective particles have been generated. Similarly, a wide range implies that particles of the respective size have been generated throughout the duration of the test.

Evaluation of tests

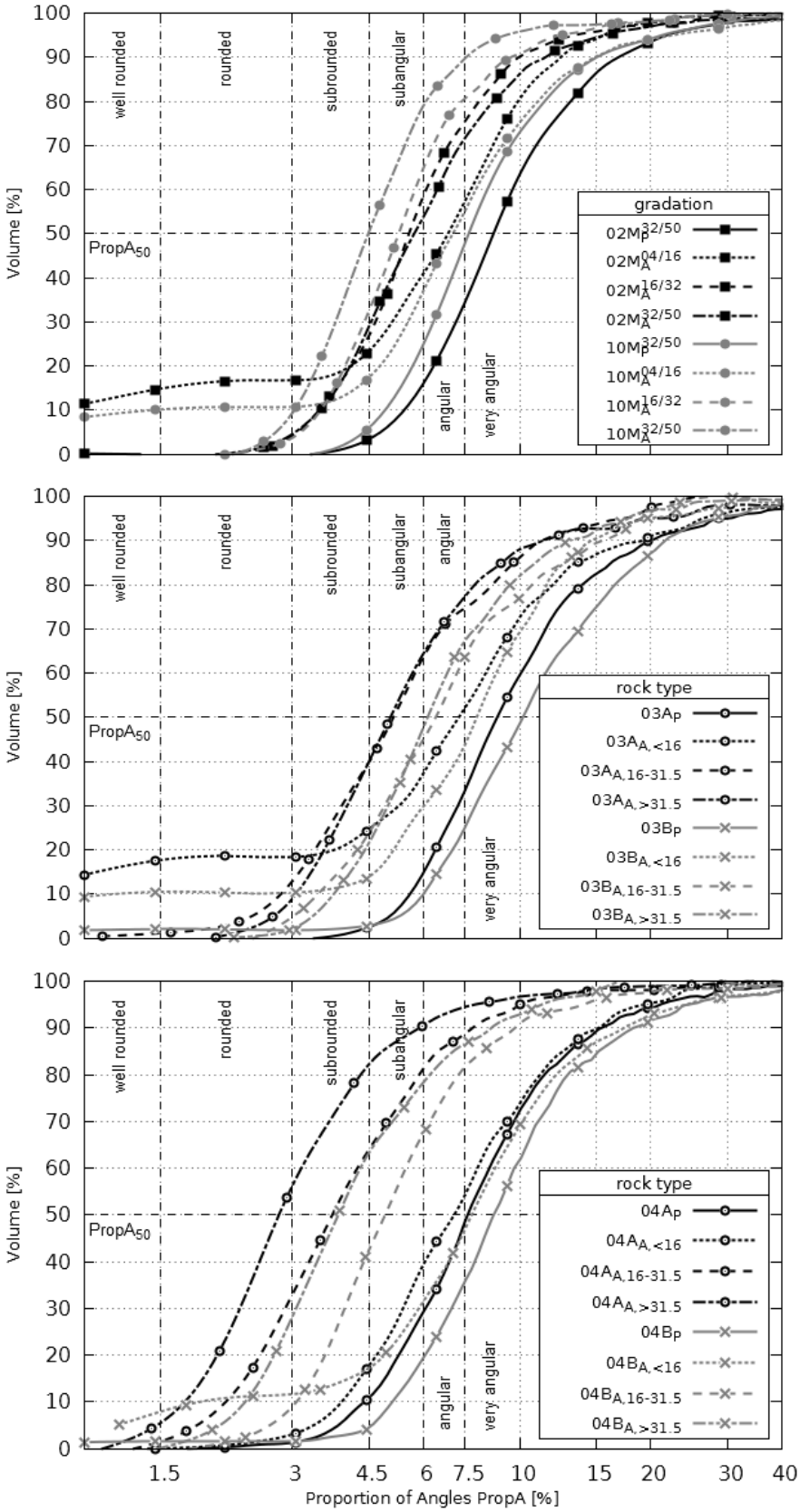

Fig. 41: LA tests - Angularity after test by gradation for rock types 02 and 10 (top), rock type 03 (center), and rock type 04 (bottom)

The similar degrees of rounding of the medium and the coarse gradation for the first group of rock types (02M, 03A and 03B) suggest that the medium sized gradation

originates from breakage processes of larger grains which then come to an end after relatively few revolutions. As the load level of the test remains constant, we can assume that the resistance to fragmentation of the respective rock types partly surpasses the load level. The weaker grains break in the course of the first dozen or hundred revolutions, whilst the stronger ones survive all 1,000 load cycles, and are only subject to rounding and abrasion. As the angularity of the fine gradation doesn't reach the respective values of the initial configuration, we can conclude that only a small part of this fraction was generated towards the end of the test (Fig. 16). It seems doubtful that the fragmentation kinetics of these two rock types are similar. The question is whether continuation of the test would result in a significant further decrease in large and medium sized particles (Wieden, Augustin & Zieger 1977).

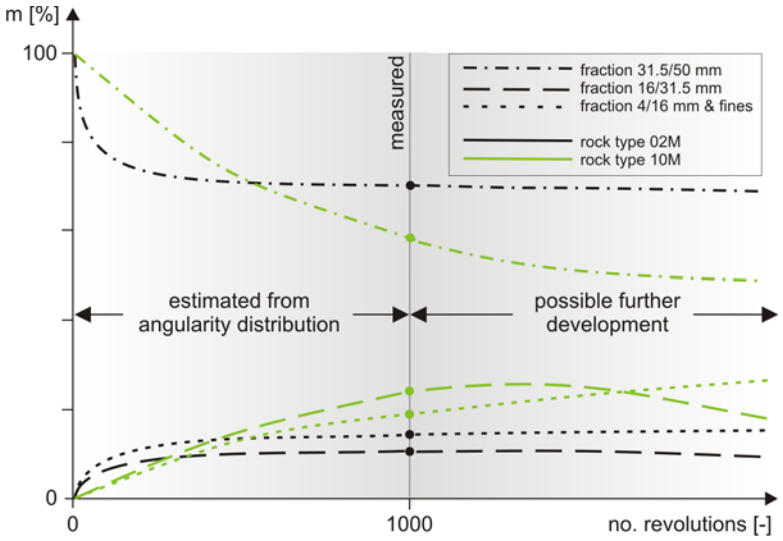

Fig. 42: fragmentation process for rock types 02 and 10 (schematic) - derived from angularity distribution

For the second group of rock types (04A, 04A and 10M), the mean angularity increases with decreasing particle size. Additionally, the smallest gradation exhibits a wide range in terms of angularity. Thus, medium sized and small sized particles must have been generated throughout the test. After 1,000 revolutions, the fragmentation processes that cause coarse sized grains to break into medium sized ones, and medium sized into small ones, are probably not yet complete. The large share of very angular particles with gradation 4/16 also indicates that fragmentation processes are still under way (Fig. 42).

5.2.4 Mass balance considerations

If we assume that rounding produces grains with d < 1.6 mm only, we can estimate the amount of volume loss due to rounding, based on the measurement of angularity before and after the test. Thus:

$$m_{d1.6,rounding}\ [\%] = 100\ (PropA_{50,P}\ [-] - PropA_{50,A}\ [-])\ m_A\ [g] / m_P\ [g] \qquad (14)$$

Fig. 43 shows that such rounding values typically range between 2.1% and 3.9%. The remaining part of the fraction $m_{d1.6}$ (=LA_{RB}) must therefore result from fragmentation (and possibly abrasion):

$$m_{d1.6,frag} = LA_{RB} - m_{d1.6,rounding} \quad (15)$$

$m_{d1.6,frag}$ varies between 10% and 21%.

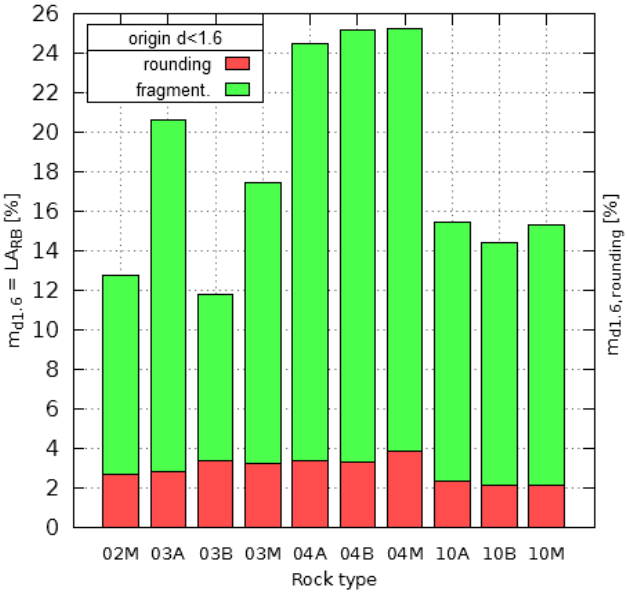

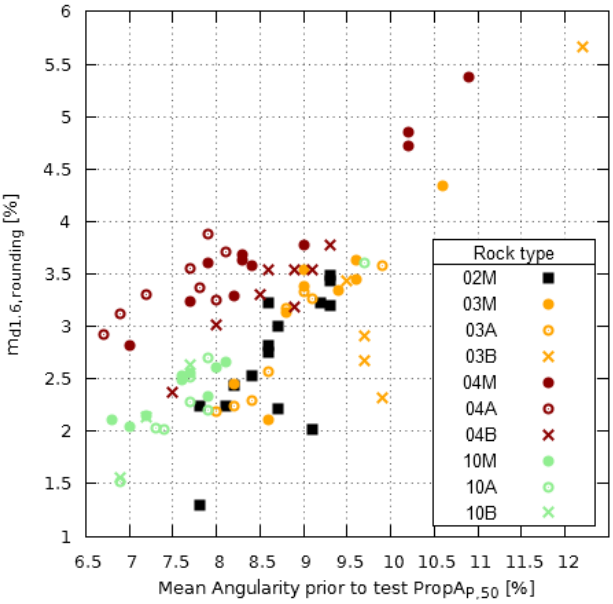

Fig. 43 (left): LA tests: fines with d < 1.6 mm - contribution by fragmentation and rounding

Fig. 44 (right): La tests - Angularity prior to test vs. loss of mass due to rounding

Note that both $m_{d1.6,rounding}$ and $md_{1.6,frag}$ hardly vary for the subclasses and the random samples of rock type 04 and 10. There is no apparent correlation with the LA-value. Rock type 03 gives a different picture: $m_{d1.6,rounding}$ shows little variety, while $m_{d1.6,frag}$ accounts for most of the observed difference in LA-values between subclass "A" and "B".

While Fig. 43 gives the results as mean values for each rock type and subclass, Fig. 44 shows the observed variety at the sample level. $PropA_{P,50}$ varies considerably within one given subclass. This is a consequence of the relatively low particle count within one sample (typically 87 to 100 particles are needed for 10 kg). For some rock types, the amount of fines generated by rounding, $m_{d1.6,rounding}$, shows a strong correlation with angularity at the subclass level (see subclasses 03A, 04A, 04B, and 10A, for example).

As a plausibility check one may contrast the number of those grains from the original sample that show a diameter < 31.5 mm after the test ("non-survived particles") with the loss of mass for the gradation 31.5/50 ($LoM_{31.5}$). Assuming only fragmentation has

occurred, and no rounding or abrasion, for a given test, both these values should be the same.

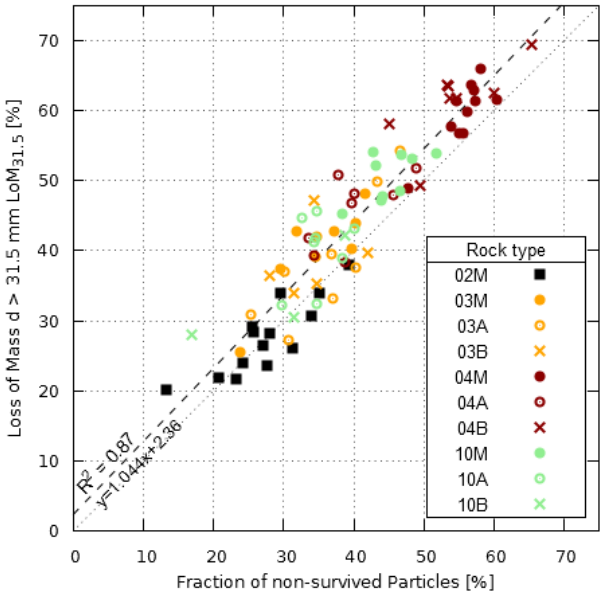

Fig. 45: LA tests - Fragmentation and loss of mass > 31.5 mm

Fig. 45 depicts the results. The strong correlation between the two values results in an almost linear relationship. $LoM_{31.5}$ exceeds the fraction of non-survived particles by 3.2% to 5.0%. This difference can only be explained by the occurrence of rounding (and possibly some abrasion) among the remaining particles. As rounding accounts for 2.1% to 3.9% of the fines, only about 1.1% can be attributed to abrasion.

The relatively small percentage of abrasion suggests that the shear stresses generated during the LA-test are minimal.

5.2.5 Particle Shape

Fig. 46 depicts the fraction of non-cuboidal particles (i.e. particles with ZINGG's (Zingg 1935) flatness ratio or elongation ratio < 0.67) both prior to test and after the test. The share of flat and elongated particles ranges from around 55% to 75 % for rock types 02 and 10, and from 75% to 90% for rock type 03. Concerning rock type 04, subclass 04A contains fewer unfavourably shaped particles than 04B.

The fraction of non-cuboidal particles typically decreases by about 10% to 12%, with minima of 0% (rock type 04B), and maxima of 20%. For some samples, chiefly from rock type 03B, the fraction of non-cuboidal particles increases in the course of the tests. If we assume that the difference between pre-test and post-test particle shape is an index for the amount of particle fragmentation, a larger share of unfavourably shaped particles should result in increased breakage. However, no such connection could be found.

Evaluation of tests

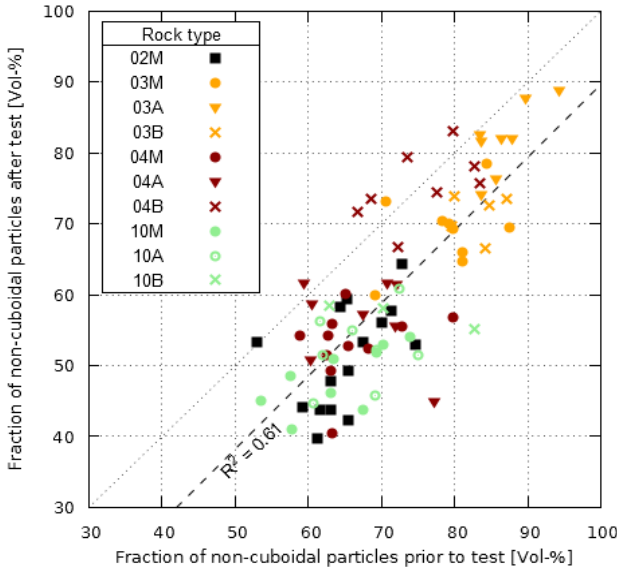

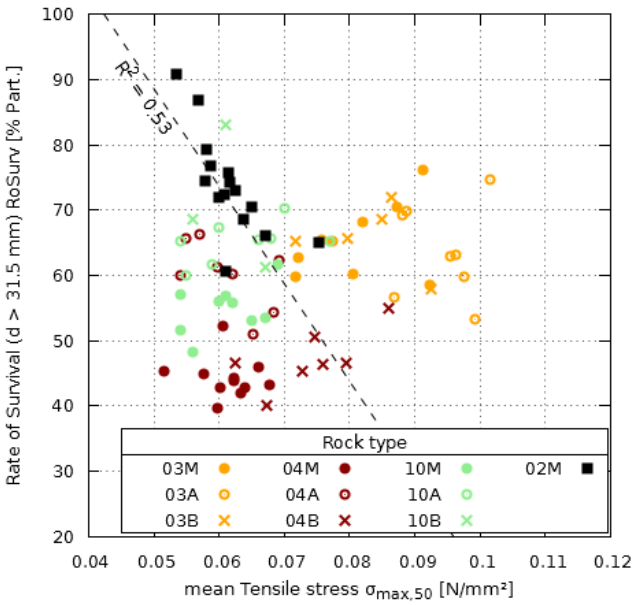

Fig. 46 (left): LA tests - Fraction of non-cuboidal particles prior to test and after test

Fig. 47 (right): LA tests – mean tensile stress $\sigma_{max,50}$ and Survival Rate of fraction 31.5/50

For rock type 02 (basalt), which is considered to be most homogenous in terms of petrographic composition, a strong correlation with the rate of survival could be detected (Fig. 47). Correlations are significantly smaller for rock types 03, 04 and 10. Here, other factors of influence (such as anisotropic material properties, large deviations of tensile strength within one rock type or one subclass, cracks caused by an inadequate crushing technique) seem to override the impact of shape.

Wieden, Auguston & Zieger (1977)'s Los-Angeles test series using gradation 10/14 mm showed that the rock type with most flat particles (a granulite) yielded the best test result, which confirms the findings of the present study.

5.2.6 Alternatives for a characteristic number

As outlined in sections 5.2.1 to 5.2.4, LA_{RB} cannot be regarded as an accurate description for the sample's resistance to fragmentation, as it

- includes fines generated by rounding and abrasion (Fig. 43) and thus inevitably overestimates the degree of fragmentation by up to 5 Mass-% (Fig. 44)
- is not representative for the particle size distributions after the test – at least for some rock types (Fig. 38, rock types 04A and 04B)

In section 3, two methods for a precise determination of the degree of fragmentation have been discussed. They are all based on the change in particle size distribution. The

Evaluation of tests

Degree of Fragmentation, based on EMPA's aggregate crushing test regulation, is easy to determine if the pre- and the post-test PSD's are known.

Fig. 48 gives the results. The fraction of fines generated by rounding (Fig. 43) is not included. The differing PSDs of rock types 04A and 04B are correctly represented, as are the differences in PSD between rock types 03A and 03B. The respective LA_{RB}-values (Fig. 36) seem to underestimate the differences in fragmentation behaviour of rock type 04A and 04B, and also seem to underestimate the respective differences of rock type 03A and 03B.

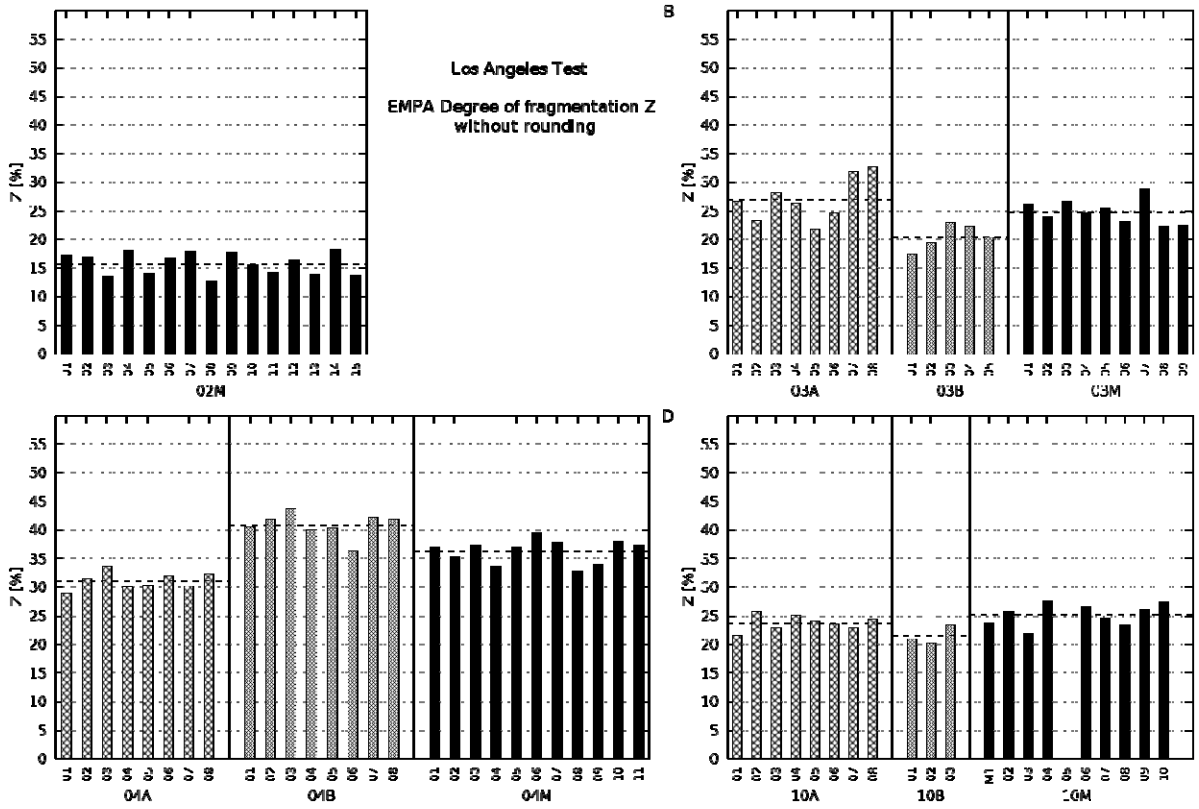

Fig. 48: LA tests – Degree of Fragmentation Z as defined by EMPA ((Wieden 1969))

Determining the particle size distribution for every Los Angeles test would improve insight into the mechanical behaviour of the sample in many ways and would yield a more precise determination of the degree of fragmentation. Using a 31.5-mm-sieve instead of a 1.6-mm-sieve would not add to cost. Using both sieves would result in two weighing processes instead of one, leading to a small increase in effort and expense.

The loss of mass values for the initial 31.5/50 mm gradation, i.e.

$$m_{1.6/31.5}\ [\%] = 100 \cdot (m_{31.5}\ [g] - m_{1.6}\ [g]) / m_P \qquad (16)$$

as shown in Fig. 49, exhibit considerable variation, especially for rock type 02 and 03. Differences in fragmentation behaviour are visible for rock types 04A and 04B but not for rock types 03A and 03B.

Correlations of Z and LA_{RB}, LoM and the fraction 1.6/31.5 mm (i.e. 100% - LoM – LA_{RB}) are compiled in Fig. 50. Correlation is generally strong for rock types 04 and 10, acceptable for rock type 03, but weak for rock type 02. Correlating Z with the fraction 1.6/31.5 mm yields the best results. Based on these observations, using an additional sieve with diameter 31.5 mm, weighing both screenings and choosing the fraction 1.6/31.5 mm as a characteristic number would be a good approximation for the degree of fragmentation. This could be done instead of using LA_{RB}.

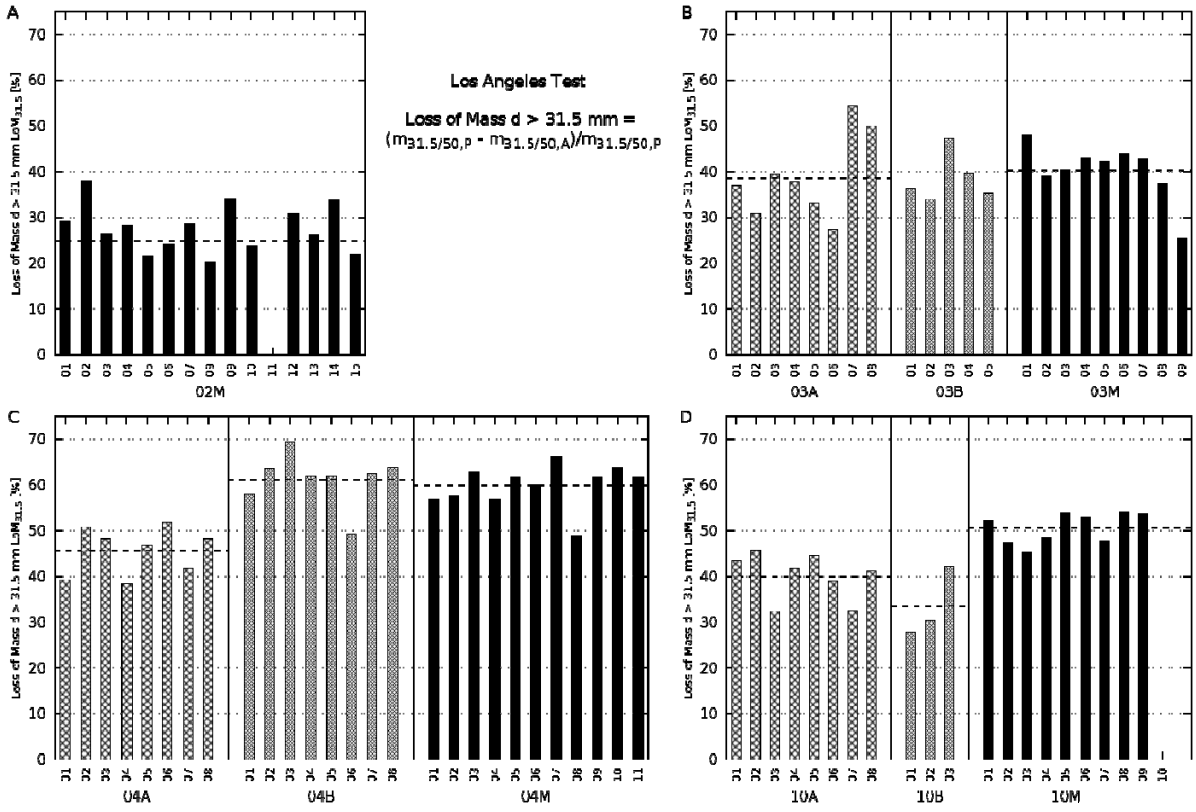

Fig. 49: LA tests – Loss of Mass d > 31.5 mm

Evaluation of tests

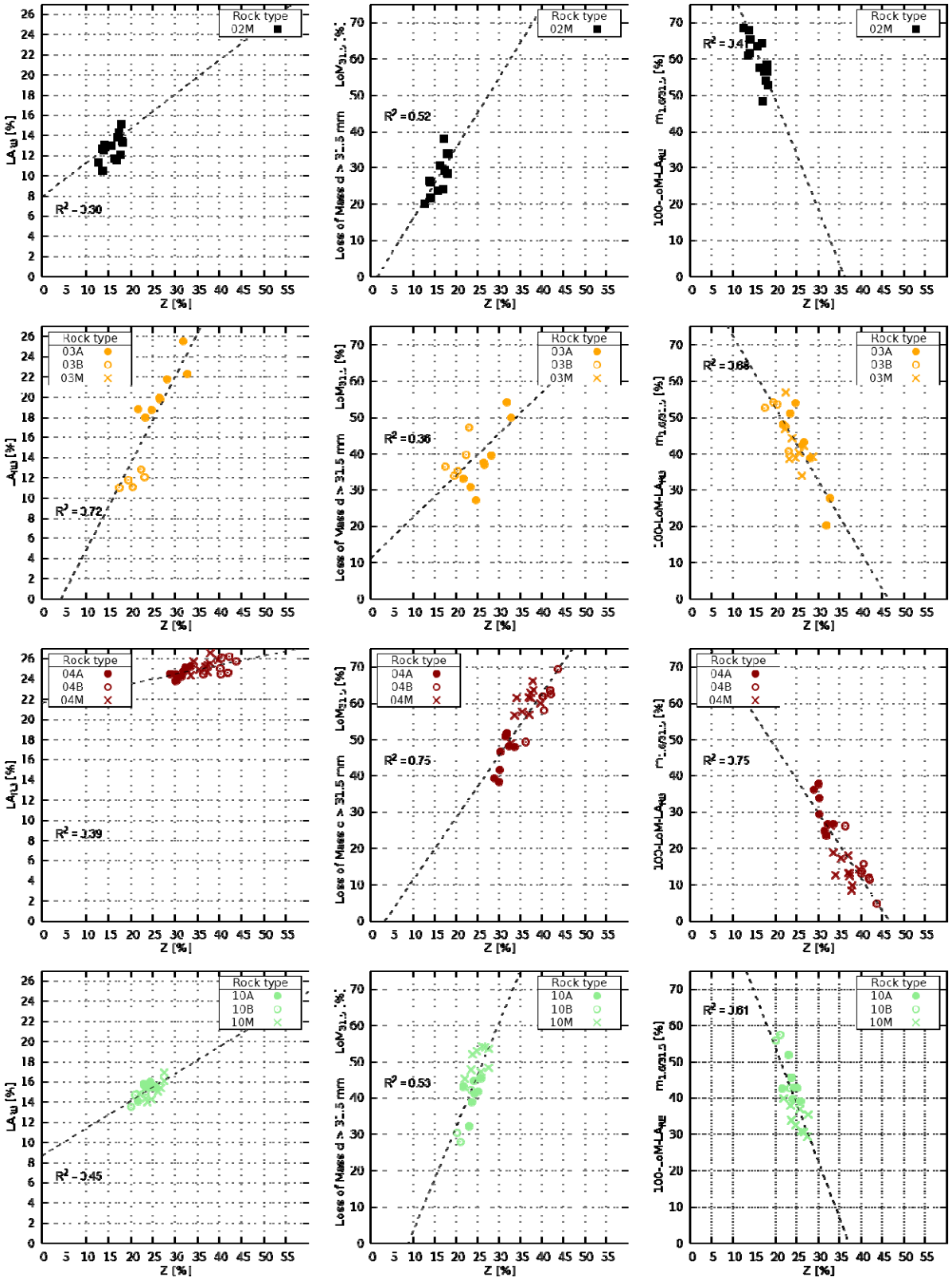

Fig. 50: LA tests – Degree of Fragmentation Z – correlations with LA_{RB} (left), Loss of Mass d>31.5 (middle) and $m_{1.6/31.5}$ (right)

5.3 Compression test (SN 670 830b)

A total of 23 compression tests according to Swiss standard SN 670 830b (Schweizerischer Verband der Strassen- und Verkehrsfachleute 2007) were carried out with samples from 2011 (Pixner 2011), including one test per rock type for types 01 & 03 to 10, two tests for rock type 11, and 12 tests for rock type 02, which, in terms of petrographic composition, was considered to be homogenous. As outlined in section 4.2, one test in terms of the standard consists of two identical sub-tests. The mean of the two sub-test results constitutes the test result. In this section, the term "test" refers to one sub-test.

The standard calls for the determination of the fraction $m_{d<22.4mm}$ only. The test series presented here also included a measurement of the pre- and post-test sample volume, a record of the load-displacement curve (test frequency 0.2 sec; recorded for rock types 01 to 05 and 07 to 11), and a determination of the particle size distribution after the test.

Fig. 51 (left) gives the results for the test result parameter DZ_{RB} per rock type (i.e. mean of all respective tests). Most rock types exhibit values between 35% and 38%, maximum values reach 50%.

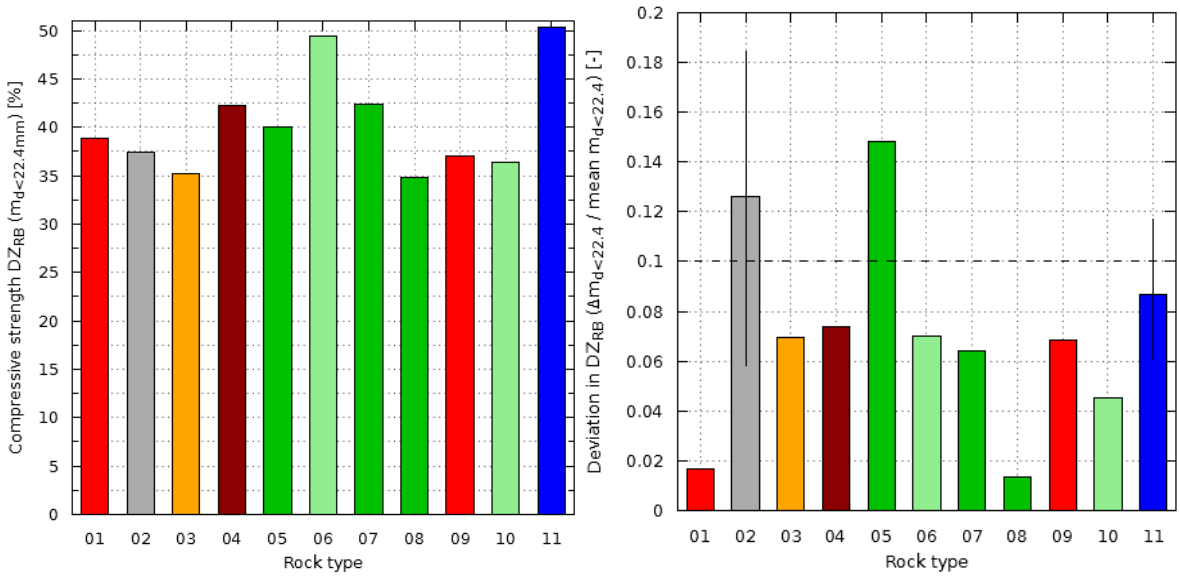

Fig. 51: Compression tests: Compressive strength DZ_{RB} (left) and its deviation (right)

Fig. 51 (right) shows the difference between the two respective test results for rock types 01 & 03 to 10 and the mean of the differences between any two results for rock types 02 and 11. The error bar indicates the inter-quartile range for these differences. For five rock types (03, 04, 06, 07 and 09) the deviation of results is about 4% to 6% of the respective mean, whilst rock types 01 and 08 show a very small deviation of less than

2%. For rock types 02, 05, and 11, the variance violates the repeatability limit of 10%, indicating that the test result needs to be discarded.

The use of DZ_{RB} = $m_{d22.4}$ as a test result parameter proved to be good characteristic for the particle size distribution after the test (Fig. 52 left). EMTA's Degree of Fragmentation Z, as described in section 3, correlates well with DZ_{RB} (R^2 = 0.93; compare Fig. 51 (left) and Fig. 52 (right)). Thus, DZ_{RB} gives an accurate description of the degree of fragmentation of the respective sample.

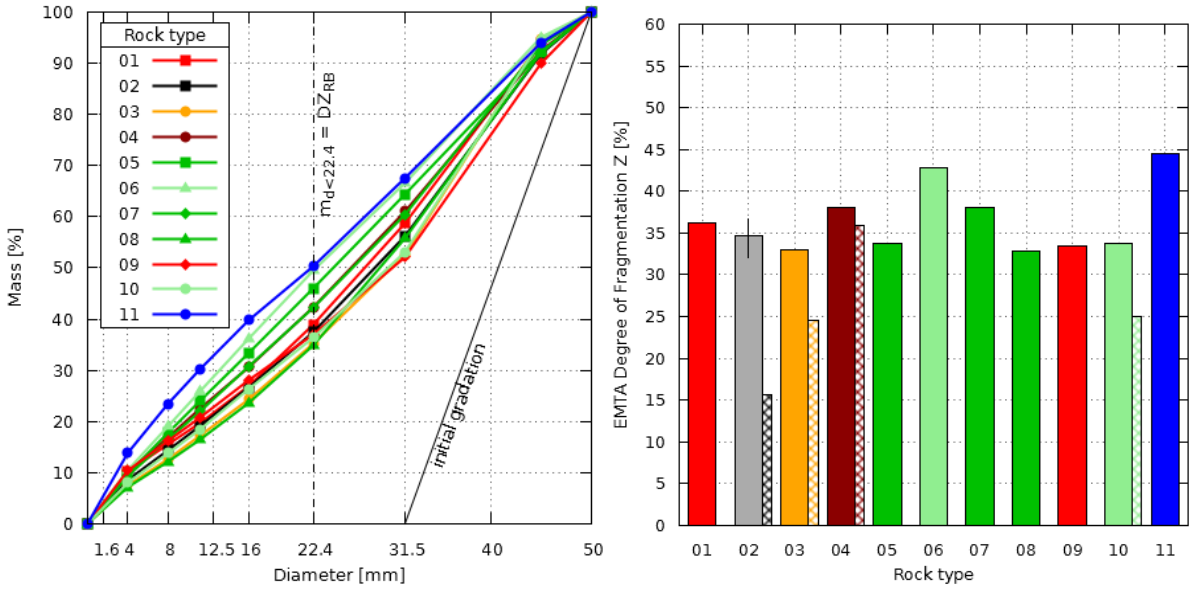

Fig. 52: Compression tests – Particle size distribution after test (left) – Degree of Fragmentation Z (right)

However, using a smaller sieve size would yield similar results. In (McDowell et al. 2004) a correlation coefficient R^2 of 98% is given for the relationship of ACV value (i.e. $m_{d2.36}$) and Hardin's Total Breakage B_t.

The degree of fragmentation, expressed as DZ_{RB}, correlates well with axial strain (Fig. 53).

Evaluation of tests

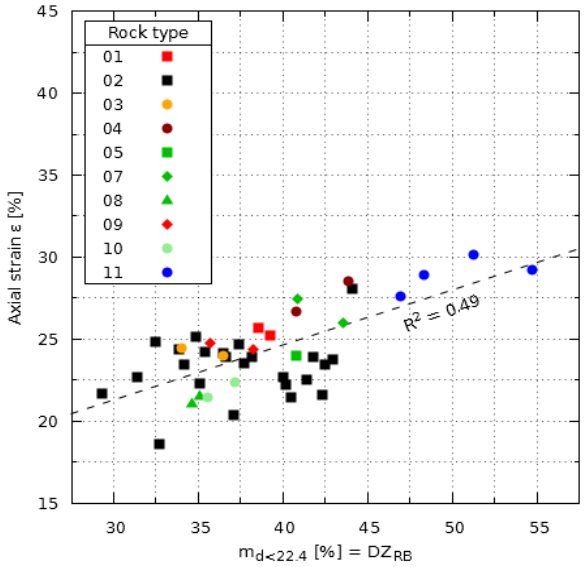

Fig. 53 (left): Compression tests – DZ_{RB} and axial strain ε

The degree of fragmentation Z decreases with increasing mineral hardness (Fig. 54). The correlation is non-linear, presumably due to the large mineral sizes of the granites type 01 and 09 and the granulite type 06. As Liu et al. (2005) showed on the examples of granite varieties, an increasing mineral size results in a decrease in uniaxial compressive strength.

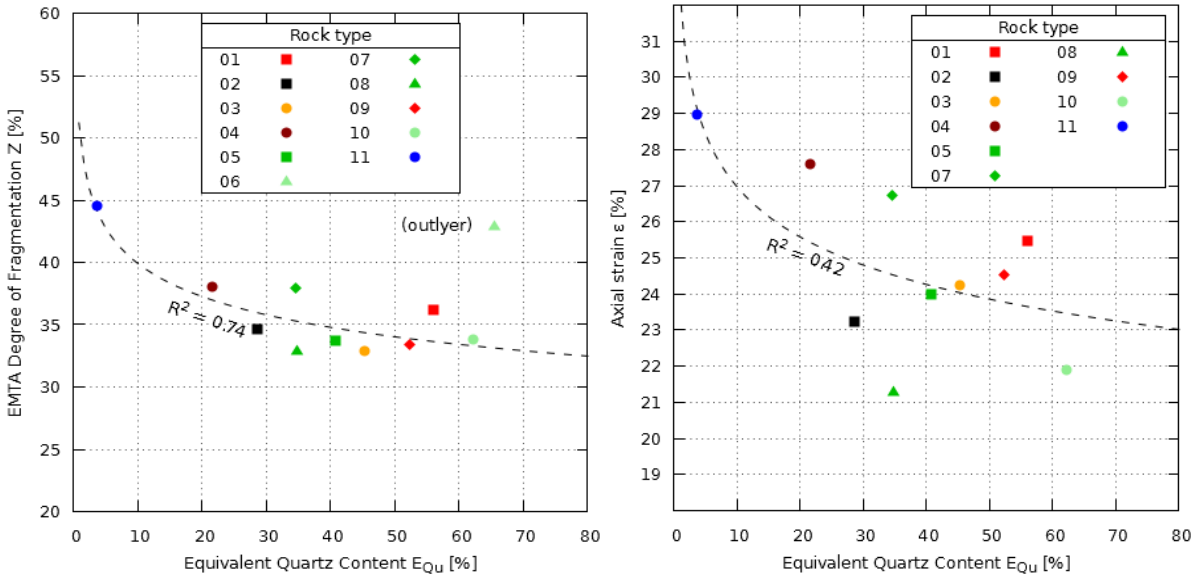

Fig. 54 (left): Compression tests – Equivalent Quartz Content E_{Qu} and Total Breakage B_T

Fig. 55 (right): Compression tests – Equivalent Quartz Content E_{Qu} and axial strain ε

Strain ε also correlates with E_{Qu} (Fig. 55), but with lower significance. This is caused in part by the fact that no uniform compactness was present, presumably due to the manual compaction method used as described in the standard. The pre-test void ratio e_{init}, based on a measurement of the position of the piston, ranged between 0.85 and

Evaluation of tests

1.04. In McDowell's comparison of standard ACV test results and the results of a large oedometer test, discrepancies between the test results were partly blamed on the different compaction methods used (vibrating table / tamping rod), although differences in e_{init} were much smaller than in the test series presented here (McDowell et al. 2004).

Compaction of the sample is also influenced by wall friction. The test cylinder is rather slim (aspect ratio H:D is 1.3 : 1). Assuming a wall friction coefficient μ of 0.5, and using McDowell 's relation (McDowell, Lim & Collop 2003)

$$\frac{\sigma_1}{\sigma_2} = e^{\left(\frac{4\mu KH}{D}\right)} \qquad \text{with K: coefficient of earth pressure at rest} \qquad (17)$$

results in a stress ratio σ_1 / σ_2 of 2.24, or an error of the order of 55%. The maximum stress at the bottom of the sample might only be 6410 kPa, with 14435 kPa applied on top.

In Fig. 56, the macroscopic stress applied is plotted on a log-scale against compaction (i.e. change in void ratio), similar to Fig. 26 (p. 37). The test results of rock type 02 (Fig. 56, A) illustrate poor repeatability in terms of initial void ratio and load-compaction behaviour. Simply judging by naked eye, the point of maximum curvature, indicating yield, is at about 70 KN to 100 KN. The corresponding strain is approx. 15% – 20%, which is clearly below McDowell & Harireche (2002)'s findings of 30% (see section 4.2). The same holds for most of the other rock types. This may partly be blamed on the comparatively small diameter of the Swiss test cylinder and on the relatively fast loading rate, which complicates particle rearrangement at low stress levels. Yielding occurs only very gradually (except for rock types 07 and 09). This is likely to be caused by the high wall friction.

The dotted lines indicate 13% of the 37% tensile strength of the particles, as postulated in McDowell & Harireche (2002) (see section 4.2). Values were calculated on the basis of Breymann's point load test results ((Breymann et al. 2011); see also Fig. 34, p. 50). Correlation is good to fair for rock types 04, 05, 07, 08 and 10, but poor concerning the other rock types.

Evaluation of tests

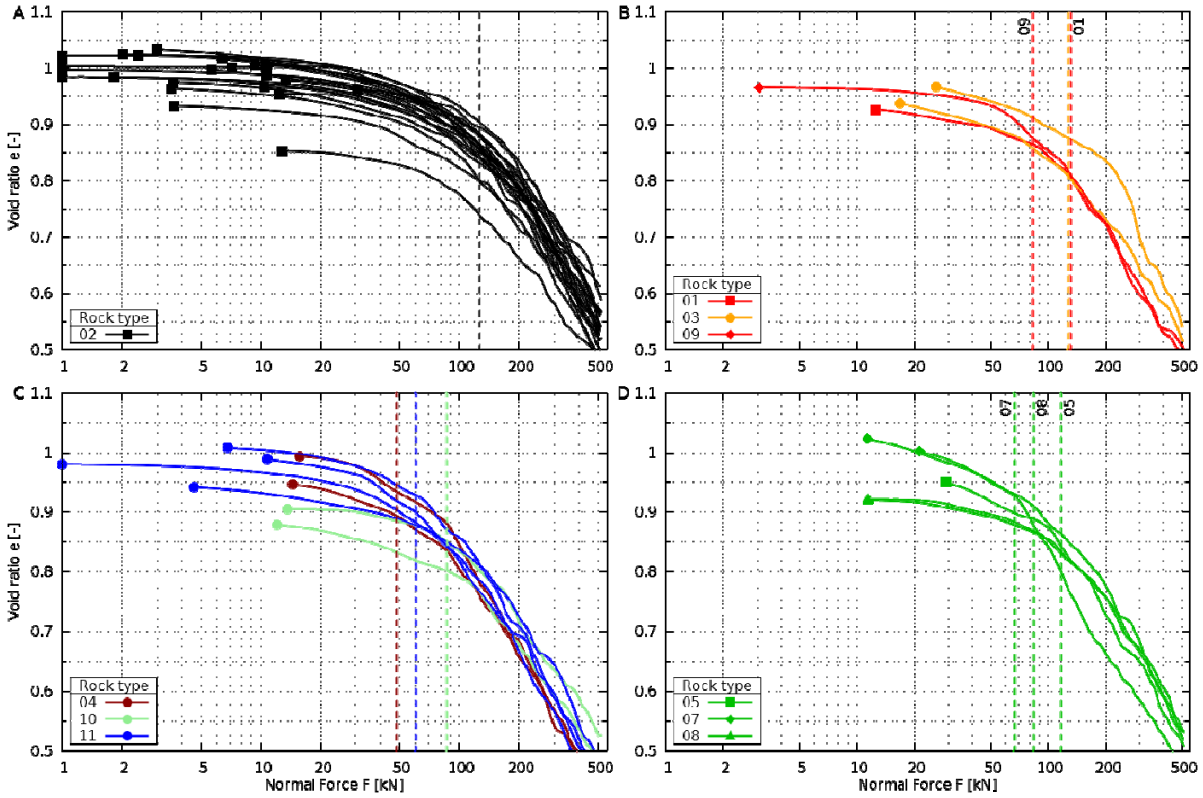

Fig. 56: Compression tests – applied force, F ($\log_{10}$ scale), and void ratio, e, for basalt (A), granites and granitic porphyry (B), diabase rocks (D) and dunite, granulite and dolomite (C) (smoothed) compared to point load test results

5.4 Deval test

The Deval tests, carried out with samples from 2011, consisted of three series (Schöck 2011):

- Two standard dry attrition tests per rock type for types 02 to 11, together with additional determination of the particle size distribution by sieving and a Petroscope® scan of the particle geometry (series Dev-I).

- Another two wet attrition tests per rock type for types 02 to 04, 06 to 08 and 10 to 11, also with additional determination of the particle size distribution and a Petroscope® scan of the particle geometry (Series Dev-II).

- Two dry attrition tests per rock type for types 02 to 11 with determination of gradation after 250, 500, 1,250, 4,000, and 10,000 revolutions in order to record the abrasion and rounding process as a function of the number of load cycles (for rock types 02 and 11, interim values were measured after 2,000, 4,000, 6,000, 8,000, and 10,000 turns). Here, too, a Petroscope® scan was carried out (Series Dev-III).

Evaluation of tests

Fig. 57 contrasts the results of the dry tests (mean of 4 tests, series Dev-I and Dev-III) and the wet tests (mean of 2 tests, series Dev-II). The WAV surpasses the DAV by a factor 1.5 to 2.9 (Fig. 58).

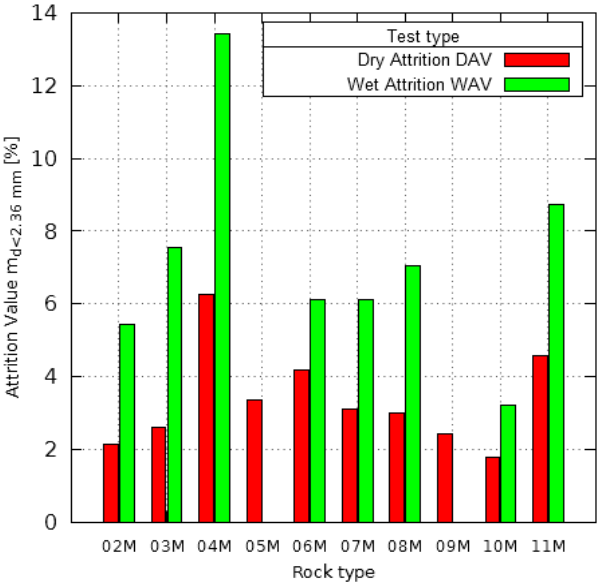

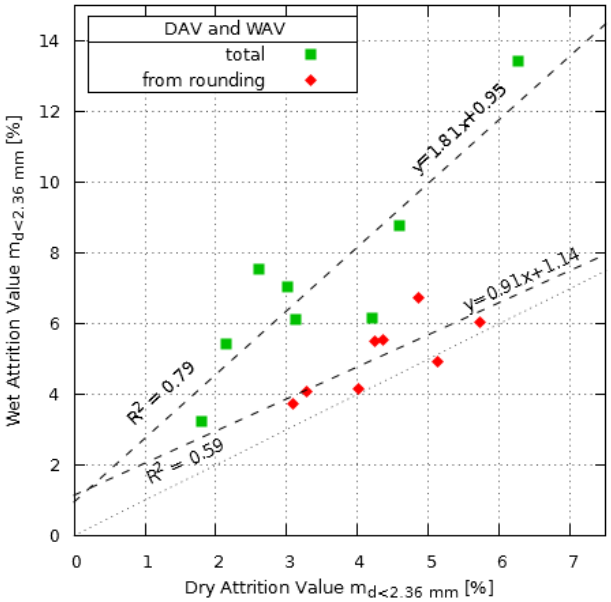

Fig. 57 (left): Deval tests – Dry Attrition value DAV and Wet attrition value WAV

Fig. 58 (right): Deval tests – DAV and WAV – total values and fines generated from rounding

As outlined in section 4.3, the wet attrition test causes increased abrasion due to the fact that newly generated fines dissolve in water and do not act as a coating, as is the case in the dry test.

A mass balance consideration is used to verify this assumption. If we assume that rounding produces grains with d < 1.6 mm only, we can estimate the amount of volume loss due to rounding, based on the measurement of angularity before and after the test. Thus

$$m_{d2.36,rounding} = (PropA_{50,P} - PropA_{50,A})\ m_A / m_P \quad (18)$$

where $PropA_{50}$ is a weighted mean of PropA, i.e. the mean angularity of the sample. $PropA_{50,P}$ refers to the configuration prior to the test, $PropA_{50,A}$ is the respective post-test value. m_A and m_P are the respective sample weights after and prior to the test. The Petroscope® scan was carried out with the fraction 4/51 after the test. No Petroscope® scan was available prior to the test. Instead, mean values from scans with ballast samples prepared for the LA tests were used (see section 5.2).

For the wet test, the fines originating from rounding surpass the respective values found in the dry test by a maximum factor 1.35 (Fig. 58). For rock types 07 and 11, there is

hardly any difference. As there is almost no fragmentation, the larger part of the remaining fines can be attributed to abrasion.

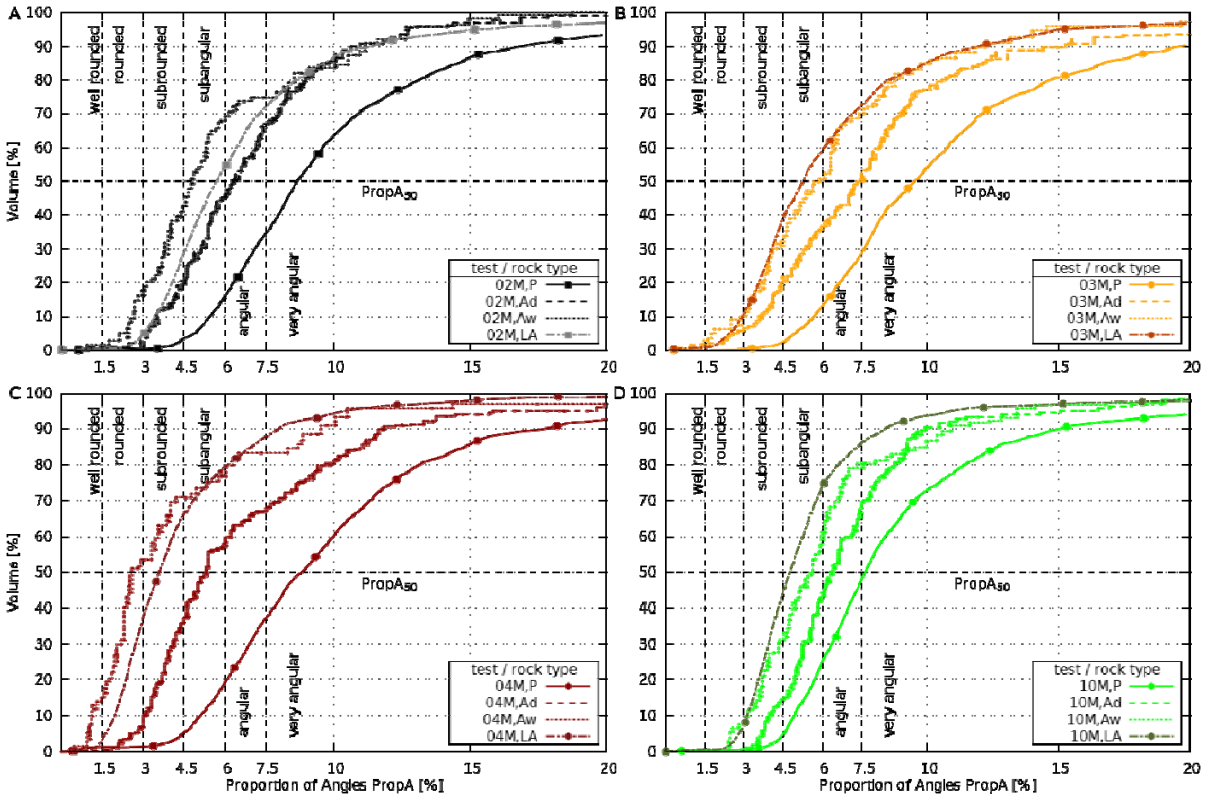

Fig. 59: Deval tests - Angularity prior to test and after test for rock types 02 to 04 and 10 (Petroscope® scan)

Fig. 59 depicts the angularity distribution before and after the test for rock types 02, 03, 04 and 10, i.e. for those rock types that underwent the Los-Angeles test series (see also section 5.2). For purposes of comparison, results of the dry ("Ad") and the wet tests ("Aw") are given (as step functions), as well as those of the respective distribution of the Los-Angeles tests ("LA") (see also Fig. 39, p. 57). Due to the small amount of mid-sized particles (04/31.5 mm; see also Fig. 64 and Fig. 65), Fig. 59 chiefly represents the initial gradation.

For all rock types, the wet test produces a larger decrease in angularity than the dry test. The wet test of rock type 04 (04M, Aw) exhibits a particularly large degree of rounding (> 50% "rounded" and "well-rounded").

The share of angular and very angular particles ranges between 40 and 65 Mass-% (with 04M,Aw again as an outlier (25%)), compared to pre-test values of 75% – 90%. The slope values (i.e the gradients) are steeper, compared to the pre-test configuration, but a uniform degree of angularity was not reached (as one might perhaps expect, considering the test duration). There is no discernible correlation between the degree of

rounding and the gradient. Post-test slope values are similar for the Deval and the LA test.

The degrees of rounding of the dry Deval tests do not surpass the respective values of the LA tests. For rock types 03 and 10, even the wet test exhibits smaller rounding than the LA test, despite the differences in load regime.

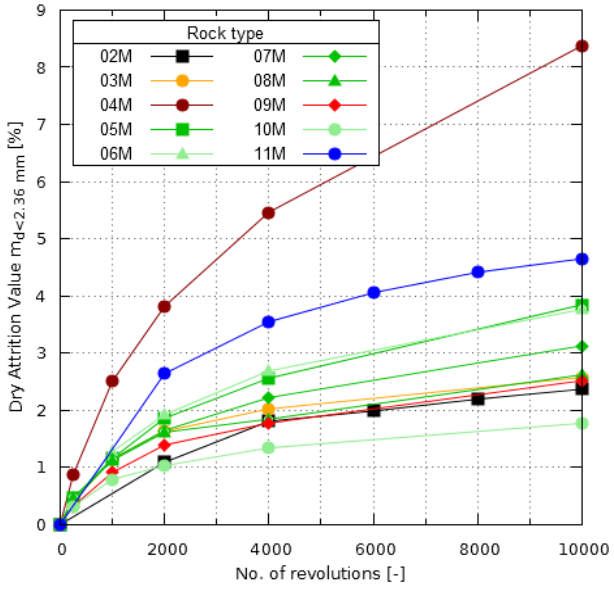

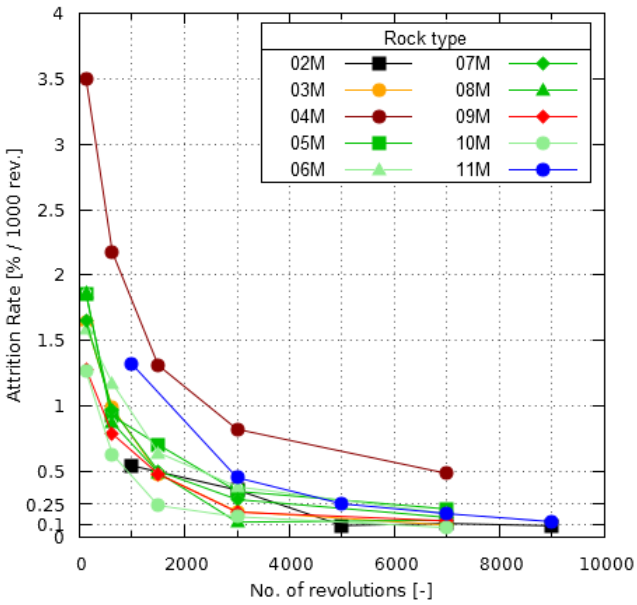

Fig. 60 (left): Deval tests (series Dev-III) – $m_{d<2.36\ mm}$ vs. no. of revolutions

Fig. 61 (right): Deval tests (series Dev-III) – Attrition rates

For the test series DV-III, the increase in fines slows down for all rock types (Fig. 60; mean of 2 tests). Fig. 61 shows the corresponding attrition rates. For most rock types, attrition rates decrease until, after some 7,000 turns, values of about 0.1% are reached.

Rock types 04 and 11, however, give a different picture: For rock type 04, the attrition rate reaches 0.5% after 7,000 turns. Additionally, the initial rates are very high (ca. 3.5%). Apparently, a quasi-stable configuration has not yet been reached at this point. Rock type 11 also exhibits high initial attrition rates, but, after a fast drop, at about 5,000 revolutions, values similar to those found for the other rock types are reached. The high DAV values of rock type 11 can thus be chiefly attributed to the high initial attrition rates.

Rock types 08 and 09 exhibit differing initial attrition rates, but show an almost identical DAV. The test result offers no hints concerning the attrition characteristics of a given rock type.

Evaluation of tests

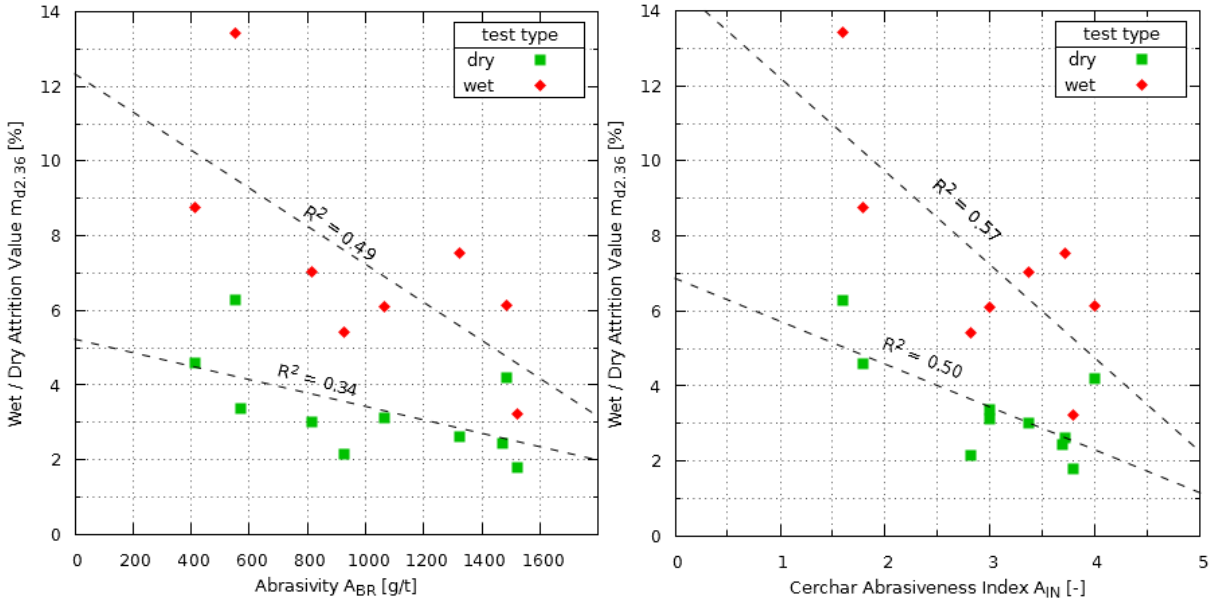

Fig. 62 (left): Deval tests – Correlations with LCPC Abroy test

Fig. 63 (right): Deval tests – Correlations with Cerchar test

As the fines produced in both variants of the Deval test result mainly from rounding and abrasion, one would expect there to be a strong correlation with the results of the tool wear tests described in section 5.5. Fig. 62 and Fig. 63 show the results for the rock types investigated (mean values; dry attrition: n = 4; wet attrition: n = 2; A_{BR}: n = 5; A_{IN}: n = 7). Higher abrasivity is related to more favourable Deval attrition values. If we assume a linear dependence, the wet tests give slightly stronger correlations. Correlations using the Cerchar tests are stronger than those found for the Abroy test, but still rather weak.

The Deval test is commonly believed to be a method "for determination of resistance to wear", and thus to be quite similar to the Micro-Deval test. Although fragmentation does occur to some extent (Fig. 64 and Fig. 65), as long as there are no or only very few fines originating from the phenomenon, it does not interfere with the DAV and WAV test results.

The bar charts on the right show that the fraction 4/16 is small for almost all rock types, regardless of the test variant (mean 0.6% dry test, 1.54% wet test). Fraction 16/31.5 is small for the wet test, but makes up 8% for the dry test. The coarse fraction 31.5/37 is the largest for all rock types. It should be noted that particles with a diameter only slightly larger than 37 mm prior to the test whose diameter falls just below 37 mm during the test (due to rounding and/or abrasion) may contribute to the fraction 31.5/37.

Evaluation of tests

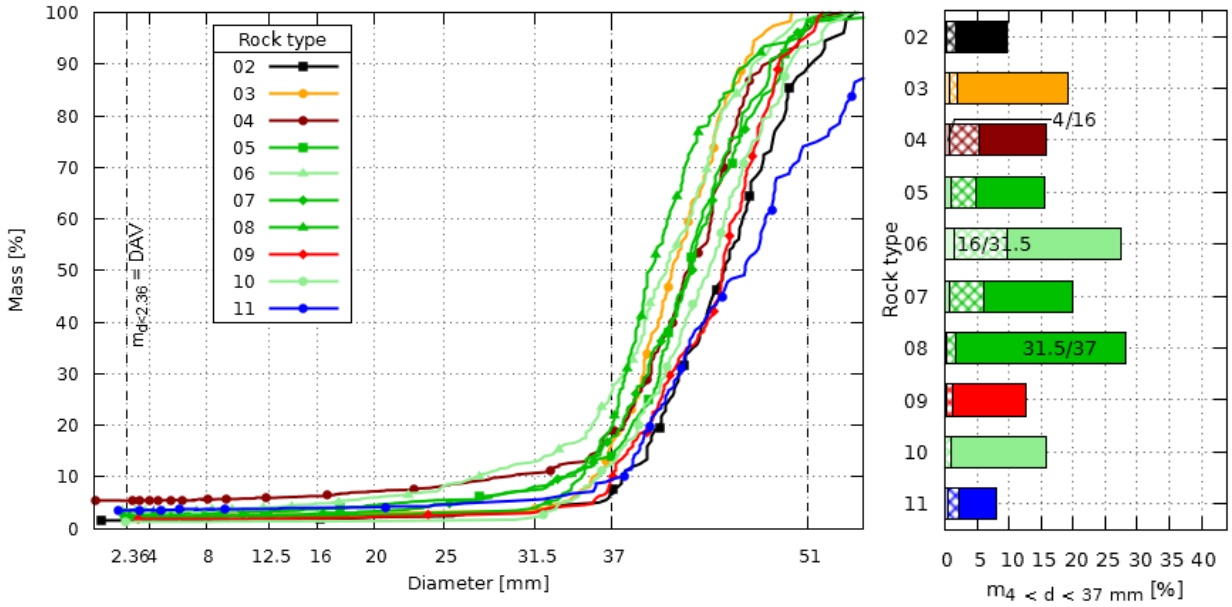

Fig. 64: Deval tests (series Dev-I & Dev-III): particle size distribution (dry tests) and fractions 04/16, 16/31.5 and 31.5/37 (Petroscope© scan data)

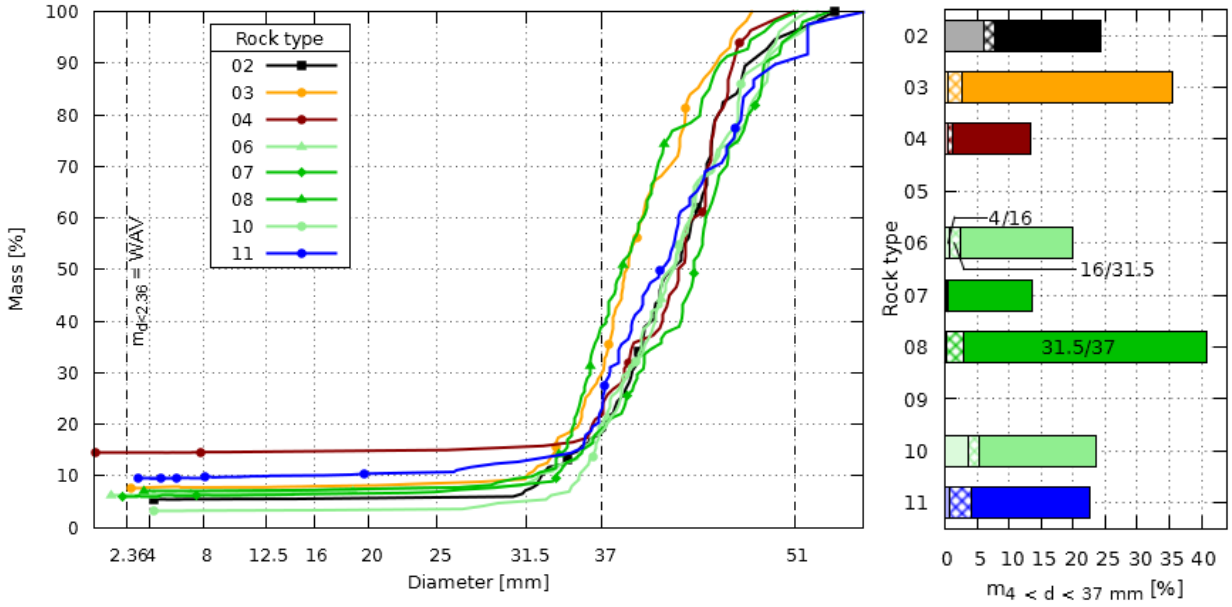

Fig. 65: Deval tests (series Dev-II): particle size distribution (wet tests) and fractions 04/16, 16/31.5 and 31.5/37 (Petroscope© scan data)

In order to estimate the impact of fragmentation on the test result, an idealized sample with no fragmentation at all (Fig. 66, black line) is compared to a sample which does not exhibit fragmentation, but does exhibit a certain decrease in particle diameter due to rounding and abrasion (Fig. 66, orange line) and finally, with a typical 'real world' test (Fig. 66, blue line).

Evaluation of tests

Thus, where no fragmentation has occurred, the red area marks the respective change in particle size distribution (or "degree of fragmentation" Z according to EMPA[1]). Where particle diameter decrease is taken into account, the respective Z-value equals the sum of the red and the green area. The lower limit of the fraction on fines due to fragmentation contained in DAW, or WAV, can then be expressed as the ratio of the blue area and the total of Z (i.e. red + green + blue area).

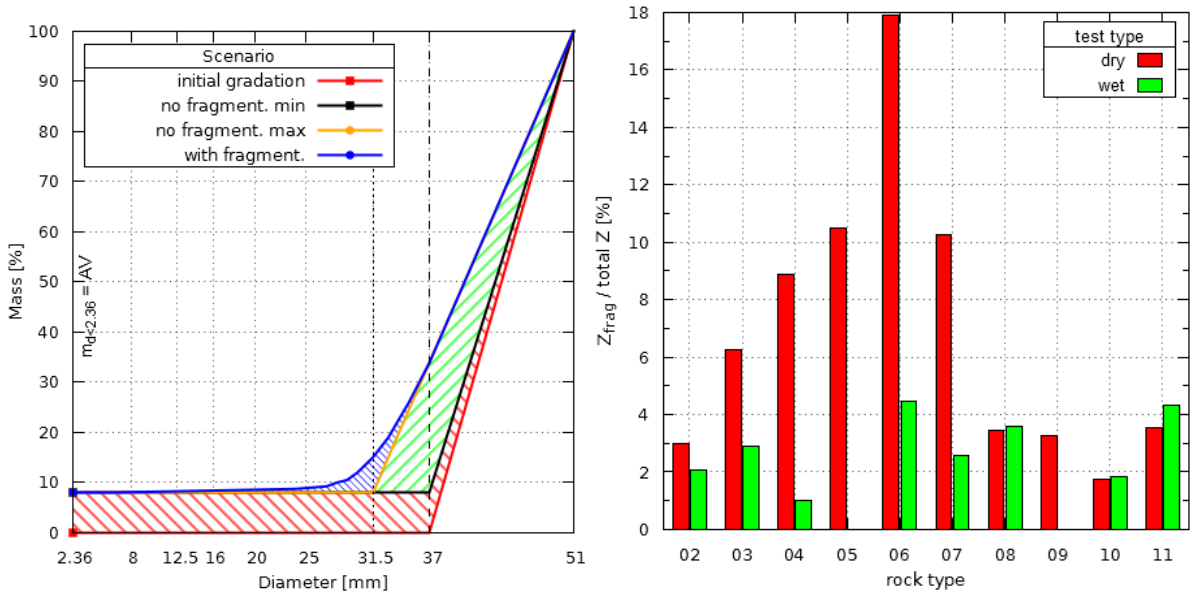

Fig. 66 (left): Deval tests – impact of fragmentation (schematic)

Fig. 67: Deval tests – ratio of degree of fragmentation Z due to true fragmentation and total Z (including rounding and abrasion)

The results are given in Fig. 67 for both test types. For most rock types, the dry test shows a much larger impact of fragmentation on the test result than the wet variant, for which values hardly exceed 4%. However, since test drum length is the main determinant in the fragmentation process, the relatively small length of the test drum (35 cm) used here (see Fig. 28), does constitute a weak point in construction design.

[1] Here, despite its name, "degree of fragmentation Z" refers to the integrated difference in particle size distribution, regardless of the underlying attrition mechanism

5.5 Abrasion tests for tool wear estimation (Abroy- and Cerchar test)

5.5.1 Results and impact of mineral hardness

The test series discussed in this section are summarized in Tab. 16.

term	Test method	Sample origin	Test per rock type/subclass	tested rock types /subclass	Sum
ABR-I	LCPC test	2011 suitability test	5	all	55
ABR-II	LCPC test	2012 suitability test	4	02, 03, 03A, 03B 04, 04A, 04B, 10, 10A, 10B	40
CAI-I	Cerchar test	2011 suitability test	7	all	77
CAI-II	Cerchar test	2012 suitability test	5	02, 03A, 03B, 04A, 04B, 10A, 10B	35

Tab. 16: Abroy- and Cerchar-Tests - test series – overview

A_{IN} and A_{BR} show a wide range of values (Fig. 68A) (Latal, Bach & Thuro (2013), Hollersbacher (2011), Uhlig (2011) and Fuchs (2012)). Mean values of A_{IN} can be classified as "abrasive" for dolomite and dunite, while all other rock types can be classified as "very abrasive", with some reaching the upper limit in this category. Looking at the A_{BR} values, a better discrimination of the rock types is possible, as abrasivity ranges from "abrasive" to "extremely abrasive". Rock types like granulites and granites yield the highest values, while the lowest values are achieved again by dolomite and dunite.

Correlation between the two alternative testing methods is strong ($R^2 = 0.77$), especially if one takes into account the relatively small number of tests per rock type and the high variability of rock types. The correlation coefficient is only slightly lower than the comparable values found for extensive test series given in the literature (e.g. Thuro & Käsling (2009)). The correlation between equivalent quartz content E_{Qu} , A_{IN} , and A_{BR}, is presented in Fig. 68B/C. Correlation coefficients are well above 70% for both tests, indicating a strong correlation.

Fig. 68D presents results of the abrasivity tests for the four rock types studied in detail (i.e. ABR-II and CAI-II). For rock types 03 and 04, a clear difference between subclass A and B is evident for both test methods.

For rock type 03, A_{IN} values differ considerably for subclass A (2.59 to 4.39) and B (2.05 to 2.83). A_{BR} values for subclass 03B show only small variations (1,120 to 1,220 g/t) while 03A exhibits the widest range of values (1,220 to 1,520 g/t). Subclass A and B of rock type 03 show nearly no overlapping values in A_{IN} and A_{BR}.

Evaluation of tests

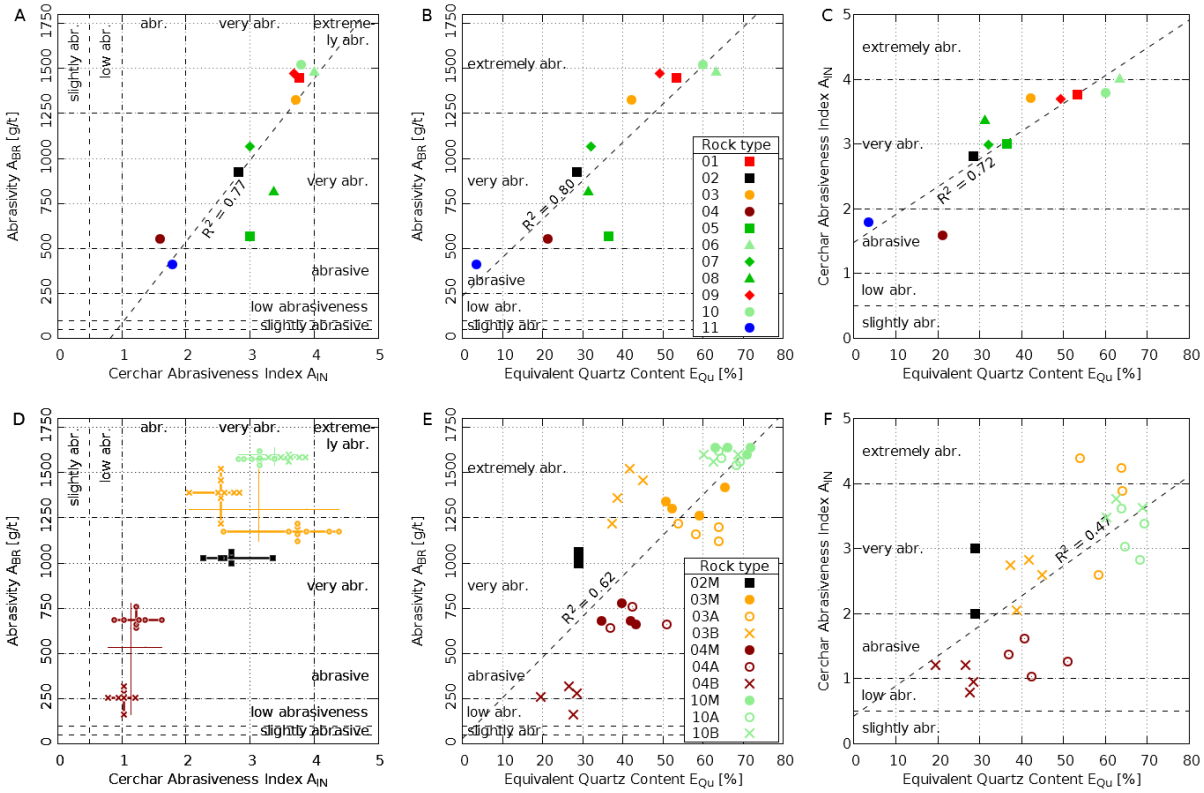

Fig. 68: Abroy- and Cerchar-Tests – correlation of the two tests (left) and influence of equivalent uartz ontent (middle & right)

For rock type 04 the difference between subclass A and subclass B results is more explicit for A_{BR}, as A_{BR} values for subclass A range from 640 g/t to 760 g/t and for subclass B from 160 g/t to 320 g/t. A_{IN} values of subclass A for rock type 04 are slightly higher but more or less in the same range as for subclass B.

For rock type 10, A_{BR} values do not differ considerably for subclass A and B, but A_{IN} values are slightly higher for subclass 10B. Rock type 02 was considered as more or less homogeneous. A_{IN} and A_{BR} values are within the value range found for the subclasses of the other rock types.

Equivalent quartz content of rock type 03B is distinctly lower than that of subclass 03A, while the respective values for 03M largely lie somewhere in between. The different abrasivity behaviour of the subclasses A and B of rock type 04 can be explained by their differing equivalent quartz content (Fig. 68E). 04M shows similar values in ABR and equivalent quartz content values to 04A. Equivalent quartz content of rock type 10 exhibits the smallest variation between A, B and M.

Note that correlation between E_{Qu} and A_{BR} and A_{IN} is weaker for test series ABR-II and CAI-II, compared to the 2011 series (ABR-I and CAI-I). The equal number of tests carried out with both subclasses is one of the reasons for this, since it leads to the impact of subclass B being over-estimated.

Evaluation of tests

As in other studies (see (Weiher 2009) for example), no relation could be found between the two Abroy test values for abrasivity A_{BR} and breakability B_R (Fig. 69). Rock types 01 and 09 (granite) exhibit larger breakability values and a smaller deviation of results than the other rock types. The Los-Angeles test series proved that on a macroscopic scale, subclass 04B is inferior in resistance to fragmentation compared to subclass 04A (see Fig. 38, p. 55). However, the Abroy test results indicate more favourable behaviour for this subclass. Subclass 03B performs distinctively better than subclass 03A, a finding which accords well with the LA test results.

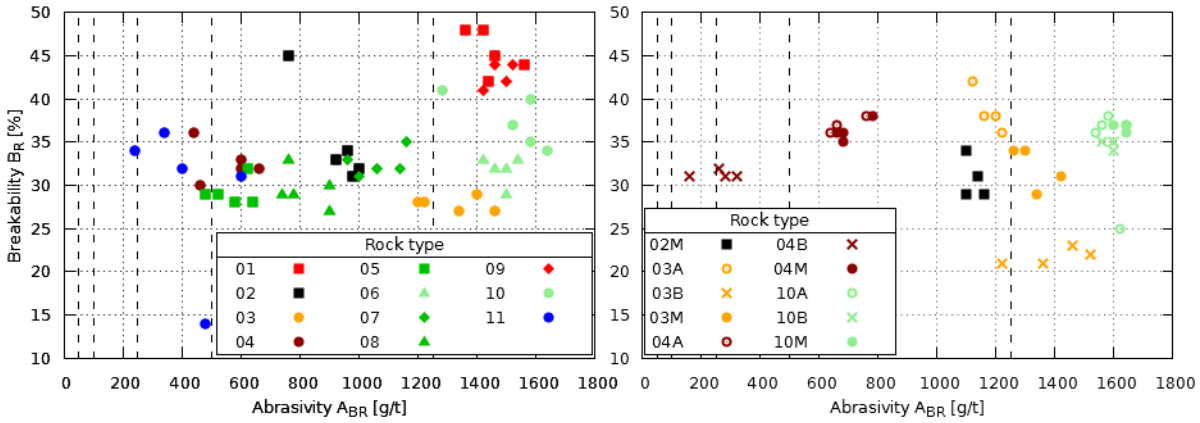

Fig. 69: Abroy test – abrasivity A_{BR} and breakability B_R for test series ABR-I (left) and ABR-II (right)

A test series carried out by Bärtschi (2010) with a wide variety of siliceous limestones from Switzerland yielded a negative correlation between A_{BR} and B_R , and between B_R and quartz content. It is questionable, however, whether these findings can be generalized with respect to other rock types, as most siliceous limestone varieties exhibit a low abrasivity value (typically < 500 g/to) but a medium to high quartz content (30 to 50%).

The present author surmises that the unsatisfactory breakability results can be explained by two phenomena:

- The fast rotation of the impeller ensures fairly constant impact momentums. However, fragmentation does not only occur in the course of particle collision with the impeller, as desired, it also takes place where two particles collide with each other at a relatively high speed, which is in fact the case in the section between the impeller's front end and the wall of the sample container. The magnitude of this unwanted phenomenon is cannot be predicted accurately at all.

- The grinding process may influence particle shape and angularity and will thus have an impact on the breakage of poorly shaped particles and on the degree of rounding, regardless of the shape and angularity characteristics of the original gradation.

Evaluation of tests

Determination of the resulting particle size distribution, as suggested in (Thuro et al. 2006), and an analysis of the sample angularity may improve the predictive powerof B_R.

5.5.2 Deviation of results

Fig. 70 depicts the normalized inter quartile range (i.e. iqr / median) for all tests on ballast from 2011 (left) and 2012 (right). For most rock types, the Abroy test exhibits a smaller deviation than the Cerchar test. Deviation is comparatively small for rock types 01 (granite), 02 (basalt), 10 (granulite) and 11 (dolomite). The diabase rocks generally show a large deviation (rock types 05, 07 and 08), which may partly be blamed on the generally larger fluctuation range of metamorphic rocks with respect to petrographic composition and textural characteristics.

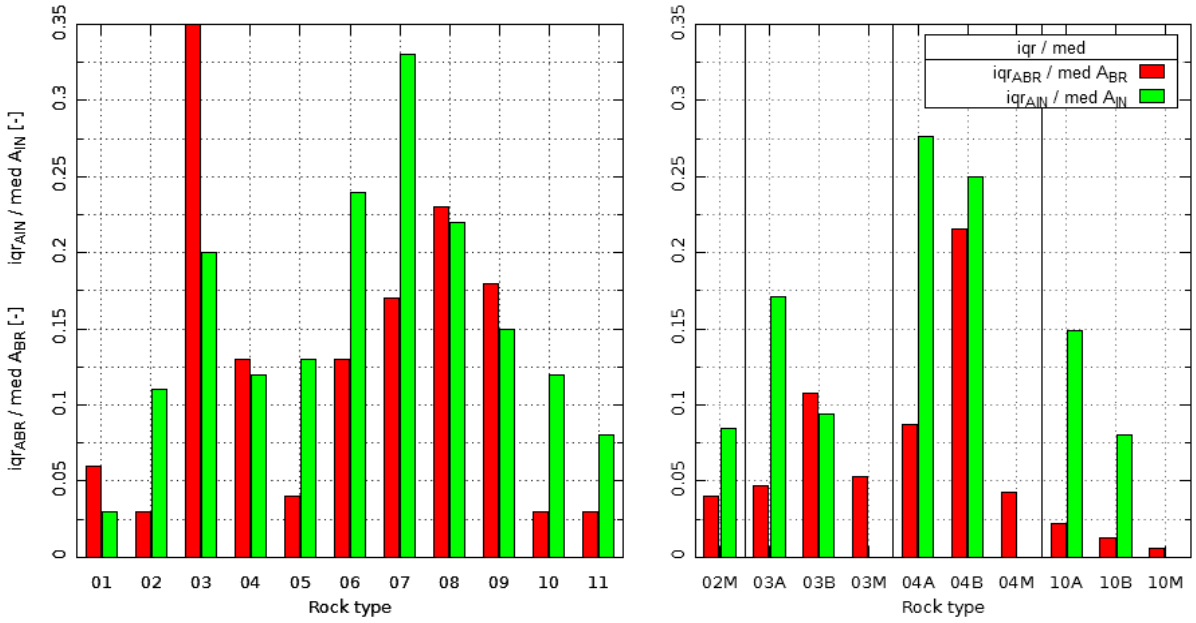

Fig. 70: Abroy- and Cerchar-Tests – Inter-quartile range of A_{Br} and A_{IN} with respect to respective med values for test series ABR-I and CAI-I (left) and for test series ABR-II and CAI-II (right)

Rock type 03 also shows a large deviation of results for both test types. Two subclasses exist for this rock type which exhibit significantly different mechanical behaviour (see also section 5.2). When the subclasses are tested separately, deviation decreases (see Fig. 70 right). The results for rock type 04 and 11, which exhibit similarly low abrasivity values for both tests, clearly demonstrate that the deviation of results does not necessarily increase for rock types with a low abrasivity.

Compared to the normalized interquartile range of the tool wear tests, the deviation of the compression test results (Fig. 51 right) proved to be much smaller. This may, however, be the result of the relatively small sample size required for both tool wear tests.

Evaluation of tests

Fig. 71 (left) shows the inter-quartile range (iqr) for the results of both tool wear tests (series ABR-I and CAI-I), with respect to the respective maximum values ($A_{BR,max}$ = 2,000 g/t; $A_{IN,max}$ = 6), i.e. the standardized iqr. For most rock types, the Cerchar-Test exhibits larger variations than the Abroy-Test (means are 4.9% for A_{BR} and 8.0% for A_{IN}).

Comparing the respective values for the two subclasses of rock types 03, 04, and 10 (Fig. 71 right) shows that the variation differs for the two associated subclasses. The respective variations of the combined tests (subclass "A" and "B" taken together) are much larger. Ignoring the existence of petrographic deviation thus results in a much larger deviation of test results.

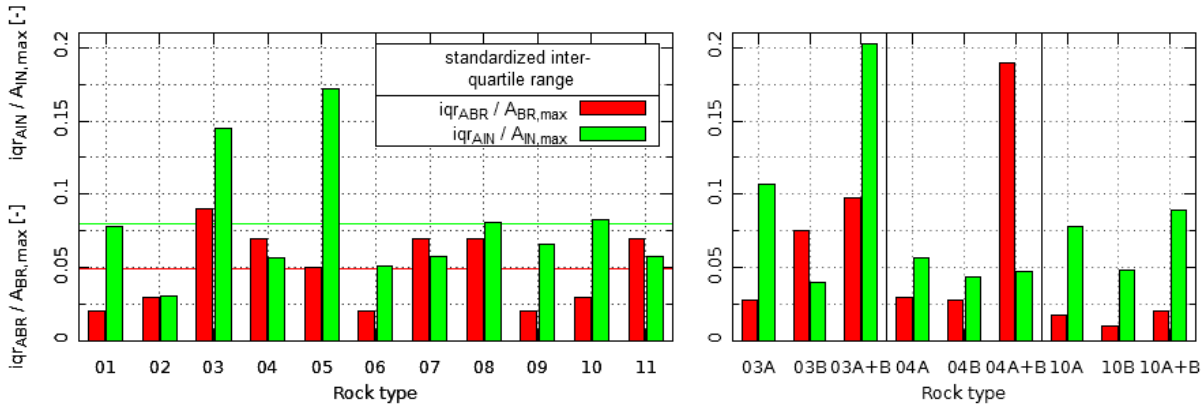

Fig. 71: Abroy- and Cerchar-Tests – Inter-quartile range of A_{Br} and A_{IN} with respect to respective max values for test series ABR-I and CAI-I (left) and for test series ABR-II and CAI-II (right)

Based on these findings it is advisable to divide the sample into subclasses, then carry out the tests separately, and evaluate the results separately for each subclass. Otherwise, large and misleading deviations in the test results will occur due to the non-representative choice of sample material. Due to the comparably small sample sizes needed for the tool wear test, the effort connected with a manual sorting of subclasses prior to the testing are considered acceptable and would yield valuable information on the degree of inhomogeneity of the respective quarry output.

LCPC and Cerchar tests are less expensive than standard test methods. Reducing test intervals may help make such tests more acceptable in economic terms.

5.5.3 Correlation to Rock Abrasivity Index

According to Plinninger (2002)'s classification scheme, seven rock types can be claimed "extremely abrasive" (RAI > 12,000), two "very abrasive" (6,000 < RAI < 12,000). Rock type 04 is "abrasive" (3,000 < RAI < 6,000) and rock type 11 is "not abrasive" (RAI < 1,000; see Fig. 72 left).

Evaluation of tests

UCS values were calculated based on Breymann (2011)'s point load test results, using Thuro (1996)'s empirical relation

$$UCS = 20.6 \cdot I_{50} = 20.6 \cdot I_S\,(D_e = 50mm) \tag{19}$$

As only the mean diameter of each respective series was known, THURO's LOGAR-method (Thuro 1996) could not be applied for conversion of I_s into I_{50}. Instead, Brook (1985)'s relation

$$I_{50} = f \cdot \frac{F}{D_e^2} = f \cdot I_s \qquad \text{with} \quad f = \left(\frac{D_e}{50}\right)^{0.45} \tag{20}$$

was used. The parameter f differed only slightly from 1 (0.97 < f < 1.04).

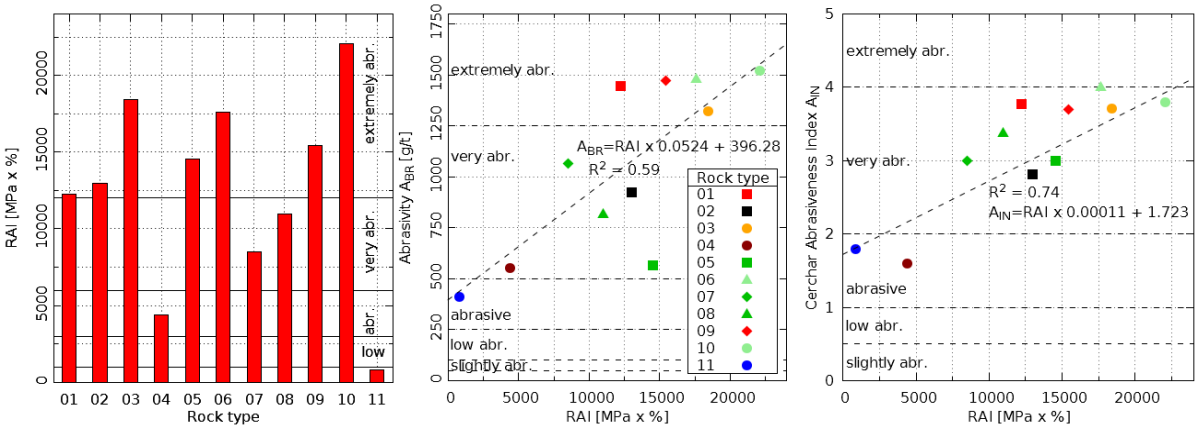

Fig. 72: Abroy- and Cerchar-Tests – Rock abrasivity index RAI (left) and correlations with Abroy- and Cerchar test (center & right)

The RAI value shows a stronger correlation to the observed tool life of core bits in tunnelling than does the equivalent quartz content E_{Qu} (Plinninger 2002). However, this does not apply for the Abroy test (Fig. 72 center). For the Cerchar test, the correlation coefficient R^2 for RAI vs. A_{IN} is approximately equal to the correlation E_{Qu} vs. A_{IN} (Fig. 72 right). It should be noted that the RAI indices for most of the tested ballast types were found to lie in the upper region of the range seen in those rock types typically encountered in tunnelling.

5.5.4 Correlations to Deval and Micro Deval tests

Given the assumption that rock types showing high abrasion on tools would show low grain to grain wear in rail tracks (see section 4.4), one would expect to find a negative correlation between the results of the traditional testing methods (Micro-Deval, Dry Attrition, Wet Attrition) and those from the alternative testing procedure. As Fig. 73 shows, this is indeed the case for all possible combinations.

Evaluation of tests

Fig. 73A shows an acceptable negative correlation between A_{BR} and $M_{DE}RB$. Rock type 04 exhibits the largest deviation with a $M_{DE}RB$ value of 18.7%. A_{IN} values also correlate with $M_{DE}RB$ (Fig. 73D), but with lower significance. Looking at dry (Fig. 73B and E) and wet attrition (Fig. 73C and F), A_{IN} values are in better accordance than A_{BR} values. Generally, A_{IN} and A_{BR} values fit better with wet attrition results than with dry ones.

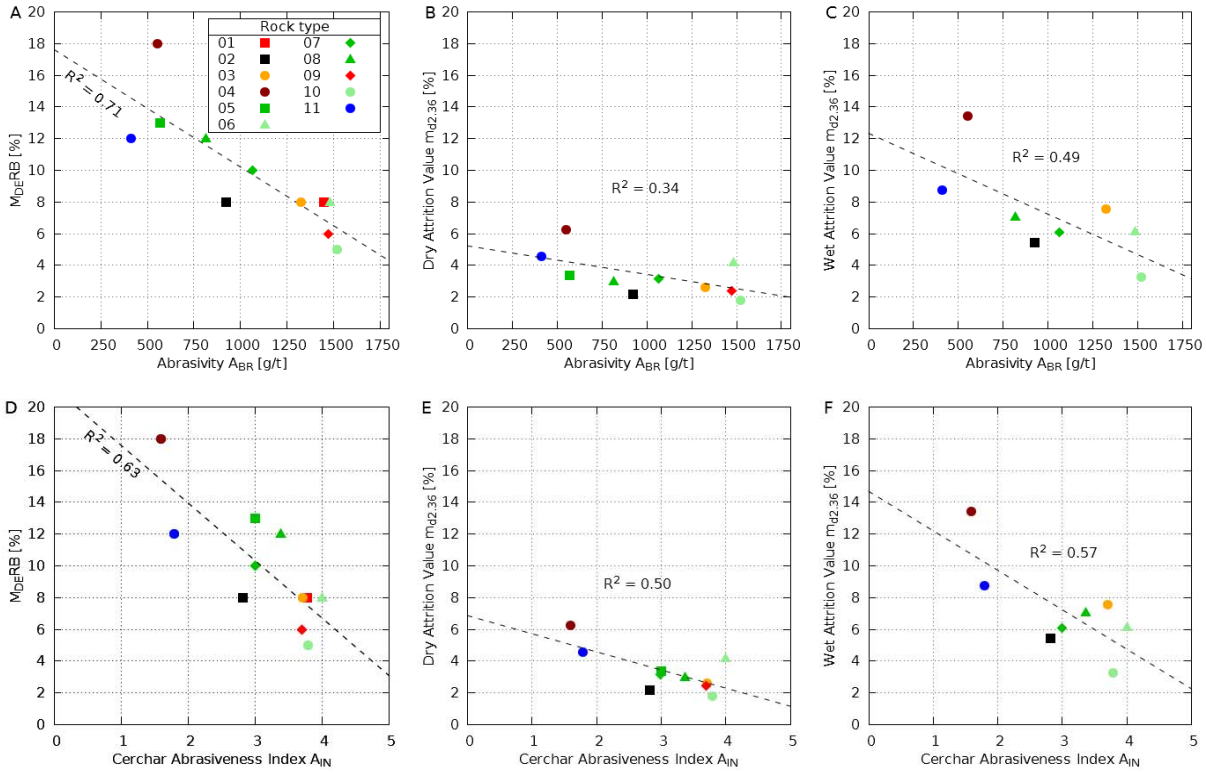

Fig. 73: Abroy- and Cerchar-Tests – correlations to Deval- and Micro-Deval tests

A_{IN} and A_{BR} values are available for a large quantity of different rock types. A detailed compilation for example is given in (Plinninger, Restner 2008), whose results fit well with the existing data, usually with high A_{IN} and A_{BR} values for igneous rocks, low values for sedimentary carbonate rocks, and a wide range for metamorphic rocks, depending on their parent rock material. Though diverse rock types were tested, strong correlations between the two testing methods could be observed.

Whilst the correlation between abrasivity and equivalent quartz content is the subject of some controversy in the literature (e.g. West (1989), Thuro et al. (2006), Thuro & Käsling (2009) and Köhler, Maidl & Martak (2011)), the results of the present study attest to a strong dependence of the abrasivity behaviour on equivalent quartz content.

Micro-Deval Tests and Deval Attrition Tests measure the resistance of aggregates to wear. In contrast, the tool wear tests measure the ability of aggregates to produce wear on tools. In case of the standard test methods the creation of fine grained material (<1.6

mm for Micro-Deval Test and <2.36 mm for Deval Test) due to grain to grain load is used as a parameter to estimate the resistance to wear of aggregates in rail tracks.

To estimate the ability of rocks to cause wear on tools, the two alternative methods measure the effect on standardized tools. In spite of these different approaches, both groups of testing methods reveal correlating results. Rock types as granites, granitic porphyry and granulites can be classified as very abrasive and show lowest grain-to-grain wear. Classification as very abrasive (especially by A_{BR}) indicates good resistance to abrasion in rail tracks.

6 Conclusions

6.1 Load regime

The respective contributions of the three attrition types described in section 3.1 (fragmentation, rounding and abrasion) was estimated for six test types, using machine vision and mass balance considerations for the determination of the angularity.

The Los-Angeles test result LA_{RB}, which is equal to the fraction of fines smaller than 1.6 mm, was found to include up to 29% residual fines from rounding (see Fig. 74 left and Fig. 43; p. 61).

The dry attrition test results in a larger share of fines due to fragmentation than the wet attrition test. Fragmentation presumably occurs when ballast particles hit the end walls of the test drum. The small length of the test drum and the combination of a rotational and a swaying movement (see Fig. 28; p. 39) represent a weakness in test design. The contribution of abrasion is higher for the wet attrition test (see Fig. 74 center and right and Fig. 67; p. 77). Fines generated during the first few rotations form a kind of protective layer and prevent polishing, thus, for most rock types, abrasion is virtually non-existent.

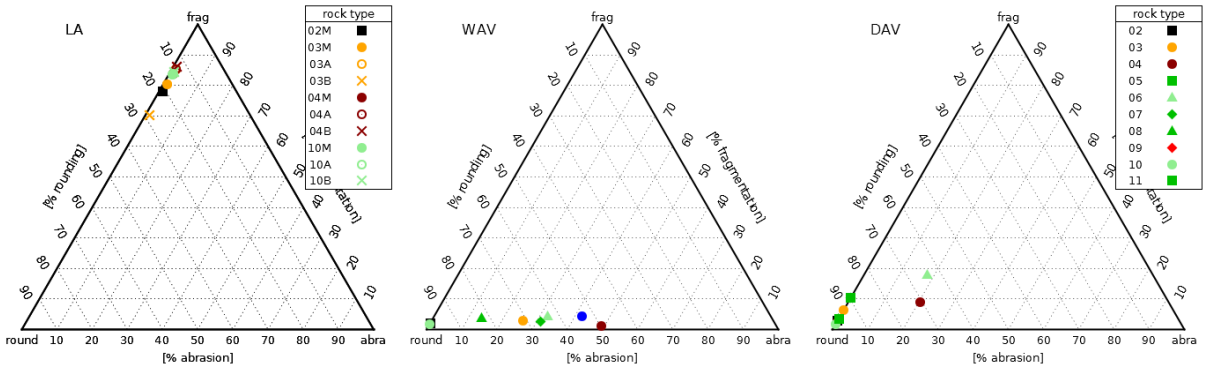

Fig. 74: Los-Angeles Test (left), Wet Attrition Value (center) and Dry Attrition Value (right) – contribution of fragmentation, rounding and abrasion to result

Whilst the Cerchar test generates abrasion only, the fines generated in the course of the Abroy test are highly unlikely to result from abrasion alone. Post-test particle size distributions, as carried out by (Thuro et al. 2006), suggest that breakage must also have occurred. However, due to the small gradation of the initial sample, it is a question of definition whether this breakage is called (macroscopic) fragmentation or abrasion. For granitic rock types, the mineral grain size almost matches the particle size. As the attrition behaviour of railway ballast is the centre of interest in the present study, the Abroy test is classified as an abrasion test.

Conclusions

Test type	Fragmentation [%]	Rounding [%]	Abrasion [%]
Cerchar test	0	0	100
Abroy test	> 0	?	< 100
Wet attrition test	1 – 4	50 – 99	0 – 50
Dry attrition test	2 – 18	75 – 100	0 – 21
Los-Angeles test	70 – 88	11 – 29	~ 1
Compression test	100	0	0

Tab. 17: test types – contribution of fragmentation, rounding and abrasion to result

6.2 Deviation of results

The impact of the following five factors on the deviation of the test results was investigated: sample size, heterogeneity in terms of petrographic composition, geometry of the test device, and, for two test types, particle shape and angularity.

As geometric and petrographic characteristics show large variability (see Fig. 32 and Fig. 33; p. 50), a sufficiently large sample size is crucial to ensure representativeness of the test result. As Tab. 18 illustrates, sample size is roughly inversely proportional to result deviation.

Test type	sample size [kg]	Gradation [mm]	particle count [-]	deviation (range and mean) [%]
Cerchar test	(> 0.2)	(> 30)	1	3-33 (16)
Abroy test	2.0 (0.5)	(> 4)	17-20	3-35 (11)
Wet attrition test	5.0	37/51	32-40	0-27 (9)
Dry attrition test	5.0	37/51	32-40	4-42 (16)
Los-Angeles test	10.0	31.5/50	87-100	2-9 (6)
Compression test	15.0	31.5/50	130-150	2-15 (7)

Tab. 18: test types – sample size and deviation of results

Geometric characteristics vary considerably from sample to sample (see Fig. 37; p. 54). The sample size of the LA test is thus too small, and causes large variability in test results (see Tab. 14; p. 53). For the user it is almost impossible to track the source of the observed variabilities. The author suggests that the unfavourable relation between gradation and sample size, resulting in a comparatively low number of particles in one sample, implies that even a very small number of particles differing in terms of shape, angularity or petrographic composition can have a relatively strong impact.

The impact of petrographic composition on the result was found to be stronger than the influence of angularity and shape. A positive correlation between angularity and the amount of fines was found for all rock types and subclasses investigated (see Fig. 44; p. 61), but the impact of the former remains comparatively small. The impact of shape on the test result could be shown for rock type 02 only (see Fig. 47; p. 63). This rock type is believed to be homogeneous in terms of petrographic composition.

Conclusions

As it is not feasible to make adaptations to the test procedure or to the geometry of the test device, there are only three ways to improve the repeatability and representativeness of the test:

1. Repetition of the test. Tab. 14 shows that a large number of test repeats is necessary to achieve a satisfactory repeatability limit. This approach is thus inefficient for most rock types.

2. Setting of additional limits for the sample in terms of shape, angularity and petrographic composition. This requires an elaborate sorting and sieving process prior to the actual test.

3. Quantifying the deviation in shape, angularity and petrographic composition for every sample and estimating their impact on the test result, using statistical methods. A correction factor can be specified or, alternatively, the impact of the measured characteristics can be quantified for a given sample.

The third approach was considered most promising. Petroscope® measures not only particle shape, but also reflectance spectra particle-wise. This allows for an automated classification of samples of unknown origin and also for a quantification of the share of the two subclasses of rock types 03, 04 and 10 within a given sample. Training data was used to build classes for the reflectance spectra. The hit rate at the subclass level (i.e. the correct class assignment) was well over 97%.

Using the geometric and spectral data of the 85 LA-tests, the respective test results as training data, and the 5-fold cross-validation technique, a statistical model for the prediction of LA_{RB} was developed and calibrated. The measured and the predicted LA-values differed by 0.51 to 0.72 mass-%, compared to a standard deviation of the results of the performed tests of 0.62 to 0.94 mass-% (see Hofer & Bach (2012)).

6.3 Performance of rock types – quality index

Test series on six attrition tests were carried out in the course of the evaluation process. Additionally, results for the equivalent quartz content E_{Qu} and the point load index I_S are also available. Furthermore, comparisons may be made with a time series of 11 suitability tests in accordance with (Österreichische Bundesbahnen (ÖBB) 2007), including micro deval tests, LA tests and impact tests in accordance with (Österreichisches Normungsinstitut 2006), including all eleven rock types, as published in Kuttelwascher (2011).

Prior to comparison, test results need to be normalized. The normalized result value, called quality index I_Q, ranges from 0% to 100%. The quality index for a given rock type

and given test type is the ratio of the median of all test results $\tilde{R}$ divided by the difference between q_{max} and q_{min}.

$$I_Q = 100 \cdot \frac{\tilde{R}}{q(R)_{max} - q(R)_{min}} \quad (21)$$

Tab. 19 gives the chosen extreme values. For most test types, the largest and the smallest result value found in any test were designated as q_{max} and q_{min} , respectively. However, in the point load test, q_{max} and q_{min} are based on the minimum 25%-quantile and the maximum 75%-quantile since using the absolute extreme values here would have led to a poor separation effect (see Fig. 34; p. 50).

Test type	Abbre-viation	q_{min} ("poor")	q_{max} ("good")	no. tests per rock type	box
quartz content	E_{Qu}	19.42	71.84	12 (rock types 02,03,04,10) 1 (other)	(iqr)
abroy	A_{BR}	160	1,640	5	iqr
cerchar	A_{IN}	0.79	4.44	7	iqr
Micro-deval	MDe_{RB}^{TS}	22	2	11	iqr
wet attrition	WAV	14.87	3.23	2	min/max
dry attrition	DAV			4	iqr
LA (time series)	LA_{RB}^{TS}	26.56	9.00	11	iqr
LA (this study)	LA_{RB}			15 (rock type 02), 9 (other)	iqr
swiss compression	DB_{RB}	54.73	29.27	12 (rock type 02), 4 (rock type 11) 2 (other)	iqr iqr min/max
impact test	SZ^{TS}	29.75	10.10	11	iqr
point load test	I_S	0.57	2.79	30	iqr

Tab. 19: quality indices – underlying range (tests results from this study colour-coded)

The results are given in Fig. 75. The sequence of the tests roughly follows the load regime: tests for determination of resistance to wear are found on the left, those for determination of resistance to fragmentation are placed on the right. The equivalent quartz content and the results of the point load tests are added at the left / right edge, respectively.

A_{BR} and A_{IN} results correlate well for most rock types. Correlation between WAV and DAV test results is good for most rock types, despite the fact that the contribution of abrasion and rounding differs considerably (Fig. 74). The LA test results from the present study correlate well with the time series means for rock types 02 and 10, but seem to have yielded results at the lower end of the long-term deviation for rock types 03 and 04.

Conclusions

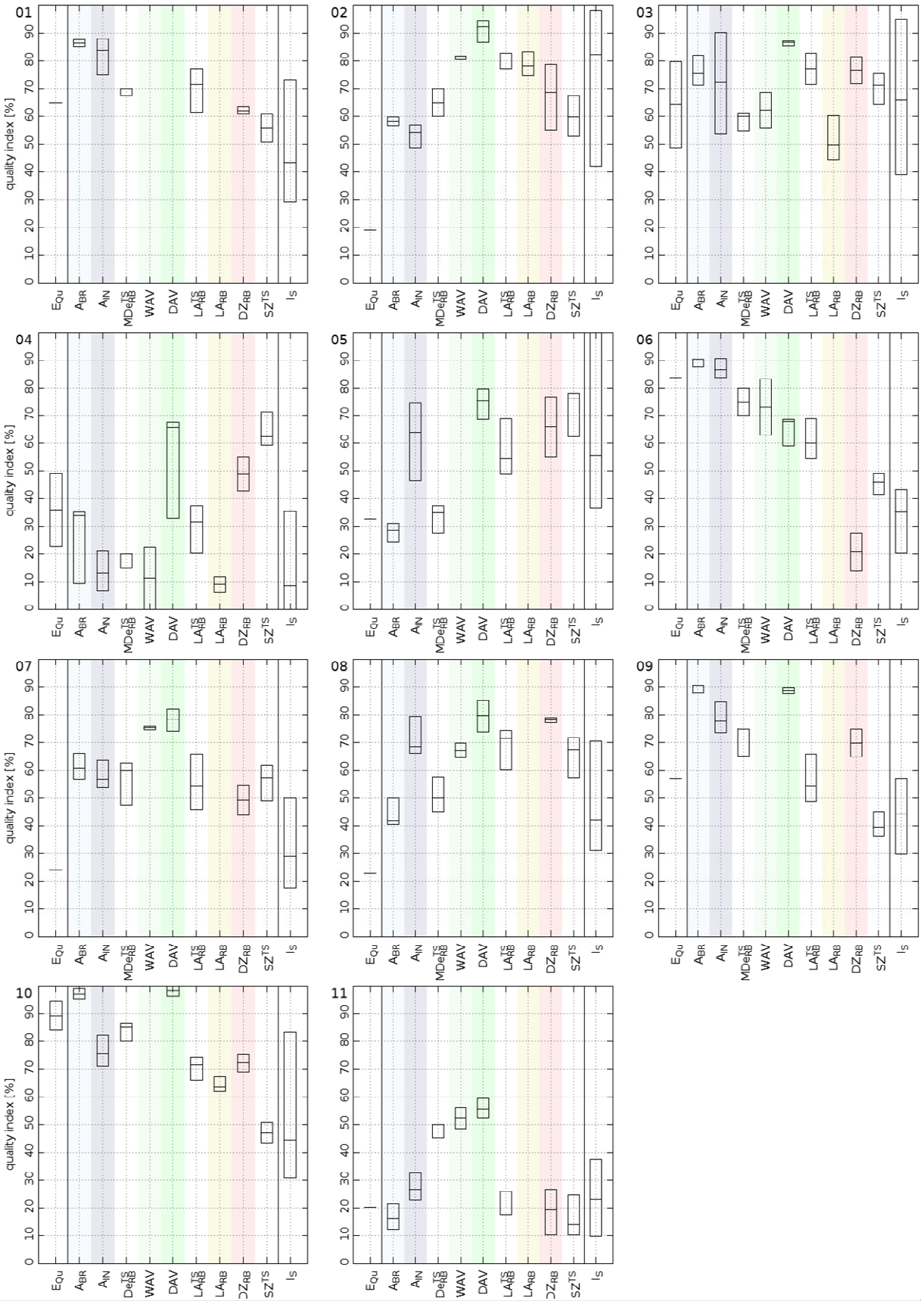

Fig. 75: quality indices for all rock types

Conclusions

The compilation of all abrasion tests (Fig. 76 top) shows consistent results for most rock types. The granitic rock types (nrs. 01, 06, 09 and 10) and the basalt (nr. 02) show the best performance. The diabatic rocks (nrs. 05, 07 and 08) perform slightly weaker, whilst the dunite (nr. 04) and the dolomite (nr. 11) exhibit low resistance to abrasion.

The quality indices for the fragmentation and impact tests are compiled in Fig. 76 (middle). For a given rock type, they exhibit greater diversity than found in the results of the abrasion tests (see rock type 04, for example). As also found by (Anthes 2006), the diabase rocks show a better performance in terms of resistance to fragmentation compared to the granitoids.

For most rock types, a high resistance to fragmentation is accompanied by a poor resistance to wear (see rock types 05 and 08) and vice versa (see rock types 01, 06, 09 and 10). Only rock types 02 and 03 perform well in both categories.

For a given rock type, the quality indices for each test type may be combined into one mean quality index which may then serve as a characteristic number for the overall quality of the respective rock type or its suitability as ballast material. (bottom) shows the sensitivity of the quality index to test mix. The test mix required by (Österreichische Bundesbahnen (ÖBB) 2007) is depicted in red, with an equal weighting of the three tests. Where resistance to wear and resistance to fragmentation is to be weighted equally, one may choose the mean of the quality indices found for the two tool wear tests and for any fragmentation (i.e. LA test, impact test, or Swiss compression test). Additionally, the mean of all attrition tests is also given, as well as the mean of all tests (i.e. all attrition tests + E_{Qu} + I_s).

The resulting rankings show little sensitivity to the chosen test type mix. The performance of rock types 04 (dunite) and 11 (dolomite) was clearly poorer than average, regardless of the chosen mix. Rock types 01 (granite), 02 (basalt), 03 (porphyry), 06 and 10 (both granulite) show the best overall performance. The fact that granulites perform well was discovered long ago by Wieden, Augustin & Zieger (1977) using standard LA-test in accordance with (Österreichisches Normungsinstitut 2006).

The diabase rocks (05, 07 and 08) exhibit a slightly lower quality index.

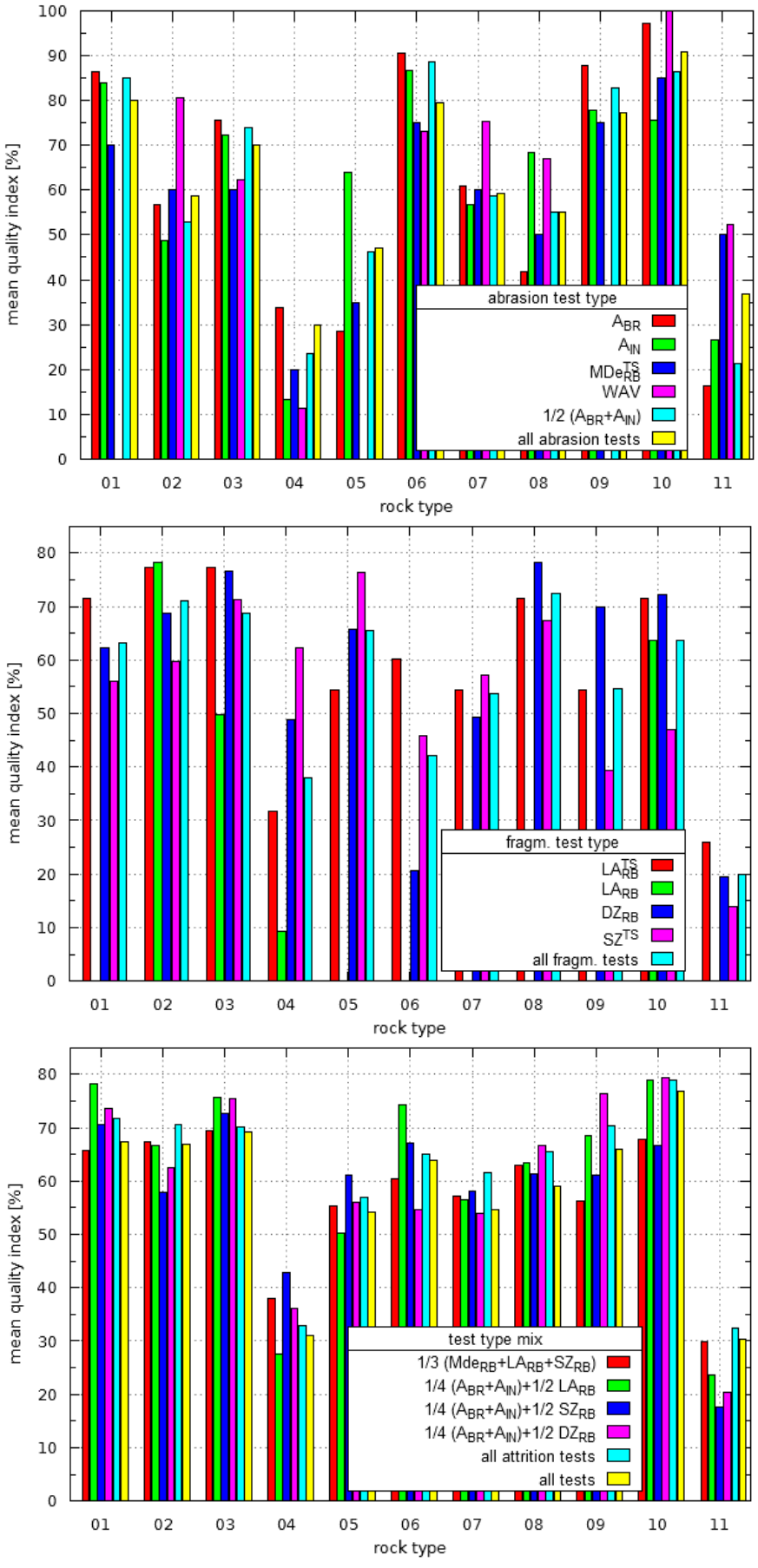

Fig. 76: mean quality index – sensitivity to chosen test type and test type mix

Conclusions

The test result values (i.e. the characteristic numbers) for all tests evaluated - except for those found in the Cerchar and the Abroy tests - are linearly proportional to the amount of fines arising due to abrasion, chipping, or fragmentation during the test . Thus, the corresponding quality index IQ also behaves linearly with respect to resistance to abrasion / fragmentation.

On the basis of such a linear relationship one is thus able to establish ballast quality classes. These classes may incorporate the weighted results of two or more test methods (see Fig. 77 for example).

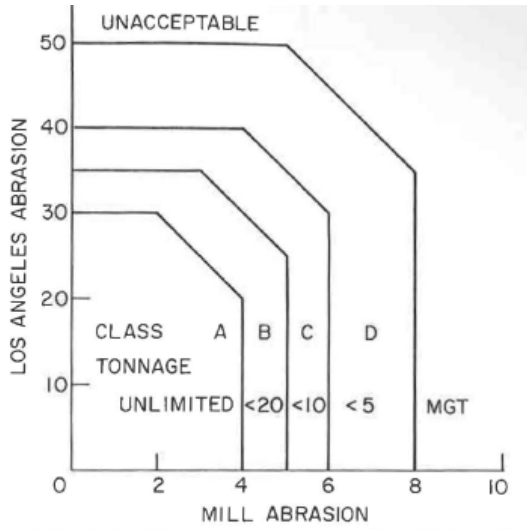

Fig. 77: load-classification diagram for ballast (Canadian Pacific railways). In Raymond & Bathurst (1985)

Austrian Railways ÖBB uses three test methods for suitability tests for railway ballast: Micro-Deval, Los-Angeles-Test and Impact test (according to EN 13450 (Österreichisches Normungsinstitut 2004a)). The corresponding quality indices I_Q are given in Fig. 76 (bottom, red bars) for all rock types.

Tab. 17 shows a proposal for three ballast quality classes (classes 1, 2 and 3) and the corresponding quality indices I_Q. The range of I_Q is divided into three classes of equal width. Four rock types would fall into class 1, five into class 2 and two into class 3.

If one takes into account that particle fragmentation is mainly governed by axle load (see also section 6.4), and that abrasion is mainly governed by the total number of load cycles, ballast class 1 should be used for highly frequented main lines with a large share of freight trains and high speed passenger trains. Ballast class 3, on the other hand, can be used for secondary lines, i.e. those lines exhibiting relatively minor freight traffic and moderate train speed.

ballast class	corresponding I_Q [%]	corresponding rock types	network rank	track rank
1	> 66 to 100	01, 02, 03, 10	core (v > 160 km/h)	a
2	> 33 to 66	05, 06, 07, 08, 09	core (v ≤ 160 km/h)	a
			secondary (high axle loads)	a
3	0 to 33	04, 11	core	b, c
			secondary	

Tab. 20: proposal for ballast classes

6.4 Attrition test results - relationship to load regime in track

In section 2.1 the relation between axle load magnitude, train speed, and the resulting sleeper load, was investigated. Using strain gauges attached to the rail, HARRISON & SELIG measured static and dynamic axle loads from combined passenger and freight traffic on the New York – Washington line (Harrison et al. (1984) and Selig & Waters (1994)). The static wheel load distribution was obtained by dividing known individual gross car weights by the corresponding number of wheels.

The results are depicted in Fig. 78A. About 20% of all axle loads exceed 22.5 tons (static), about 10% exceed 30 tons. Less than 1% of the dynamic loads exceed 40 tons. The latter occurred mainly in the case of high speed trains with wheel imperfections. Using the axle load – sleeper load relationship shown in Fig. 7 (p. 17), the respective sleeper loads were calculated (Fig. 78B).

Based on the concept of coordination number, and on the knowledge of the particle size distribution, void ratio, and particle shape, the magnitude of the point loads acting between adjacent ballast particles (section 2.2) may be deduced from the sleeper load. Lu & McDowell (2007)'s numerical back-analysis of a box test resulted in a peak point load of a magnitude of 10% of the macroscopic load. The peak load was measured immediately below the sleeper. In Fig. 78C, the resulting peak point loads are given together with the 13% of the 37% tensile strength of the ballast particles for rock type 01 to 11 (from Breymann et al. (2011)). At about 13% of the 37% tensile strength, the production of coarse aggregate subject to uniaxial pressure complies with McDowell & Harireche (2002)'s theoretical considerations and experimental findings. The tensile strength of all rock types investigated in the present study is exceeded by 40% to 80% of all axle loads. This implies that either fragmentation occurs immediately after the first

few axle passages, or, alternatively, particle rearrangement takes place, resulting in a more favourable coordination number and thus in smaller point loads (see also Fig. 13, p. 24).

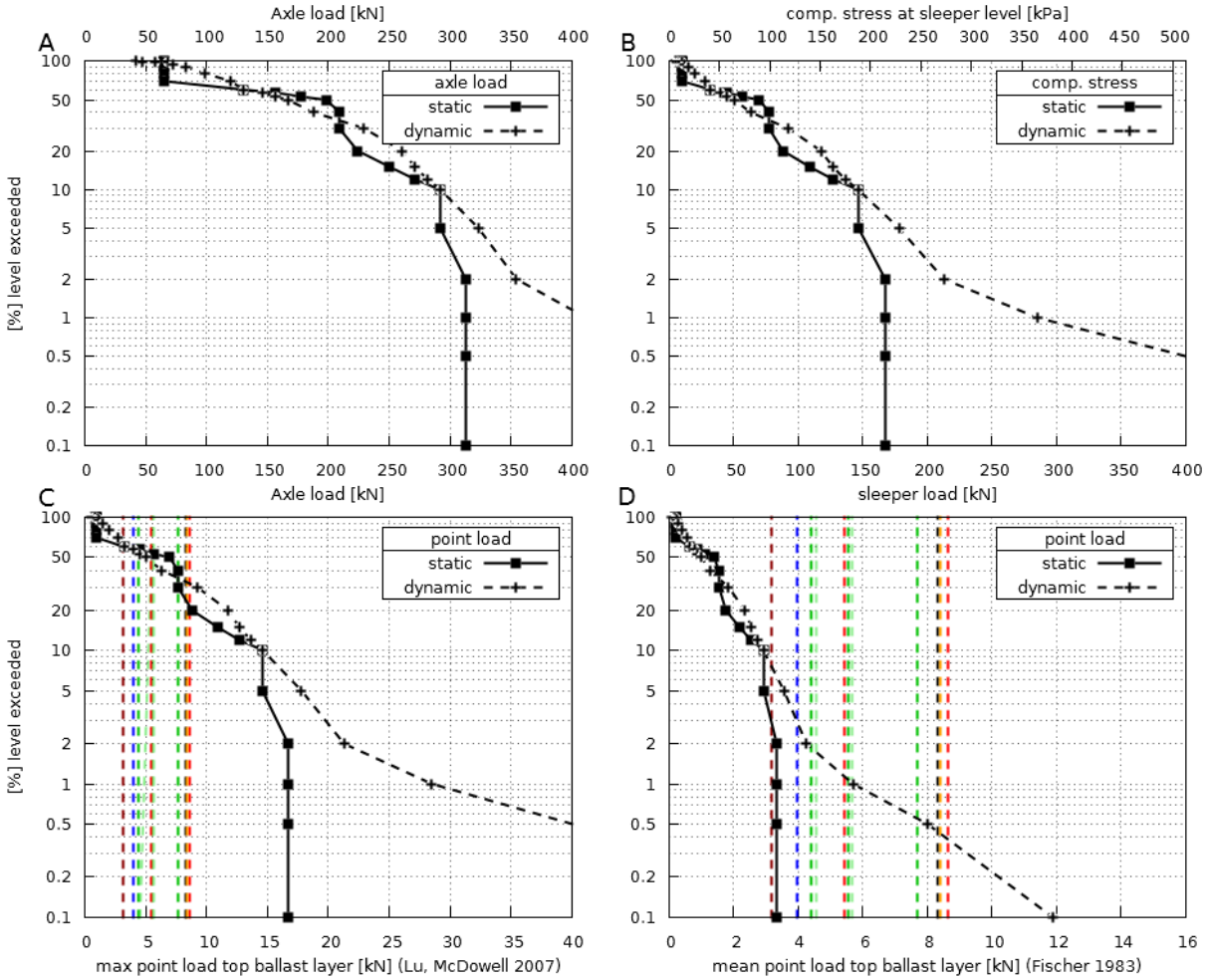

Fig. 78: (A) static and dynamic axle loads from combined passenger and freight traffic (from Selig & Waters (1994)) (B) respective sleeper loads from numerical model (see Fig. 7) (C) maximum point load for top ballast layer (according to Lu & McDowell (2007)) and 13% of the 37% tensile strength of the particles for rock type 01 to 11 (from Breymann et al. (2011)) (D) mean point load for top ballast layer (according to Fischer (1983)'s lacquer method)

Fischer (1983)'s experiments with dyed ballast particles in a shear box (see Fig. 9; p. 18) resulted in a ratio of macroscopic load to mean point load of approx. 50 for the uppermost ballast layer. The resulting load distribution is depicted in Fig. 78D, once again together with the 13% of the 37% tensile strength of all rock types. The tensile strength of rock type 04 is exceeded by 3% to 8% of all axle loads, of rock type 11 by 2.5%, and of rock type 06 by 1.5%. All other rock types withstand more than 99% of the passing axle loads.

It should be noted that FISCHER's findings only allow for an estimation of mean point load magnitudes, but that the generation of fines usually occurs gradually (see Fig. 56; p.

71). Fragmentation does not occur all at once. However, Fig. 78C and D illustrate that there is no linear relationship between the tensile strength of a given rock type and its survival probability at a given load level. Even a rock type with a comparably small rock strength, such as rock type 04 or 11, would show no or only little fragmentation where the macroscopic load level (i.e. the axle load) never or hardly ever exceeded about 250 kN.

The present author supposes that the relatively long life of railway ballast observed on some Austrian secondary lines (on which ballast of low rock strength is used in parts) is mainly caused by the comparatively small axle loads of the rolling stock and the small number of freight trains operating on these lines.

7 Summary and suggestions for further research

The load regime in track was investigated using numerical models, test results and findings from literature.

- Experimental results and results from numerical analyses indicate that the load at sleeper level increases disproportionately with increasing gross axle load. The respective ratio ranges from approx. 25% for small axle load to 50% and more
- The number of contacts per ballast particle (the 'coordination number') can be estimated using experimental data, the results of particle models, and geometrical considerations. Respective values range from 2.7 to 8.6. Experiments and numerical models indicate that only somewhere between 2.7 and 5.3 contact points per particle actually transmit loads.
- The ratio between the sleeper load and the peak point load acting at a particle-to-particle contact point is approx. 10:1. The respective mean value is approx. 50:1 to 100:1.

The load regime of the test procedures was investigated, and shortcomings of the test procedure located.

- The test kinetics of the Los-Angeles test for railway ballast result in impact momentums that range between 0.14 kg m/s and 1.05 kg m/s. Mean values are approx. 0.37 kg m/s and drop to approx. 0.25 kg m/s over the course of the test, and as fragmentation occurs
- In the Deval test impact momentums ranging between 0.11 kg m/s and 0.43 kg m/s occur when particles hit the end wall

The particle geometry of ballast samples originating from eleven sources (suppliers) was measured, using the test device "Petroscope®4D", Additionally, two subclasses were defined for three rock types.

- All evaluated ballast types exhibit large deviations in terms of shape and angularity. 75% to 85% Volume-% are "angular" or "very angular".
- There is an almost uniform distribution of the flatness ratio between 0.4 and 1.0 and of the elongation ratio (between 0.55 and 1.0). The mean flatness ratio varies between 0.62 and 0.69 and the mean elongation ratio between 0.73 and 0.78.
- For two rock types, the respective subclasses exhibited distinctly different shape characteristics

An extensive series of 85 Los-Angeles Tests was performed, with a determination of the particle geometry prior to and after the test, using the test device "Petroscope®4D".

Summary and suggestions for further research

- Three out of four rock types exhibited large repeatability limits for the Los-Angeles test result, LA_{RB}. For two rock types, the two subclasses showed distinctly different LA_{RB} values, and a different degree of fragmentation
- The number of necessary test repeats necessary in order to reach a confidence interval of 95% on a confidence level of $^1/_{20} \cdot LA_{RB}$ ranged between 5 and 25. One of the reasons for this is the fact that as a result of the comparably small particle count within one sample, geometric parameters vary considerably from sample to sample.
- For any single rock type, the result parameter LA_{RB} does not reflect the degree of fragmentation
- At the level of rock type, no general correlation was found between the initial angularity and the degree of rounding
- The progress of the fragmentation processes during the test can be estimated by analysing the post-test angularity distribution. For two of the four rock types examined, the fragmentation process appears to be still under way even at the end of the test, while for other rock types, the process comes to an end after only relatively few revolutions of the test drum.
- The test result LA_{RB} not only contains fines generated by fragmentation, but also those generated by rounding. By measuring the angularity distribution sample-wise prior to and after the test, the contribution of rounding processes can be quantified. Typical magnitudes are in the range of 2 to 4 Mass-%.
- The impact of variations in petrographic composition on the degree of fragmentation proved stronger than the impact of shape. Differences in particle shape only come into play for rock types which are petrographically homogeneous.

A series of 34 Swiss compression tests was carried out with samples from eleven quarries.

- The Swiss compression test shows excellent correlation with the degree of fragmentation, but deviation of results is large for some rock types.
- The degree of fragmentation correlates well with the mineral hardness E_{Qu}. Correlation with axial strain is weaker. This is probably due to the presence of wall friction, and to insufficient pre-test sample compaction.
- The compression test gives a good indication of the load level for yield and of the brittleness of the sample, i.e. whether yielding occurs at once or rather gradually. However, results are less than satisfying for some rock types, probably, again, as a result of high wall friction. The aspect ratio chosen for the test cylinder appears to be detrimental here.

A third test series involved the Wet and the Dry Deval Attrition test. Ten rock types were testes. For the dry test, intermediate test results were obtained.

Summary and suggestions for further research

- The wet deval test produces more fines than the dry test and induces a larger degree of rounding
- The degree of rounding is proportional to the result parameters DAV and WAV
- The degrees of rounding of the dry Deval test do not surpass the respective value of the LA test. For two rock types the wet test exhibits smaller rounding than the LA test
- The attrition rates of the dry test show a drop after their high initial values. The DAV does not distinguish between whether a given rock type exhibits high initial attrition rates followed by a quick drop in rate, or medium initial values, followed by a gradual decrease.
- In terms of mass balance, the contribution of fragmentation to the test result is typically 2% to 4% for the wet test, and 2% to 10 % for the dry test.

The fourth test series included Cerchar and Abroy abrasiveness tests. Both tests are well-known and wide-spread test methods for tool wear estimation in tunneling.

- A strong correlation between the results of both tool wear tests was found
- Both tests show a strong dependency on mineral hardness and a slightly weaker dependency on rock abrasivity, as revealed by the index RAI.
- A clear difference between the results for the two subclasses is evident for all rock types and for both test methods
- For the Abroy test, no relation could be found between abrasivity A_{BR} and breakability B_R.
- Owing to the smaller sample size, the Cerchar test yielded a larger deviation in results than the Abroy test,. Division into subclasses and the use of separate tests for the subclasses allows for an estimation of degree of abrasivity variability.
- Both tool wear tests exhibit a negative correlation with the two Deval test variants and with the Micro-Deval test. The correlation with the Micro-Deval test result was found to be strongest

Most test series resulted in large result deviations. The following strategies for dealing with these deviations were developed:

- In order to achieve a satisfactory confidence interval, a large number of test repeats are necessary. Alternatively, additional limits with respect to particle shape, angularity and homogeneity of petrographic composition may also be imposed.
- In the Los-Angeles test, measurement and quantification of the shape and angularity characteristics as well as of the deviation in petrographic composition were undertaken. A statistical model estimates the test results, using the above mentioned characteristics for calibration. The accuracy of the prediction model turned out to be very satisfactory (an error of 0.5 to 0.7 mass-%).

Summary and suggestions for further research

The extensive test series incorporated a multitude of test methods and rock types. A performance ranking of these rock types was worked out one the base of the test results.

- For most rock types, a high resistance to fragmentation is accompanied by a poor resistance to wear and vice versa. Only two rock types (basalt and granitic porphyry) performed well in both categories.
- Using normalized test results, a mean quality index may be introduced to include test results for abrasion and fragmentation tests. The overall ranking of the eleven tested rock types shows only a relatively small dependency on the chosen test mix.

Concerning the relation of test results and performance in track:

- The crushing strength of the ballast may be determined using compression tests or single particle crushing tests. Superimposing the resulting strength distribution on the respective distribution of the particle-to-particle point loads in track may help to estimate the performance of a given ballast type in track for a given axle load distribution.

An insufficient sample size proved to be the main source of the variability observed in test results. Thus, petrographic composition, shape and angularity vary considerably from sample to sample, even though the variability of the respective quarry output does not usually constitute a problem in practice, as the variabilities tend to cancel each other out.

Further research should thus concentrate on an estimation of the magnitude of such variations at the sample level, on their impact on results and on the techniques needed to overcome the problem (of insufficient sample size).

- The deviations in result values need to be investigated for a wide range of rock types, for the LA test, and for other attrition tests that are likely to suffer from similar inadequacies and restrictions, such as the Deval Attrition test, the Micro-Deval test, the impact test and the Swiss compression test.
- The statistical model introduced in section 6.2 allows for an estimation of the test result to be made, based on the measurement of particle shape, angularity and petrographic composition. This model should be developed further to allow for quantification of those factors influencing test results.
- The connection between axle load, sleeper load, particle-to-particle point load within the ballast layer, and respective rock strength, were shown using the example of initial gradation of the ballast. The results suggest that the degradation characteristics of the track quality are governed by the peak particle-to-particle load level and by the ballast strength. In turn, the peak particle-to-particle load level is influenced by the fragmentation behaviour of the ballast. Ballast samples from the

track are needed, and these are to be taken at various stages of use. Based on the respective particle size distributions, the increase in the number of load chains and the corresponding decrease in the mean and peak particle-to-particle load level can then be calculated and may be compared to the ballast strength.

- Static compression tests such as the AGV test and the Swiss compression test allow estimation of yield load, as well as of degree of brittleness, i.e. the span in load level for which yielding takes place. However, an appropriate shape of test device (aspect ratio) also has to be chosen in order to minimize wall friction. A slow loading rate allows for particle rearrangement at low load levels. Precise pre-test sample compaction ensures a satisfactory repeatability limit. The Swiss compression test is thus in need of further development here.
- The result parameter B_R of the Abroy test turned out to be of little significance. The degree of rounding and the post-test particle size distribution of the sample ought to be investigated for a wide range of rock types in order to find a more specific breakability parameter.

References

Aikawa, A. 2009, "Techniques to Measure Effects of Passing Trains on Dynamic Pressure Applied to Sleeper Bottoms and Dynamic Beshavior of Ballast Stones", *Quarterly Report of Railway Technical Research Institute*, vol. 50, no. 2, pp. 102-109.

Anthes, G. 2006, *Grundlagenerhebung zu Vorkommen von Granitgesteinen in Österreich*, Report, Projekt Ü-LG-050.

Aschenbrenner, B. 1956, "A new Method of expressing Particle Sphericity", *J Sediment Petrol*, vol. 26, no. 1, pp. 15-31.

Association française de normalisation (afnor) 2006, P 94-430-1 *Roches - Détermination du pouvoir abrasif d'une roche*, Paris.

Association française de normalisation (afnor) 1990, P 18-579 *Granulats - Essai d'abrasivité et de broyabilité*, Paris.

Augustin, S. 2002, *Untersuchungen zur Lagestabilität des Schotteroberbaus*, Dissertation, Institut für Bodenmechanik und Felsmechanik der Universität Fridericiana in Karlsruhe.

Augustin, S., Gudehus, G., Huber, G. & Schünemann, A. 2003, "Numerical Model and Laboratory Tests on Settlements of Ballast Track" in *System Dynamics and Long-Term Behaviour of Railway Vehicles, Track and Subgrade*, eds. K. Popp & W. Schiehlen, Springer-Verlag, Berlin, pp. 317-336.

Bach, H. 2012, "Beanspruchungscharakteristik von Schotter im Gleis" in *Forschungstag 2012 (Schriftenreihe 1)*, ed. Institut für Eisenbahnwesen und Verkehrswirtschaft an der TU Graz, Graz, pp. 76-93.

Bach, H. & Enzi, M. 2013, *Petroscope - Wirtschaftliche Bewertung - Business Case Petroscope*, Report, Institut für Eisenbahnwesen und Verkehrswirtschaft - TU Graz.

Bach, H. & Latal, C. 2013, "Attrition Kinetics of the Los Angeles Test", *Engineering Geology*, vol. p submitted.

Baeßler, M. & Ruecker, W. 2003, "Track Settlement Due to Cyclic Loading with low Minimum Pressure and Vibrations" in *System Dynamics and Long-Term Behaviour of Railway Vehicles, Track and Subgrade*, eds. K. Popp & W. Schiehlen, Springer-Verlag, Berlin, pp. 337-356.

Bärtschi, C.J. 2010, *Kieselkalke der Schweiz: Charakterisierung eines Rohstoffs aus geologischer, petrographischer, wirtschaftlicher und umweltrelevanter Sicht*, Dissertation, ETH Zürich.

Blott, S.J. & Pye, K. 2008, "Particle shape: a review and new methods of characterization and classification", *Sedimentology*, vol. 55, pp. 31-63.

Bond, F.C. 1952, "The third theory of comminution", *Transactions of the Society of Mining Engineers of AIME*, vol. 193, pp. 484-494.

Breymann, H., Nerat, M., Treffer, C., Hueber, P. & Schweinberger, M. 2011, *Mechanische Kriterien für den Gleisschotter - Punktlastversuch - Zertrümmerung*, Master Project, Höhere Technische Bundeslehranstalt Saalfelden - Abteilung Bautechnik - Tiefbau.

References

Breymann, H., Nindl, G. & Scharler, D. 2012, *Mechanische Kriterien für den Gleisschotter - Punktlastversuch - Zeitreihen*, Master Project, Höhere Technische Bundeslehranstalt Saalfelden - Abteilung Bautechnik - Tiefbau.

British Standards Institution 1990, BS 812-110:1990 *Testing Aggregates: Methods for Determination of Aggregate Crushing Value (ACV)*, Milton Keynes.

British Standards Institution 1951, BS 812:1951 *Testing Aggregates: Method of determination of aggregate abrasion value - Deval Attrition*, Milton Keynes.

Brook, N. 1985, "The equivalent core diameter method of size & shape correction in point load testing", *International Journal of Rock Mechanics and Mining Sciences & Geomechanical Abstracts*, vol. 22, no. 4, pp. 61-70.

Cerchar 1986, "*The Cerchar abrasiveness index*", ed. Centre d´Études et des Recherches des Charbonages de France, Verneuil.

Daniel, J.S. & Lowe, J. 2011, *Petroscope Evaluation*, Report, University of New Hampshire - Department of Civil Engineering.

Descantes, Y., Fosse, Y. & Milcent, F. 2006, "Automated Measurement of Railway Ballast Angularity", *Journal of Materials in Civil Engineering*, vol. 18, no. 4, pp. 612-618.

Drucker, P. 2011, "Validity of the LCPC abrasivity coefficient through the example of a recent Danube gravel", *Geomechanik und Tunnelbau*, vol. 4, no. 6, pp. 681-691.

EUREKA 2005, *Petroscope II.*, Brussels.

EUREKA 2001, *Petroscope – an optical analyser for construction aggregates and rocks.*, Brussels.

Field, W.G. 1963, "Towards the statistical definition of a granular mass" in *Proc. 4th Australian and New Zealand Conference on Soil Mechanics*, pp. 143-148.

Filep, L. 1936, *Egyenló gömbökból âlló halmazok*, Vizügyi Közlemények, Budapest.

Fischer, J. 1983, *Einfluss von Frequenz und Amplitude auf die Stabilisierung von Oberbauschotter*, Dissertation, Institut für Eisenbahnwesen und Verkehrswirtschaft an der TU Graz.

Fuchs, R. 2012, *Untersuchungen der Abrasivität von Gleisschottermaterial*, Master Project, Institut für angewandte Geowissenschaften, Technische Universität Graz.

Führer, G. 1978, *Oberbauberechnung*, 1. Aufl. edn, transpress VEB Verlag für Verkehrswesen, Berlin.

Gerstberger, U., Knothe, K. & Wu, Y. 2003, "Combined Modelling of Track Models and Subgrade Models - Vertical and Lateral Dynamics" in *System Dynamics and Long-Term Behaviour of Railway Vehicles, Track and Subgrade*, eds. K. Popp & W. Schiehlen, Springer-Verlag, Berlin, pp. 247-264.

Hardin, B.O. 1985, "Crushing of Soil Particles", *Journal Geotechnical Engineering*, vol. 111, no. 10, pp. 1177-1192.

References

Harrison, H.D., Selig, E.T., Dean, F.E. & Stewart, H.E. 1984, *Correlation of concrete tie track performance in revenue service and at the facility for accelerated service testing - Vol. 1*.

Heibaum, M. & Warnecke, W. 2012, "Versuche zum Abriebverhalten von Gesteinen bei hydraulischen Einwirkungen", *geotechnik*, vol. 35, no. 2, pp. 94-108.

Heineke, S.A. 2001, *Experimentelle und numerische Untersuchungen zur Gleislagestabilität*, Dissertation, Institut für Geotechnik der Technischen Universität Darmstadt.

Hofer, V. & Bach, H. 2012, "Statistical monitoring for continuous quality control of railway ballast", *European Journal of Operational Research*, vol. p submitted.

Hofer, V., Bach, H., Latal, C. & Neubauer, A. 2012, "Impact of geometric and petrographic characteristics on the variability of LA test values for railway ballast", *Mathematical Geosciences*, in print.

Hofer, V., Pilz, J. & Helgason, T.S. 2006, "Statistical classification of different petrographic varieties of aggregates by means of near and mid infrared spectra", *Mathematical Geology*, vol. 38, no. 7, pp. 851-870.

Hollersbacher, K. 2011, *Mineralogische Charakterisierung und Erfassung des Abrasivitätsverhaltens von ausgewählten Graniten und Metamorphiten Österreichs*, Master Project, Institut für angewandte Geowissenschaften, Technische Universität Graz.

Holtzendorff, K. 2003, *Untersuchung des Setzungsverhaltens von Bahnschotter und der Hohllagenentwicklung auf Schotterfahrbahnen*, Dissertation, Technische Universität Berlin.

Indraratna, B., Lackenby, J. & Christie, H.D. 2005, "Effect of confining pressure on the degradation of ballast under cyclic loading", Géotechnique, vol. 55, no. 4, pp. 325-328.

Jankovic, A., Dundar, H. & Metha, R. 2010, "Relationships between comminution energy and product size for a magnetite ore", *The Journal of The Southern African Institute of Mining and Metallurgy*, vol. 110, no. 3, pp. 141-146.

Käsling, H., Thiele, I. & Thuro, K. 2007, "Abrasivitätsuntersuchungen mit dem Cerchar-Test - eine Evaluierung der Versuchsbedingungen" in *Veröffentlichungen von der 16. Tagung für Ingenieurgeologie*, ed. F. Otto, Technische Fachhochschule "Georg Agricola" Bochum, Bochum, pp. 229-235.

Katzenbach, R. & Heineke, S.A. 2003, "Experimental and Numerical Investigations on the Track Stability" in *System Dynamics and Long-Term Behaviour of Railway Vehicles, Track and Subgrade*, eds. K. Popp & W. Schiehlen, Springer-Verlag, Berlin, pp. 395-410.

Kick, F. 1883, "Das Gesetz der proportionalen Widerstände und seine Anwendung auf Sanddruck und Sprengen", *Polytechnisches Journal*, vol. 250, pp. 141-145.

Köhler, M., Maidl, U. & Martak, L. 2011, "Abrasivness and tool wear in shield tunneling in soil", *Geomechanik und Tunnelbau*, vol. 4, no. 1, pp. 36-53.

References

Kuttelwascher, C. 2011, "Oberbauschotter in Österreich" in *Proc. 10. Unterbau-Expertentreffen DACH-Staaten, Nürnberg*.

Lanaro, F. & Tolppanen, P. 2002, "3D characterization of coarse aggregates", *Engineering Geology*, vol. 65, pp. 17-30.

Lassnig, K., Latal, C. & Klima, K. 2008, "Impact of Grain Size on the Cerchar Abrasiveness Test", *Geomechanik und Tunnelbau*, vol. 1, no. 1, pp. 71-76.

Latal, C., Bach, H. & Thuro, K. 2013, "Application of the methods for tool wear in quality control of railway ballast", *Rock Mechanics and Rock Engineering*, in preparation.

Lee, J.R.J., Smith, M.L. & Smith, L.N. 2007, "A new approach to the three-dimensional quantification of angularity using image analysis of the size and form of coarse aggregates", *Engineering Geology*, vol. 91, pp. 254-264.

Lee, J.R.J., Smith, M.L., Smith, L.N. & Midha, P.S. 2005, "A mathematical morphology approach to image based 3D particle shape analysis", *Machine Vision and Applications*, vol. 16, no. 5, pp. 282-288.

Lichtberger, B. 2010, *Handbuch Gleis*, 3. Aufl. edn, Eurailpress, Hamburg.

Lim, W.L. 2004, *Mechanics of Railway Ballast Behaviour*, Dissertation, University of Nottingham.

Lim, W.L., McDowell, G.R. & Collop, A.C. 2005, "Quantifying the relative strength of railway ballasts", *Geotechnical Engineering*, vol. 158, no. GE2, pp. 107-111.

Liu, H., Kou, S., Lindqvist, P., Lindqvist, J.E. & Aakesson, U. 2005, *Microscope Rock Texture Characterization and Simulation of Rock Aggregate Properties*, Geological Survey of Sweden, Stockholm.

Lobo-Guerrero, S. & Vallejo, L.E. 2006, "Discrete Element Method Analysis of Railtrack Ballast Degradation during Cyclic Loading", *Granular Matter*, vol. 8, no. 3-4, pp. 195-204.

Lu, M. & McDowell, G.R. 2006, "Discrete element modelling of ballast abrasion", *Géotechnique*, vol. 56, no. 9, pp. 651-655.

Lu, M. & McDowell, G.R. 2007, "The importance of modelling ballast particle shape in the discrete element method", *Granular Matter*, vol. 9, pp. 69-80.

Maerz, N.H. & Zhou, W. 1999, "Flat and elongated: advances using digital image analysis" in *Proc., 7th Annual ICAR Symp.* Austin, Tex., pp. B1-4-1-B1-4-12.

McDowell, G.R. & Amon, A. 2000, "The Application of Weibull Statistics to the Fracture of Soil Particles", *Soil and Foundations*, vol. 40, no. 5, pp. 133-141.

McDowell, G.R. & Bolton, M.D. 1998, "On the micromechanics of crushable aggregates", *Géotechnique*, vol. 48, no. 5, pp. 667-679.

McDowell, G.R., Bolton, M.D. & Robertson, D. 1996, "The fractal Crushing of Granular Materials", *Journal of the Mechanics and Physics of Solids*, vol. 44, no. 12, pp. 2079-2102.

McDowell, G.R. & Harireche, O. 2002, "Discrete element modelling of yielding and normal compression of sand", *Géotechnique*, vol. 52, no. 4, pp. 299-304.

References

McDowell, G.R., Lim, W.L. & Collop, A.C. 2003, "Measuring the strength of railway ballast", *Ground Engineering*, vol. 36, no. 1, pp. 25-28.

McDowell, G.R., Lim, W.L., Collop, A.C., Armitage, R. & Thorn, N.H. 2004, "Comparison of ballast index tests for railway trackbeds", Geotechnical Engineering, vol. 157, no. GE3, pp. 151-161.

Neubauer, A. 2013, *Effect of petrographic Composition of railway Ballast on the Los-Angeles Test*, Master thesis, Institut für angewandte Geowissenschaften, Technische Universität Graz, in preparation.

Österreichische Bundesbahnen (ÖBB) 2007, BH 700 *Technische Lieferbedingungen für den Oberbauschotter*, Wien.

Österreichische Bundesbahnen (ÖBB) 2002, *Richtlinie für das Entwerfen von Bahn-anlagen – Hochleistungsstrecken (directive for the design of railway infrastructure – High speed railways)*, Wien.

Österreichische Bundesbahnen (ÖBB) 1962, BH 700 *Vorläufige Technische Lieferbe-dingungen für Oberbauschotter*, Wien.

Österreichisches Normungsinstitut 2006, EN 1097-2 *Prüfverfahren für mechanische und physikalische Eigenschaften von Gesteinkörnungen - Teil 2: Bestimmung des Widerstandes gegen Zertrümmerung*, Wien.

Österreichisches Normungsinstitut 2004a, EN 13450 *Gesteinskörnungen für Gleis-schotter*, Wien.

Österreichisches Normungsinstitut 2004b, EN 1097-1 *Prüfverfahren für mechanische und physikalische Eigenschaften von Gesteinkörnungen - Teil 1: Bestimmung des Widerstandes gegen Verschleiß (Mikro-Deval)*, Wien.

Pham, A.M., Descantes , Y. & Larrard, F.d. 2010, "Determination of sieve grading curves using an optical device", *Mechatronics*, [Online], , pp. 2011-01-28.

Pixner, P. 2011, *Durchführung und Auswertung von Laborversuchen über mechanische Eigenschaften von Gleisschotter*, Master Project, Institut für Eisenbahnwesen und Verkehrswirtschaft an der TU Graz.

Plinninger, R. 2007, "Geotechnische Einflüsse auf den Werkzeugverschleiß beim Bohren in Festgestein" in *58. Berg- und Hüttenmännischer Tag - Kolloquium 4: Innovative Bohrtechnologien für Flach-, Tief- und Großlochbohrungen*, ed. Technische Universität Bergakademie Freiberg, Freiberg, pp. 1-15.

Plinninger, R. 2002, *Klassifizierung und Prognose von Werkzeugverschleiß bei kon-ventionellen Gebirgslösungsverfahren im Festgestein*, Münchner Geologische Hefte Reihe B: Angewandte Geologie, München.

Plinninger, R. & Restner, U. 2008, "Abrasiveness Testing, Quo Vadis? - A Commented Overview of Abrasiveness Testing Methods", *Geomechanik und Tunnelbau*, vol. 1, no. 1, pp. 61-70.

Powers, M.C. 1953, "A new Roundness Scale for Sedimentary Particles", *J Sediment Petrol*, vol. 23, no. 2, pp. 117-119.

References

Raymond, G.P. & Bathurst, R.J. 1985, "Repeated-load response of aggregates in relation to track quality index", *Canadian Geotechnical Journal,* vol. 31, no. 4, pp. 547-554.

Ridgway, K. & Tarbuck, K.J. 1967, "The random packing of spheres", *British Chemical Engineering,* vol. 12, no. 3, pp. 385ff.-1.

Riessberger, K., Jörg, A., Semprich, S., Bach, H. & Feldbacher, R. 2007, *Under Ballast Mats - Theoretical Reserach*. Report.

Rittinger, R.P. 1867, *Lehrbuch der Aufbereitungskunde,* Ernst & Sohn, Berlin.

Rosival, A. 1916, "Neuere Untersuchungsergebnisse über die Härte von Mineralien und Gesteinen - Ein absolutes Maß für die Härte spröder Körper", *Verhandlungen der kaiserlich-königlichen geologischen Reischsanstalt Wien,* vol. 5 & 6, pp. 117-147.

Rosival, A. 1896, "Neue Untersuchungen über die Härte von Mineralen und Gesteinen", *Verhandlungen der kaiserlich-königlichen geologischen Reichsanstalt Wien,* vol. 17 & 18, pp. 475-491.

Röthlisberger, F., Däppen, J., Kurzen, E. & Würsch, E. 2005, " Los Angeles Prüfung für Gleisschotter - Aussagekraft und Folgerung ", *Eisenbahntechnische Rundschau,* vol. 54, no. 6, pp. 355-361.

Salas Cazón & Milton Antonio 2002, *Untersuchungen zur abrasiven Beanspruchung von Feststoffpartikeln in einem Rührreaktor*, Dissertation, Technische Universität Berlin - Fakultät III – Prozesswissenschaften.

Scharinger, F. 2007, *A Multilaminate Model for Soil incorporating Small Strain Stiffness*, Dissertation, Institut für Bodenmechanik und Grundbau - Technische Universität Graz.

Schimazek, J. & Knatz, H. 1976, "Die Beurteilung der Bearbeitbarkeit von Gesteinen durch Schneid- und Rollenbohrwerkzeuge", *Erzmetall,* vol. 29, no. 3, pp. 113-119.

Schöck, M. 2011, *Deval-Versuch - Untersuchungen zur Verschleißcharakteristik verschiedener Gesteinsarten*, Master thesis, Institut für Eisenbahnwesen und Verkehrswirtschaft an der TU Graz.

Schweizerischer Verband der Strassen- und Verkehrsfachleute 2007, SN 670 830b *Prüfverfahren für mechanische und physikalische Eigenschaften von Gesteinskörnungen - Verfahren zur Bestimmung der Druckfestigkeit von Gleisschotter am Haufwerk*, Zürich.

Selig, E.T. 2009, *Guidelines to Best Practices for Heavy Haul Railway Operations - Infrastructure Construction and Maintenance Issues,* International Heavy Haul Association, Virginia Beach.

Selig, E.T. & Waters, J.M. 1994, *Track Geotechnology and Substructure Management,* Thomas Telford, London.

Smith, W.O., Foote, P.D. & Busang, P.F. 1929, "Packing of homogeneous spheres", *Physical Review,* vol. 34, pp. 1271-1274.

Thuro, K. 1996, *Bohrbarkeit beim konventionellen Sprengvortrieb,* Dissertation, Münchner Geologische Hefte Reihe B: Angewandte Geologie, München.

References

Thuro, K. & Käsling, H. 2009, "Classification of the abrasiveness of soil and rock", *Geomechanik und Tunnelbau*, vol. 2, no. 2, pp. 179-188.

Thuro, K., Singer, J., Käsling, H. & Bauer, M. 2006, "Soil Abrasivity Assessment Using the LCPC Testing Device", *Felsbau*, vol. 24, no. 6, pp. 37-45.

Tolppanen, P. 2001, *3-D Characterization and Degradation Analysis of Rock Aggregates*, Dissertation, Division of Engineering Geology - Department of Civil and Environmental Engineering - KTH Stockholm.

Tolppanen, P., Stephansson, O. & Stenlid, L. 2002, " 3-D Degradation analysis of railroad ballast ", *Bulletin of Engineering Geology and the Environment*, vol. 61, pp. 35-42.

Uhlig, E. 2011, *Mineralogische Charakterisierung und Erfassung des Abrasivitäts-verhaltens von ausgewählten Metamorphiten, Dolomit und Vulkaniten Österreichs*, Master Project, Institut für angewandte Geowissenschaften - Technische Universität Graz.

Wadell, H. 1935, "Volume, Shape and Roundness of Quartz Particles", *Journal of Geology*, vol. 43, pp. 250-280.

Weiher, B.M. 2009, *Kennwertprognose in der Natursteinindustrie als Hilfestellung für Erkundung und Qualitätssicherung*, Dissertation, Institut für Ingenieurgeologie TU München.

West, G. 1989, "Technical Note – Rock Abrasiveness Testing for Tunnelling", *International Journal of Rock Mechanics and Mining Sciences & Geomechanical Abstracts*, vol. 26, no. 2, pp. 151-160.

Wieden, P. 1969, " Erfassung der Gesteinseigenschaften durch Schlag- und Zertrümmerungswert und Los-Angeles-Test", *Berg- und Hüttenmännische Monatshefte*, vol. 114, no. 10, pp. 310-315.

Wieden, P., Augustin, H. & Zieger, M. 1977, *Versuche zur Verbesserung des Los Angeles-Tests*, in *Straßenforschung 86*, ed. Bundesministerium für Bauten und Technik, Wien.

Winkler, E. 1867, *Die Lehre von der Elastizität und Festigkeit*, Dominicus, Prag.

Yanagisawa, E. 1978, "Relation between the shear modulus and void ratio in granular media", *The Technology Reports of Tohoku University*, vol. 43, no. 1, pp. 211-220.

Zimmermann, H. 1941, *Berechnung des Eisenbahnoberbaues*, 3rd edn, W. Ernst & Sohn, Berlin.

Zingg, T. 1935, *Beitrag zur Schotteranalyse - Die Schotteranalyse und ihre Anwendung auf die Glattalschotter*, Dissertation, Abteilung für Naturwissenschaften an der ETH Zürich.

WISSEN ▪ TECHNIK ▪ LEIDENSCHAFT

Institut für Eisenbahnwesen
und Verkehrswirtschaft
Technische Universität Graz
Rechbauerstrasse 12/II
8010 Graz
+43 316 873 6216
office.ebw@tugraz.at
www.ebw.tugraz.at